To the Graduate Council:

I am submitting herewith a thesis written by Peter Evan Fryberger entitled "A Simplified Analytical Pressure Prediction Model of an Aerodynamically Separated Interceptor Shroud." I have examined the final copy of this thesis for form and content and recommend that it be accepted in partial fulfillment of the requirements for the degree of Master of Science, with a major in Mechanical Engineering.

Ahmad D. Vakili

Dr. Ahmad Vakili, Major Professor

We have read this thesis
and recommend its acceptance:

Roy J. Schulz

Roger Crawford

Accepted for the Council:

CW Minkel

Associate Vice Chancellor
and Dean of The Graduate School

In presenting this thesis in partial fulfillment for a Master's degree at The University of Tennessee, Knoxville, I agree that the Library shall make it available to borrowers under rules of the Library. Brief quotations from this thesis are allowable without special permission, provided that accurate acknowledgment of the source is made.

Permission for extensive quotation from or reproduction of this thesis may be granted by my professor, or in his absence, by the Head of Interlibrary Services when, in the opinion of either, the proposed use of the material is for scholarly purposes. Any copying or use of the material in this thesis for financial gain shall not be allowed without my written permission.

Signature ____________________

Date 28 April 1993

# A SIMPLIFIED ANALYTICAL PRESSURE PREDICTION MODEL OF AN AERODYNAMICALLY SEPARATED INTERCEPTOR SHROUD

A Thesis
Presented for the
Master of Science
Degree
The University of Tennessee, Knoxville

Peter Evan Fryberger

May 1993

DEDICATION

This Thesis is dedicated to my parents

Mr. Charles Theodore Fryberger II

and

Mrs. Nancy Ann Barnett Fryberger

who have given me invaluable support,

nourishing freedom, and unlimited opportunity.

ACKNOWLEDGMENTS

First and foremost I would like to express my thanks to my wife, Maralyn, for her patience, support, and love. Its your turn now. Next, I would like to thank my employer, SY Technology, Inc., and the U.S. Army for providing the resources which supported much of this work. I would also like to thank my major professor, Dr. Ahmad Vakili, for his flexibility and guidance throughout my studies. Thanks also goes to the other committee members, Dr. Roy Schulz and Dr. Roger Crawford, for their help and general scholastic efforts throughout my post-graduate years. Finally, thanks again to my father, Charles Theodore Fryberger II, and my mother, Nancy Ann Barnett Fryberger, for everything.

## ABSTRACT

A FORTRAN computer code has been written to simulate the removal of a shroud which protects seeker hardware on a ballistic missile interceptor. The removal process is characterized by the aerodynamic filling and venting of the cavity defined by a four petal conic shroud. The resulting cavity pressure increase causes the shroud petals to rotate and release from the interceptor, exposing the seeker on the interceptor forebody. The code predicts the shroud petal motion and the pressures on the interceptor forebody at designated locations over the duration of the shroud separation event.

The code has been written to be used as a low cost aerodynamic environment prediction tool for evaluating initial designs of interceptors which rely on aerodynamic forces to remove cone shaped shrouds consisting of two or more petals. Typically, interceptor forebodies which rely on this design experience mechanical shock related to the aerodynamics of the shroud removal process, which could jeopardize interceptor hardware.

The results of the code for the case of the Army's High Endo-atmospheric Defense Interceptor (HEDI) are compared with HEDI ground and flight test data. It was found that the code's modeling of a constant speed moving shock produced petal motion and forebody pressure data which compared well to the ground and flight test data.

# TABLE OF CONTENTS

LIST OF TABLES

LIST OF FIGURES

## NOMENCLATURE

| | |
|---|---|
| AAV | Designed conic shroud half angle |
| Aflow | Flow cross sectional area at a given flight station |
| A_FRONT | Flow capture area at moving shock flight station |
| AGAP | Total gap area between petals downstream of moving shock |
| AL_P | Petal angular acceleration |
| AT | Tetracone cross sectional area at a given flight station |
| Atotal | Total area within the petals at a given flight station |
| AZINIT | Initial radial acceleration at time of petal unhinge |
| CHKRAT | Fill/vent mass flow ratio |
| DGAP | Gap distance between two petals |
| DT | Time increment |
| FE1 | Petal external pressure force |
| FI1 | Petal internal pressure force upstream of moving shock |
| FI2 | Petal internal pressure force downstream of moving shock |
| F_MDOT | Mass flow rate into the shroud cavity |
| G | Ratio of specific heats |
| J | Tetracone geometry description parameter |
| OM_P | Petal angular velocity |
| P2 | Static pressure behind a shock/expansion |
| P2P1 | Static pressure ratio across a shock/expansion |
| P_CAV | Instantaneous cavity pressure |
| PETL | Total length of a petal |
| PETL2 | Distance along the petal from the petal base to the moving shock location |
| PETM | Petal mass |

| | |
|---|---|
| PI | Pi |
| PI2 | Petal internal pressure downstream of the moving shock |
| PINF | Free stream static pressure |
| PPETEXT | Petal external pressure |
| PPETINT | Petal internal pressure upstream of the moving shock |
| PT2 | Total pressure downstream of a shock/expansion |
| PT2PT1 | Total pressure ratio across a shock/expansion |
| PTINF | Free stream total pressure |
| Rb | Tetracone base radius |
| Reff | Radius from the axis of symmetry to closed petal internal surface at a given flight station |
| RGAS | Universal gas constant |
| RHO2 | Density downstream of a shock/expansion |
| RHO_IN | Density of the gas downstream of the moving shock |
| RHOINF | Free stream density |
| RMINF | Free stream Mach number |
| RM1N | Upstream normal Mach number component |
| RM2 | Mach number downstream of a shock/expansion |
| RS | Sphere radius of tetracone tip |
| RTCR | Radius from axis of symmetry to tetracone surface at a given flight station |
| RTHP | Radius from axis of symmetry to rotated petal internal surface at a given flight station |
| SA1 | Petal surface area upstream of the moving shock |
| SA2 | Petal surface area downstream of the moving shock |
| SAT | Total petal surface area |
| SUM_M | Moment sum about the petal hinge or its c.g. |

| | |
|---|---|
| T2 | Static temperature downstream of a shock/expansion |
| T2T1 | Static temperature ratio across a shock/expansion |
| T_CAV | Temperature downstream of the moving shock |
| THDIFF | Angle between a line drawn from a point on a rotating petal through the petal base and a horizontal line through the point on the petal |
| THP | Instantaneous petal rotation angle |
| THPT | Angle between a line drawn from a point on a closed petal through the petal base and a horizontal line through the point on the petal |
| THS | Angle between a line drawn from a point on the tetracone sphere tip surface to the center of the sphere and a vertical line through the point on the sphere |
| TINF | Free stream static pressure |
| TMASS | Total mass of the gas downstream of the moving shock |
| TTINF | Free stream total pressure |
| VINF | Free stream velocity |
| V_MDOT | Mass flow rate out through the petal gaps |
| VT | Total captured flow volume downstream of the moving shock |
| VZINIT | Initial radial velocity of the petal at time of unhinge |
| X | Flight station of point of interest on internal surface of rotating petal |
| X1P | Flight station of point of interest on internal surface of closed petal |
| X20 | Flight station of petal hinge point |
| X_CG | Distance along petal from petal base to petal center of gravity |
| XMOI | Moment of inertia about petal hinge or its c.g. |

| | |
|---|---|
| XNUM | Prandtl-Meyer function |
| XPET1 | Moment arm from center of pressure on petal internal surface area upstream of the moving shock to the petal center of rotation |
| XPET2 | Moment arm from center of pressure on petal internal surface area downstream of the moving shock to the petal center of rotation |
| XPET3 | Moment arm from center of pressure on petal external surface to petal center of rotation |
| XUN | Same as X_CG |
| XT | Distance from tetracone virtual origin to a given flight station |
| Y | Tetracone geometry description parameter |
| Z | Tetracone geometry description parameter |

# CHAPTER I

# INTRODUCTION

## Background and General Information

The High Endoatmospheric Defense Interceptor (HEDI - Figure 1) and related interceptor programs rely on an infrared seeker to track and intercept incoming threat re-entry vehicles. The infrared seeker is housed inside the tetracone forebody of the HEDI kill vehicle (Figure 2). The seeker is protected from aerodynamic and heating loads by a window on the tetracone forebody when the missile is actively tracking and intercepting the threat.

During initial flyout of the interceptor, the seeker window is also protected from debris, and aerodynamic and heating loads by a protective shroud (Figure 2). Shroud separation is initiated at a predetermined time in the trajectory of the interceptor. Shroud separation occurs by detonation of a charge in the nosecap which effectively splits and discards the nosecap (Figure 3a). Freestream fluid then fills the shroud cavity until the aerodynamic forces cause the four shroud petals to rotate about (and then out of) the hinges at the base of the tetracone forebody (Figure 3b). The petal motion is such that they fall away clear of the interceptor missile.

Table 1 summarizes the nominal development ground tests that were conducted for the HEDI missile to evaluate performance of the "fly-away" shroud concept and to determine the thermal and aerodynamic loads imparted on the seeker window during shroud separation. In addition, two successful HEDI flight tests have been

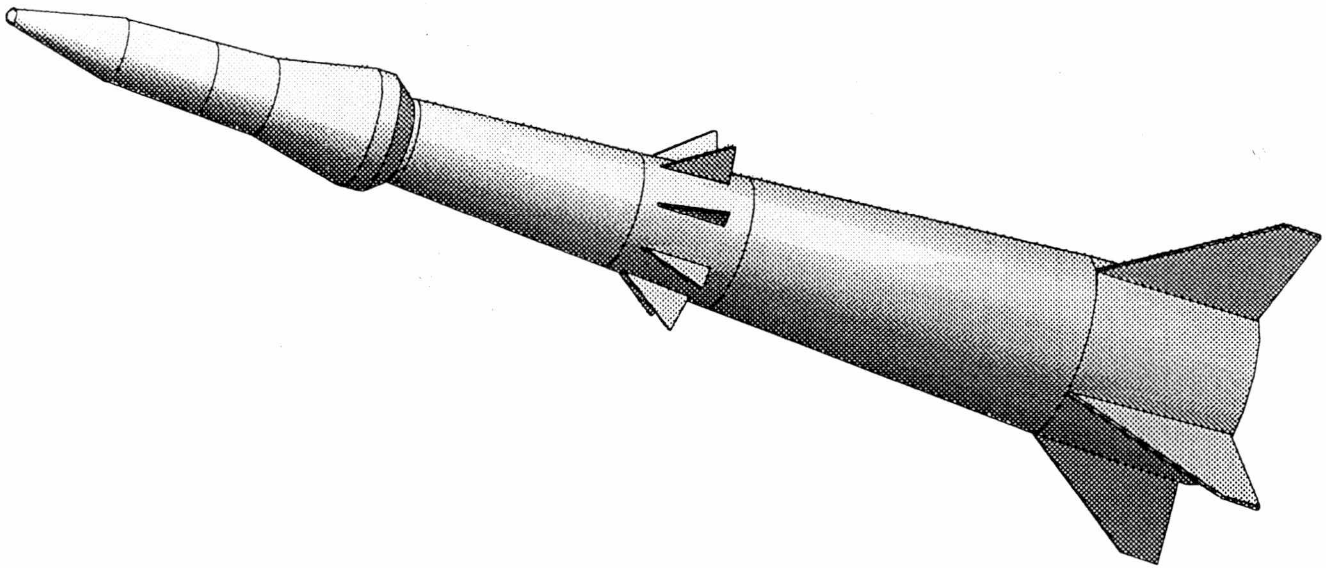

Figure 1. High Endoatmospheric Defense Interceptor (HEDI)

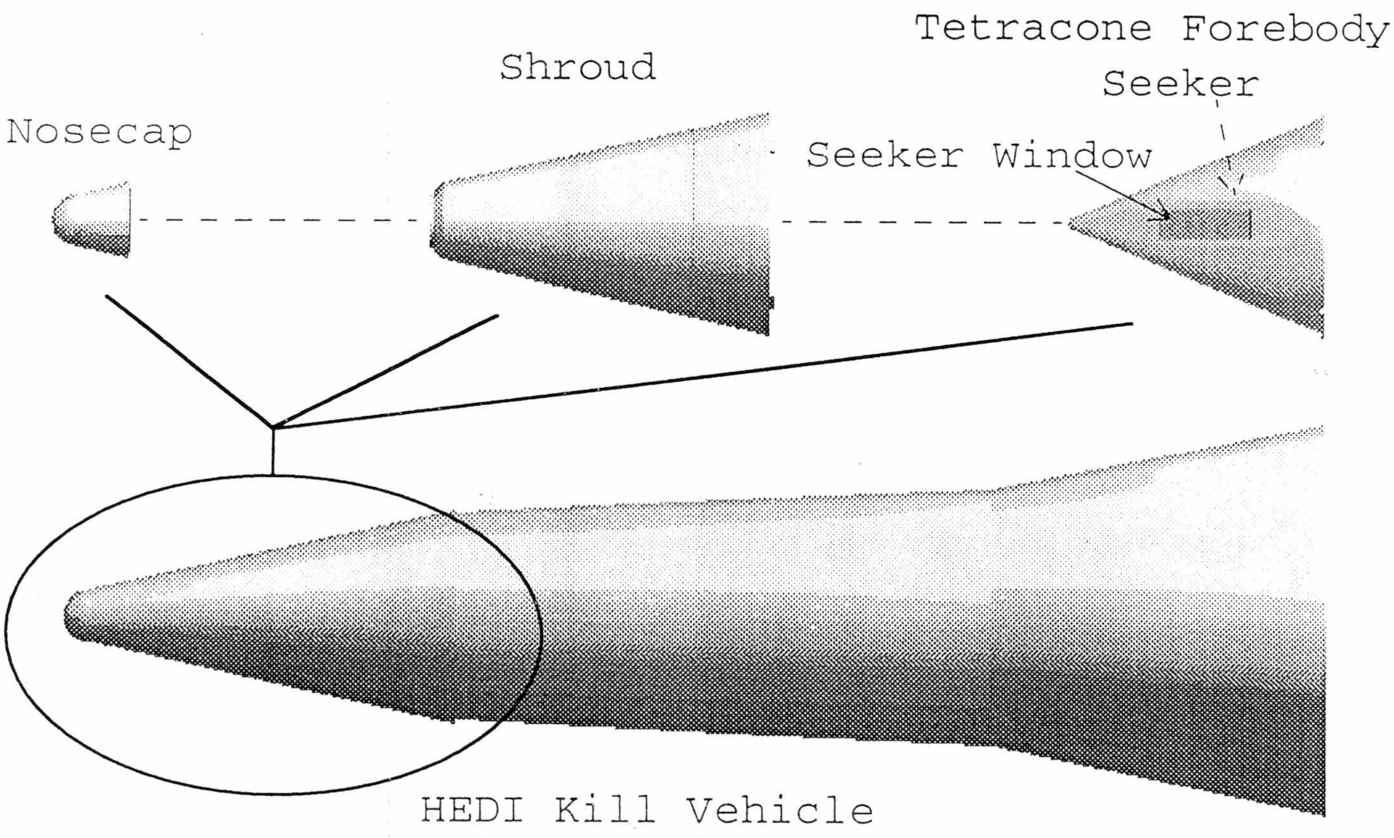


Figure 2. HEDI Kill Vehicle and Forebody Components

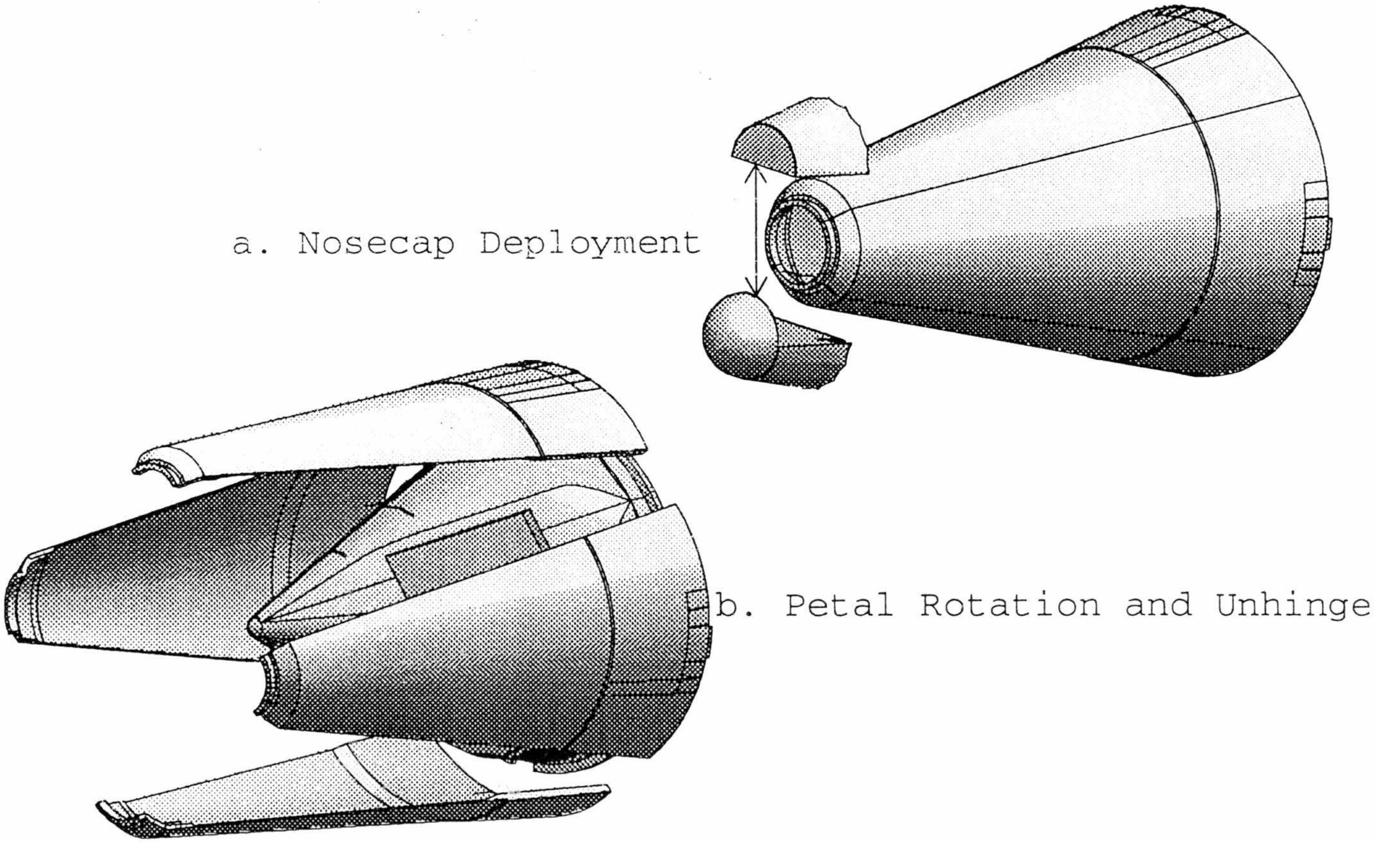


Figure 3. HEDI Shroud Separation

Table 1. HEDI Shroud Removal Test Summary

| Facility | Scale | Mach # | Gas | $\gamma$ | R (ft-lbf/lbm-$^oR$) | Total Pressure (PSIA) | Total Tempertature ($^oR$) |
|---|---|---|---|---|---|---|---|
| Langley Research Center (LARC)-HTT | 0.5 | 6.2 | $N_2$-$O_2$ | 1.38 | 55 | 1150 | 3400 |
| Naval Surface Warfare Center (NSWC)-Tunnel 9 | 0.3 | 10.3 | $N_2$ | 1.4 | 54.77 | 16925 | 2000 |
| NSWC Tunnel 9 | 0.3 | 14.1 | $N_2$ | 1.4 | 54.77 | 15175 | 3669 |
| NSWC Tunnel 9 | 1.0 | 7.87 | $N_2$ | 1.4 | 54.77 | 18009 | 1798 |
| White Sands Missle Range (WSMR) - Flight | 1.0 | 6.7 | Air | 1.4 | 53.35 | 17873 | 4322 |
| WSMR-Flight | 1.0 | 5.07 | Air | 1.4 | 53.35 | 2773.8 | 2579 |

conducted. Test results reflect expected and unexpected trends. The nature of the aerodynamics responsible for a particular unexpected result is the focus of this thesis.

## Thesis

Forebody data recorded for each HEDI test reveal a pressure rise on each face of the forebody tetracone just after nosecap removal associated with the cavity fill process. As the pressure on the inside of the shroud petals caused moments about the petal hinges of enough magnitude to overcome the moments created by the external petal pressures, the petals began to rotate. A second, strong transient pressure was then measured on the forebody (Figure 4).

The aerodynamics responsible for the high magnitude pressure pulse are of great interest to the interceptor community. The magnitude of the pressure imparted on the forebody drives the design of the seeker window, and contributes to the mechanical shock imparted to the interceptor's on-board hardware. Therefore, there is a need to predict the aerodynamics of the shroud separation process during the design phase of future interceptors which use similar fly-away shroud concepts.

Computational Fluid Dynamics (CFD) codes exist which can do an impressive job of predicting the pressure histories relating to the shroud separation process (Chamberlin and Baltar [1]). Unfortunately, the cost and time associated with obtaining a full history of the separation process from the CFD codes is well beyond what would be acceptable for a flexible design tool. Instead, a need exists to efficiently model the aerodynamics of the shroud separation

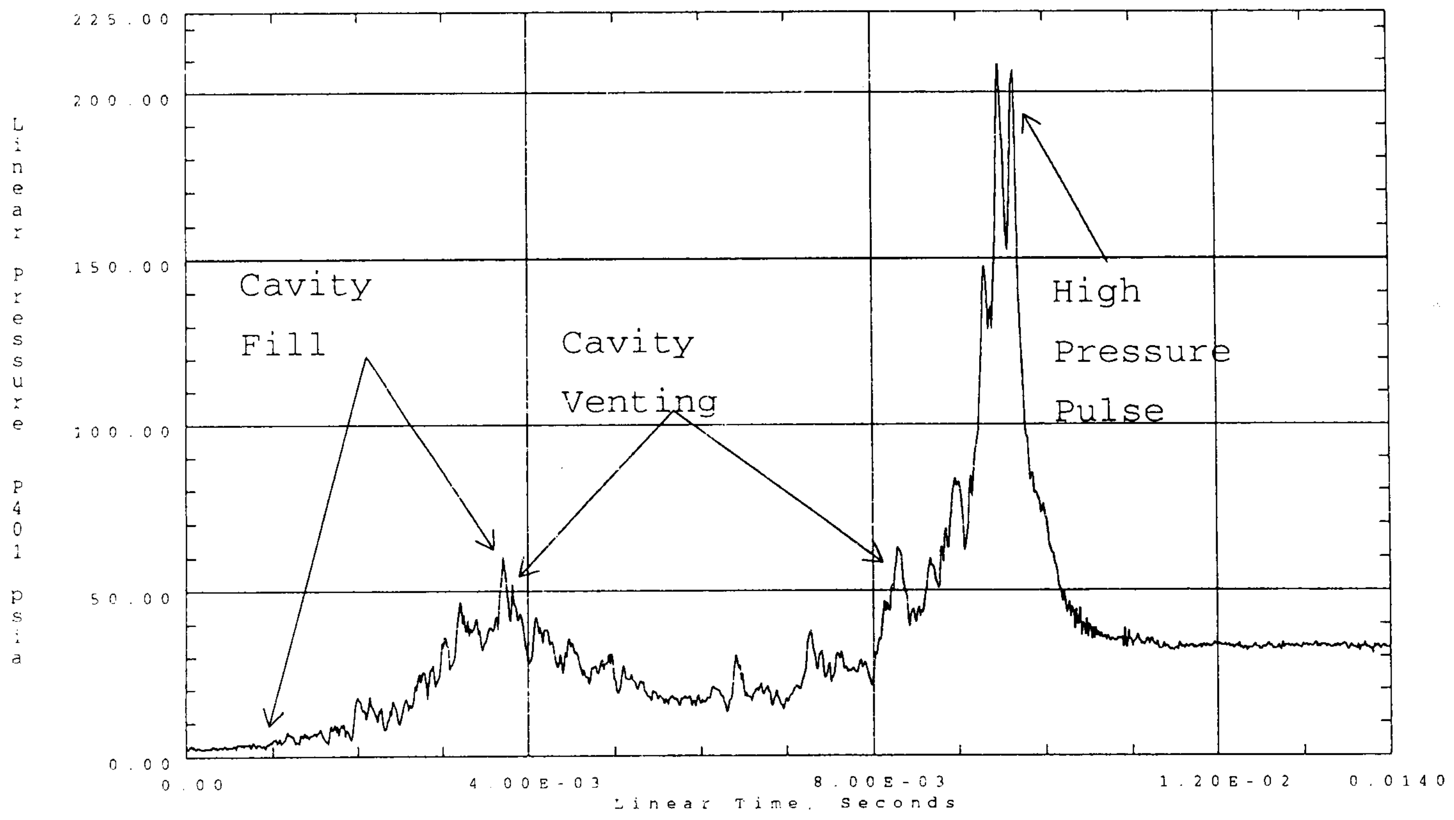


Figure 4. Typical Shroud Separation Forebody Pressure History

process with enough detail to satisfy the engineering involved in the initial design process of fly-away shrouds, and then use CFD later to validate the design. The focus of the work that follows is the development of a relatively simple aerodynamic prediction code which can model the shroud separation process accurately.

## Motivation

The ultimate goal of the engineer designing an interceptor which relies on infrared seeker technology is to maximize seeker wavelength flexibility. An unfortunate side effect is that this goal requires reducing seeker window material strength. In addition, the engineer must be confident that the internal hardware which controls the interceptor will not be compromised by large mechanical shocks imparted to the vehicle. Therefore, use of the program developed (modified for the geometry of the proposed design) would aid the engineer in converging on the best design before any expensive tests or CFD codes would have to be run. In addition, the code can be used by the United States (U.S.) Government to evaluate proposed interceptor design concepts.

## Hypothesis

To create a simple model of the shroud separation aerodynamics without the benefit of a full fledged CFD solution, the mechanism for the strong pressure pulse had to be determined. After a relatively short literature search, it became obvious that very little research was published with respect to hypersonic flow filling a variable area duct undergoing variable venting. Therefore, the following possible explanations were considered:

1. The shocks generated by the tetracone forebody interact with the shocks generated by the rotating petals. The result of the interaction causes the locally high pressure pulse when the interaction passes. This theory is similar to the explanation given by McDonnell Douglas Space Systems Company (MDSSC - the HEDI prime contractor) after the HEDI screening test (Tincher [2]). They said:

> "(MDSSC) used the filtered pressure data to categorize forebody pressure histories into two phases. The first, or cavity fill, phase is caused by applying stagnation conditions to an acoustic cavity. The pressure achieved is a function of gas bulk modulus, cavity volume, and stagnation pressure levels. The pressure histories exhibit an upward slope as ram-air enters the petal opening. Pressures then level and oscillate until the petals quickly begin to rotate, whereupon the histories enter the next phase.
>
> The second, or shock-on-shock, phase is caused by the formation and interaction of shocks within the petal boundaries. Initially, strong traveling shocks form and pass through the cavity. A hyperextended bow shock is formed from the shroud opening due to the large pressure seen between the shock, petals, and forebody. As the petals continue to rotate, and these shocks pass the tetracone forebody, the main bow shock remains on the forebody with attached shocks forming on the petal leading edges. The forebody bow shock interacts with the petal leading-edge shocks to transmit local short-duration pressure pulses to the forebody. The net pressures continue to rise since the petal capture area is substantially larger than the venting area. Once the petal hinges approach and pass their release angles, the high pressure is quickly vented and this phase is complete. Free flow establishes over the forebody and the forebody pressures quickly ramp down to quasi-static levels."

Prediction of the location on the forebody of the interaction's effect relative to the measured effect during testing would help to prove or disprove this theory. Also, if the MDAC description is correct, the pressure measured on the forebody after the high pulse passage and before the petals unhinge and depart should be something other than that behind an attached shock generated by the forebody.

2. A moving "pseudo-normal" shock starts out as a bow shock ahead of the petals before they open, then travels downstream as the petal gap area increases. This theory could be proven by finding fairly uniform motion of the pressure pulse on all faces of the forebody - independent of individual petal motions. The shock motion should be more a function of total vent area than petal angle. Additionally, an independent analysis of the theoretical time of passage of a moving bow shock (as a function of back pressure, most likely) compared with test data could be a convincing argument for or against this theory.

Theory 2, the movement of a pseudo-normal shock, was determined to be the most likely based on the evidence from the test data, as will be shown. The hypothesis, therefore, is that after nosecap detonation, the cavity fills and builds pressure to the point where the petals begin to rotate. Upon rotation, the gap area downstream of the cavity opening increases until the mass flow out of the cavity is equivalent to the mass flow into the cavity. At this point, a pseudo-normal shock begins travelling downstream. The details of this process are described in the following text.

# CHAPTER II

# GROUND TEST DISCUSSIONS

## Theories

Chapter 1 brought to light two possible theories for the occurrence of the strong pressure pulse measured on the HEDI forebody during the shroud separation event. For each theory, a method for proving or disproving the theory was suggested. Using the ground test data from the Naval Surface Warfare Center (NSWC) Tunnel 9 full scale HEDI shroud separation test, the two theories will now be addressed in more detail.

## Theory 1

Shocks generated by the tetracone forebody interacting with those generated by the rotating petals is the basis for theory 1. The idea here is that the interacting shocks cause a type I Edney jet (Edney [3]), whose interaction with the boundary layer causes the high pressure pulse, and/or something similar to the MDSSC screening test explanation occurs.

To test these possibilities, an analysis of the intersection of the attached shocks according to petal rotation angle would locate the vicinity of the impending effects. The results of such an analysis could then be compared to the time history of the peak pressures measured to see if the local passage area is coincident. In addition, to test the related explanation by MDSSC, local pressures measured after the peak pressure but prior to petal unhinge should be something other than the pressure measured behind an attached shock generated by the tetracone forebody.

The shroud petals, prior to nosecap deployment, make up a 13 degree cone. Therefore, as the petals begin to rotate, expansion will occur within the shroud cavity immediately downstream of the petal leading edges until the petals pass through 0 degrees, at which time compression will take place, forming an oblique shock (Figure 5). Eighteen dynamic pressure transducers (3 at each of 6 axial model stations - Figure 6) were attached to the HEDI forebody during the NSWC Tunnel 9 test. The test conditions were:

| Gas | Mach # | Static Pressure (psia) | Static Temperature (deg R) |
| --- | --- | --- | --- |
| Nitrogen | 7.87 | 2.06 | 134.3 |

Table 2 documents the time of peak pressure measurement at each transducer location, the measured pressure value, and the measured petal angle. From this information, it can be seen that the peak pressures occur on the tetracone forebody when the petal angles are less than or just greater than zero. The implication is that the peak pressures listed in Table 2 could not have been a result of an effect relating to internal petal compression because the petals are not producing significant forebody directed oblique shocks until they have rotated well past the horizontal plane (Figure 5).

Furthermore, as can be seen in Figure 4, the pressure measured immediately after pulse passage is on the order of the static pressure behind an attached shock coming off the tetracone forebody. At the time of pulse measurement at the first two axial transducer locations, additional venting caused by petal detachment is not yet a

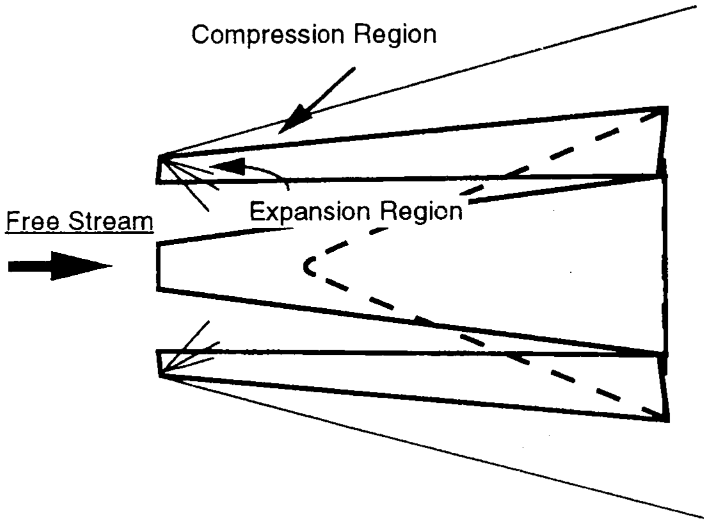


a. Petal angle less than 0°

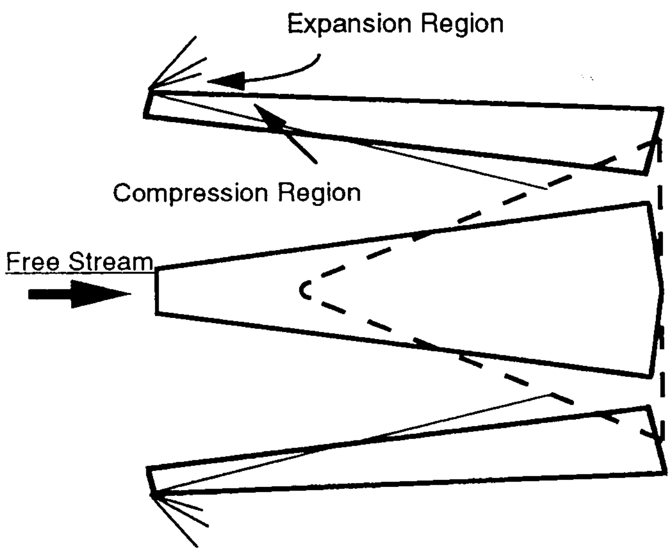


b. Petal angle greater than 0°

Figure 5. Petal Aerodynamics

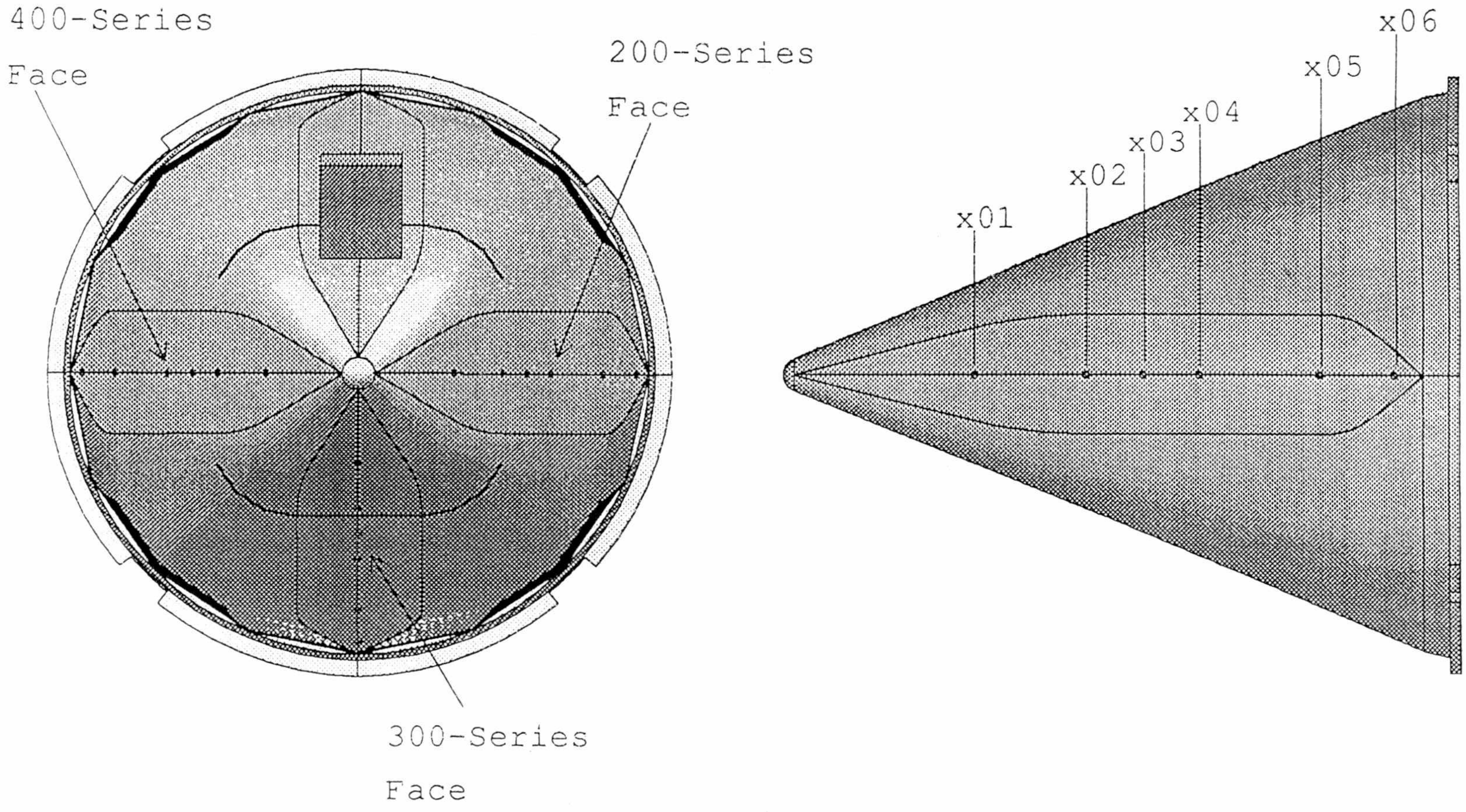


Figure 6. NSWC Tunnel 9 Transducer Locations

Table 2. Peak Forebody Pressure Measurement History

| Time After Nosecap Deployment (sec) | Transducer | Measured Pressure (psia) | Petal Angles (degrees) 1 | 2 | 3 | 4 |
|---|---|---|---|---|---|---|
| 0.0086 | FP201 | 225.15 | -1.63 | -2.76 | 3.59 | -2.34 |
| 0.0093 | FP301 | 192.13 | 0.24 | -2.96 | 6.56 | -2.08 |
| 0.0095 | FP401 | 208.55 | 0.74 | -3.25 | 7.38 | -2.22 |
| 0.0096 | FP202 | 247.55 | 0.98 | -3.44 | 7.77 | -2.34 |
| 0.0102 | FP203 | 200.36 | Petal Accelerometer Data Discontinued | | | |
| 0.0103 | FP302 | 207.23 | | | | |
| 0.0104 | FP402 | 163.68 | | | | |
| 0.0104 | FP303 | 203.86 | | | | |
| 0.0106 | FP403 | 243.99 | | | | |
| 0.0107 | FP304 | 175.98 | | | | |
| 0.0107 | FP404 | 193.47 | | | | |
| 0.0109 | FP204 | 176.22 | | | | |
| 0.0117 | FP205 | 184.60 | | | | |
| 0.0117 | FP405 | 170.00 | | | | |
| 0.0118 | FP305 | 163.37 | | | | |
| 0.0121 | FP206 | 207.99 | | | | |
| 0.0121 | FP406 | 163.91 | | | | |
| 0.0123 | FP306 | 153.72 | | | | |

factor, suggesting that the MDSSC screening test explanation is not likely. Therefore, theory 1 was rejected.

## Theory 2

A moving normal shock controlled by the petal gap area as the petals open is the basis for theory 2. The concept here is that the bow shock present prior to nosecap removal remains during the cavity fill process. As the petals begin to rotate, venting through the gaps occurs and the bow shock becomes a pseudo-normal shock which moves downstream, with its speed controlled by the characteristics of the captured gas it's "pushing" (Figure 7).

To test theory 2, ground test data should show that the peak pressures measured at each axial station on the forebody occurred at approximately the same time on all of the instrumented faces with no specific relation to independent petal angles. Also, the local pressure measured at the time of the pulse passage should be on the order of the total pressure immediately downstream of a moving normal shock. Finally, the pressure measured immediately after shock passage should be that which would be measured behind an attached shock coming off the tetracone forebody.

Referring back to Table 2, it can be seen that indeed there was fairly uniform passage of the high pressure pulse independent of individual petal angles. In addition, a mean speed of the travelling pulse can be determined from the data in Table 2 by simply dividing the distance between the furthest upstream and furthest downstream axial transducer location by the elapsed time between the first

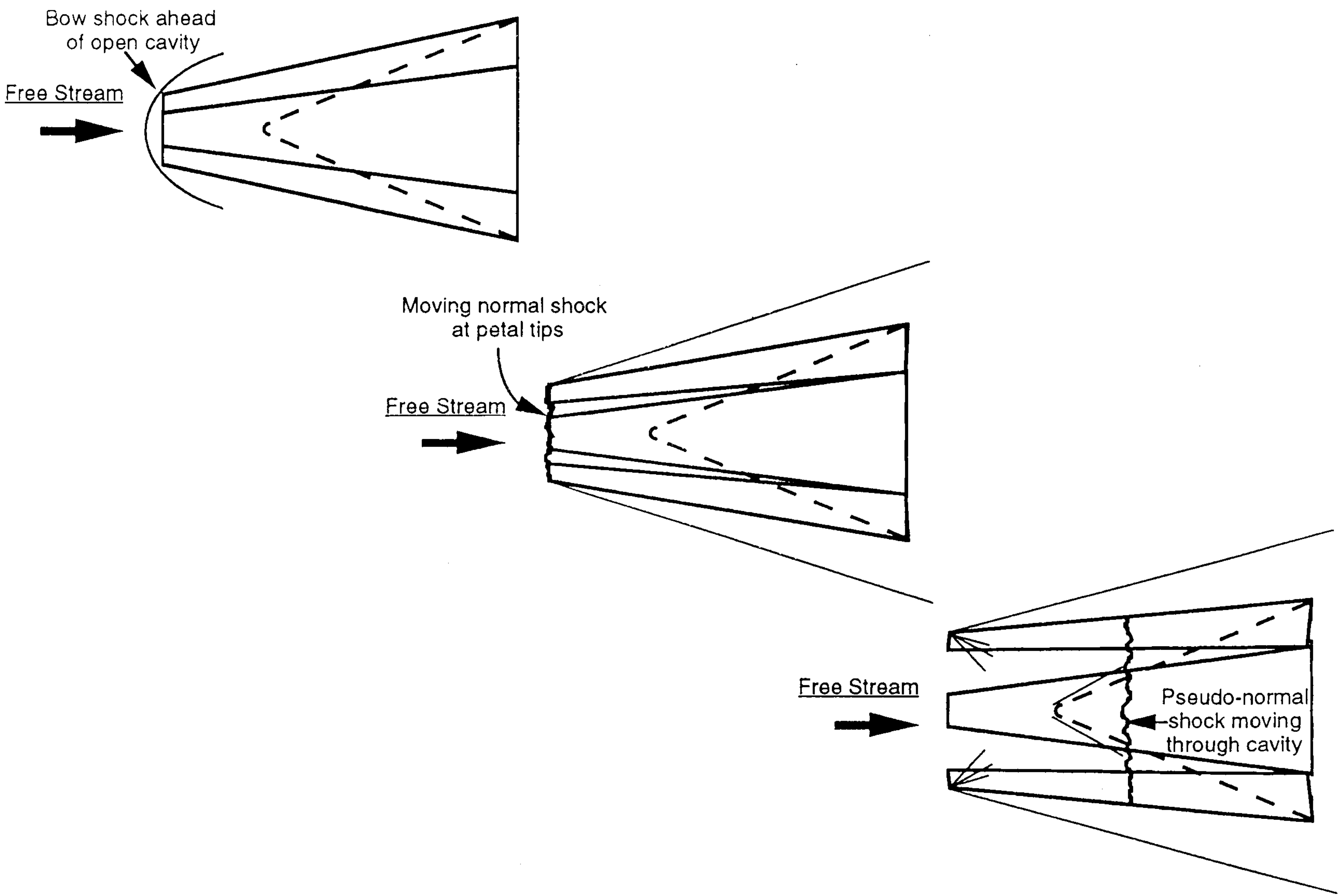


Figure 7. Petal Shock Influence

measured pulse and the last measured pulse. The result of this calculation is a pulse speed of 267 ft/sec.

To check the expected pressure associated with the theorized pseudo-normal moving shock, calculations were performed to estimate the total pressure downstream of a normal shock subject to the free-stream conditions, with an adjustment to the Mach number to account for the motion of the shock. The conceptual details and calculations are presented in Figure 8. The resulting calculated pressure ($Pt_2$ = 215.2 psia) compares very well to the average measured peak pulse pressure of 193.4 psia, and is well within the range of measured values.

Finally, calculating the static pressure behind an attached shock coming off the 23 deg tetracone forebody (using a cone solution) one gets $P_{cone}$ = 31.4 psia. This value compares very well to the constant pressure of ~31 psia measured at all transducer locations immediately after shock passage (Figure 4). Therefore, theory 2 was accepted as the model theory.

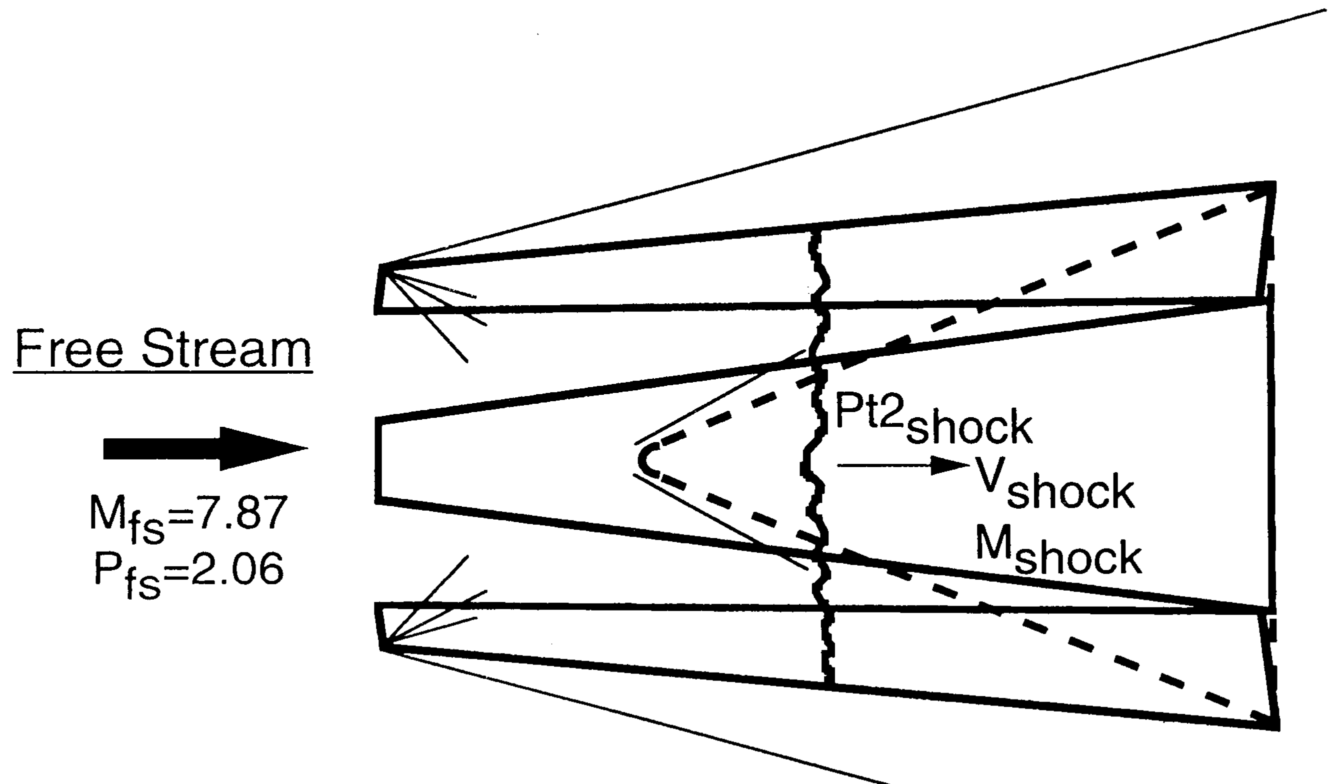


$V_{shock} = dx_{shock}/dt$

$M_{shock} = V_{shock}/(\gamma RT)^{0.5}$

$DM_{shock} = M_{fs} - M_{shock}$

$Pt2_{shock}/P_{fs} = Fn(DM_{shock}$ , ref. NACA 1135 equation#100)

Figure 8. Moving Shock Strength Determination

# CHAPTER III

## METHODS AND ASSUMPTIONS

### Overview

Prior to shroud nosecap removal, there exists a bow shock just upstream of the nosecap. The moving shock theory pursued begins at the instant after the nosecap ordnance has been fired and the nosecap has been propelled away from the shroud cavity opening. What follows is the "cavity fill" process characterized by rapid pressurization of the shroud cavity as the mass flow in is compressed. The capture area into the cavity is assumed to be the area encapsulated by the ends of the petals (Figure 9a).

As the internal pressure forces increase, the moments they create about the petal hinges become larger than the restraining moments caused by the external pressures, and the petals begin to rotate.

Cavity fill continues until the gaps formed between the rotating petals become so great that the mass flow exiting the gaps becomes greater than or equal to the mass flow entering the cavity. At the time the fill/vent mass flow ratio becomes less than or equal to one, the "vent and travel" process begins.

During the vent and travel process, the bow shock is ingested into the cavity, and now moves continuously downstream. Flow continues to enter the cavity, however the volume of interest now becomes that containing the fluid mass trapped downstream of the shock front plane. Capture area is now defined by the area

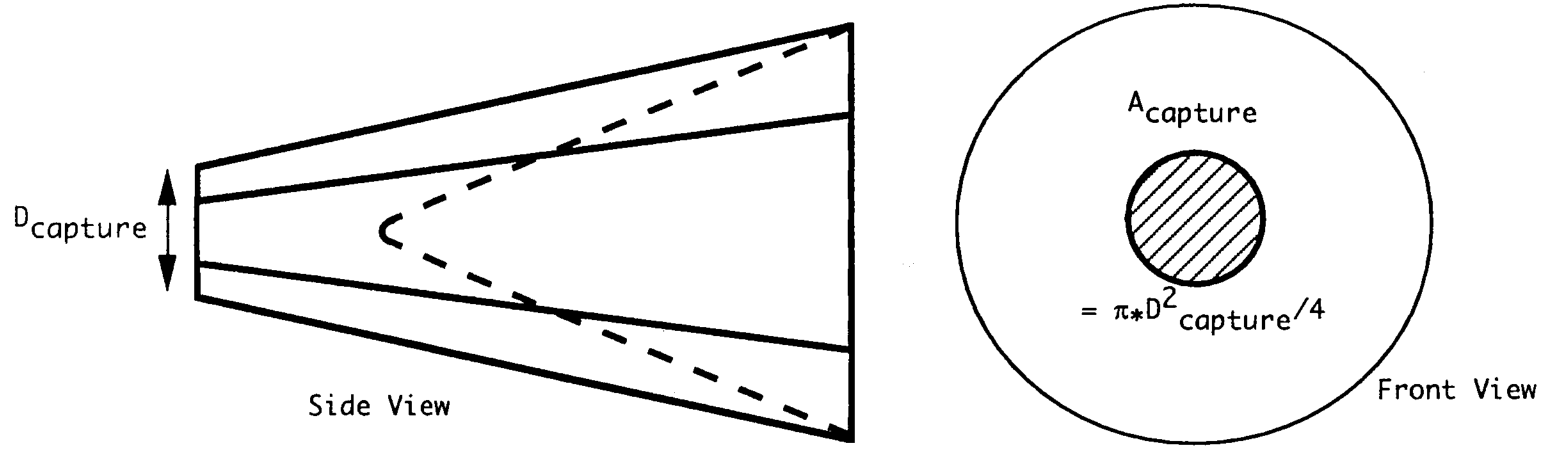


a. Pre petal rotation

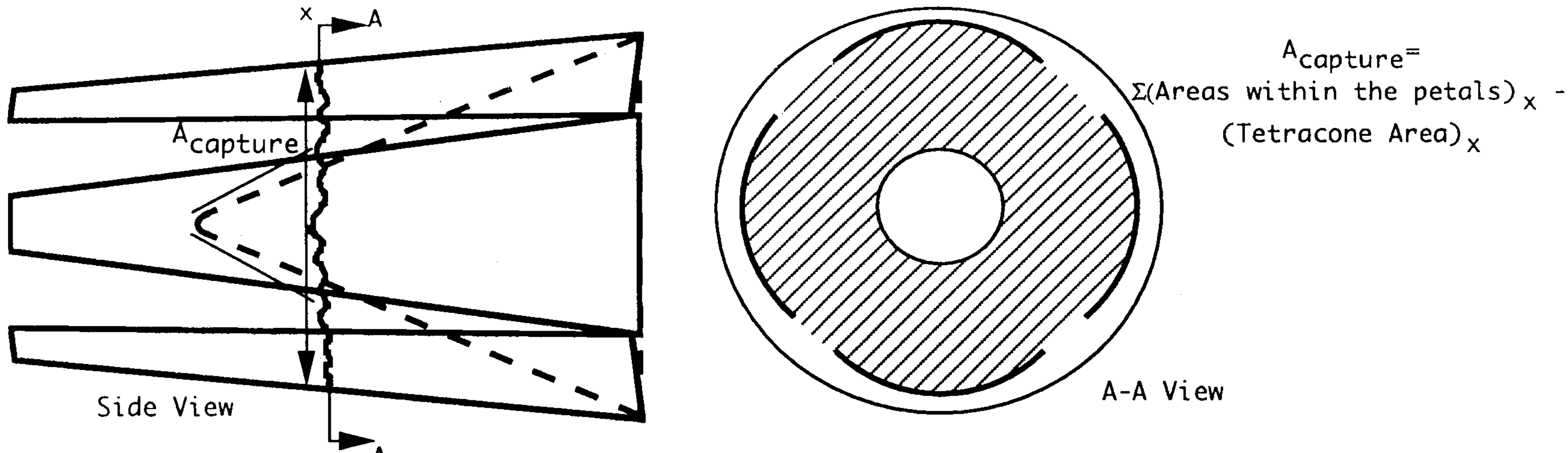


b. Post shock movement

Figure 9. Petal Capture Area

encapsulated by the petal walls at a flight station (FS) defined by the location of the shock plane (Figure 9b).

Petal release from the hinges occurs by design, allowing additional venting as the gap between the petals and tetracone base increases. Petal motion characteristics change because the petals now rotate about their centers of mass. Shock motion continues downstream until the shock passes FS 100 (the hinge point at the base of the tetracone) at which time the event is considered over.

## Cavity Fill Process

Forebody pressure data obtained from the full scale HEDI test conducted in the NSWC Tunnel 9 are presented in Figure 10. The flow into the cavity just after nosecap deployment resembles flow in a classic shock tube experiment (Anderson [4]). Initially, it was considered that the acoustic shock which immediately enters the cavity, reflects off the base of the tetracone/shroud seal, and travels back out to the cavity opening may be tied to the events measured. Subsequent calculations revealed that this shock travels much too fast (cycles through cavity in less than 3 milliseconds) and with minimal strength, to be responsible for the phenomena being investigated. Evidence of early internal shock activity can be witnessed in the "ringing" effect recorded by the most downstream pressure transducers (x06 series) during the first 4 milliseconds of the NSWC Tunnel 9 experiment (Figure 10).

To avoid getting into the complex details of the initial internal aerodynamics associated with a variable area shock tube, the cavity fill process was handled as a bulk mass flow problem. The

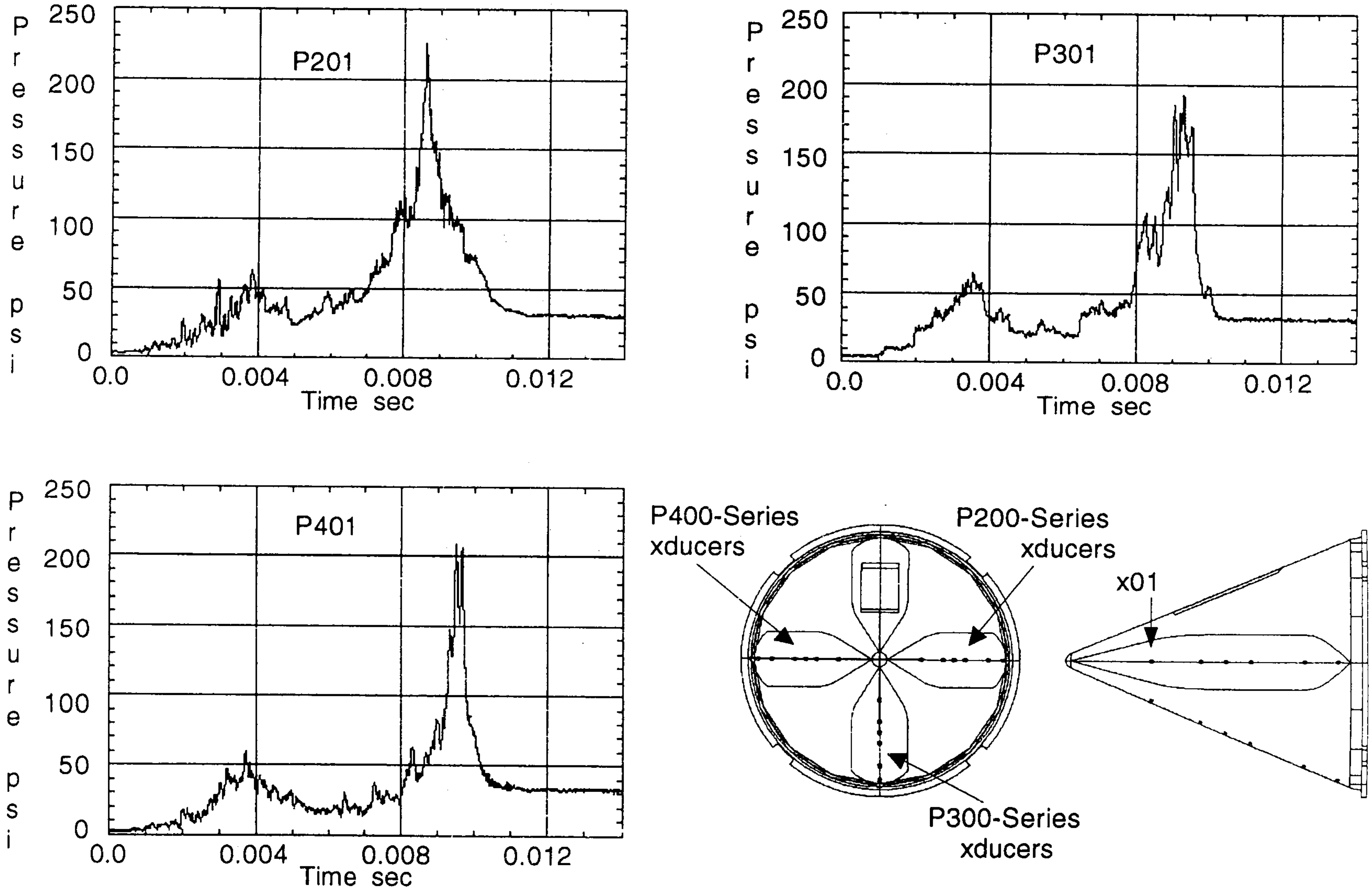


Figure 10. HEDI Forebody Pressure Histories From The NSWC Tunnel 9 Shroud Separation Test

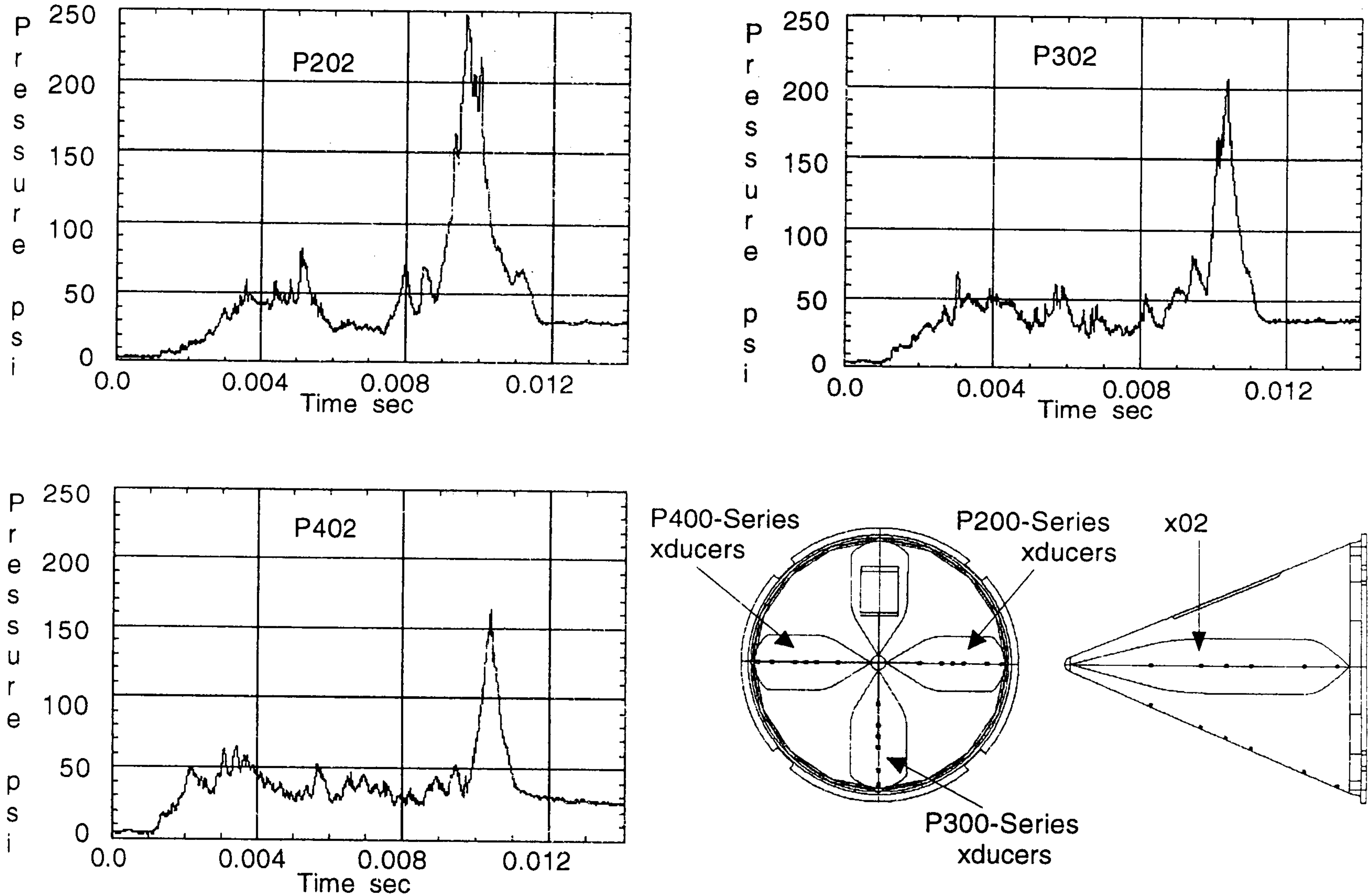


Figure 10. Continued

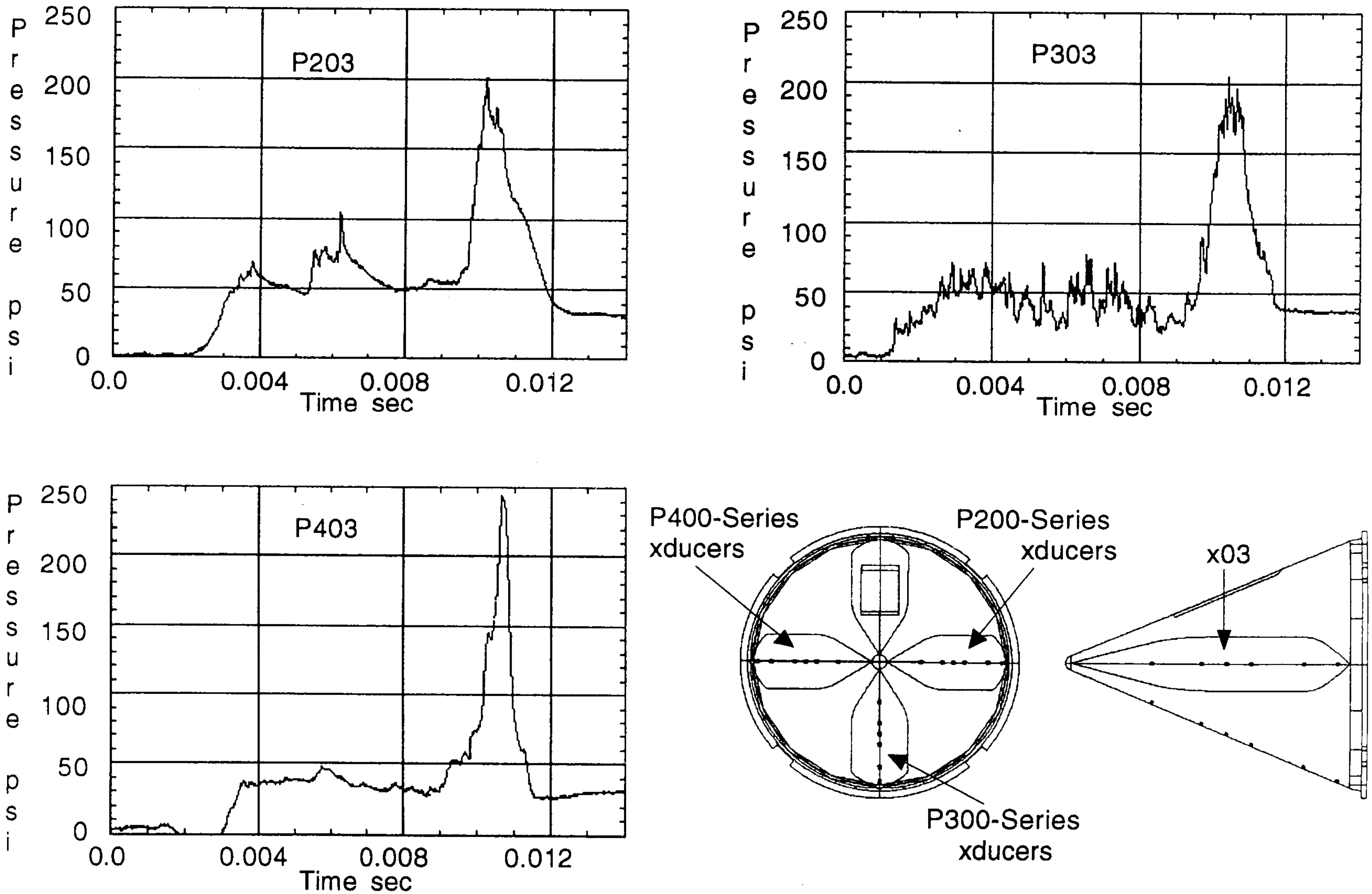


Figure 10. Continued

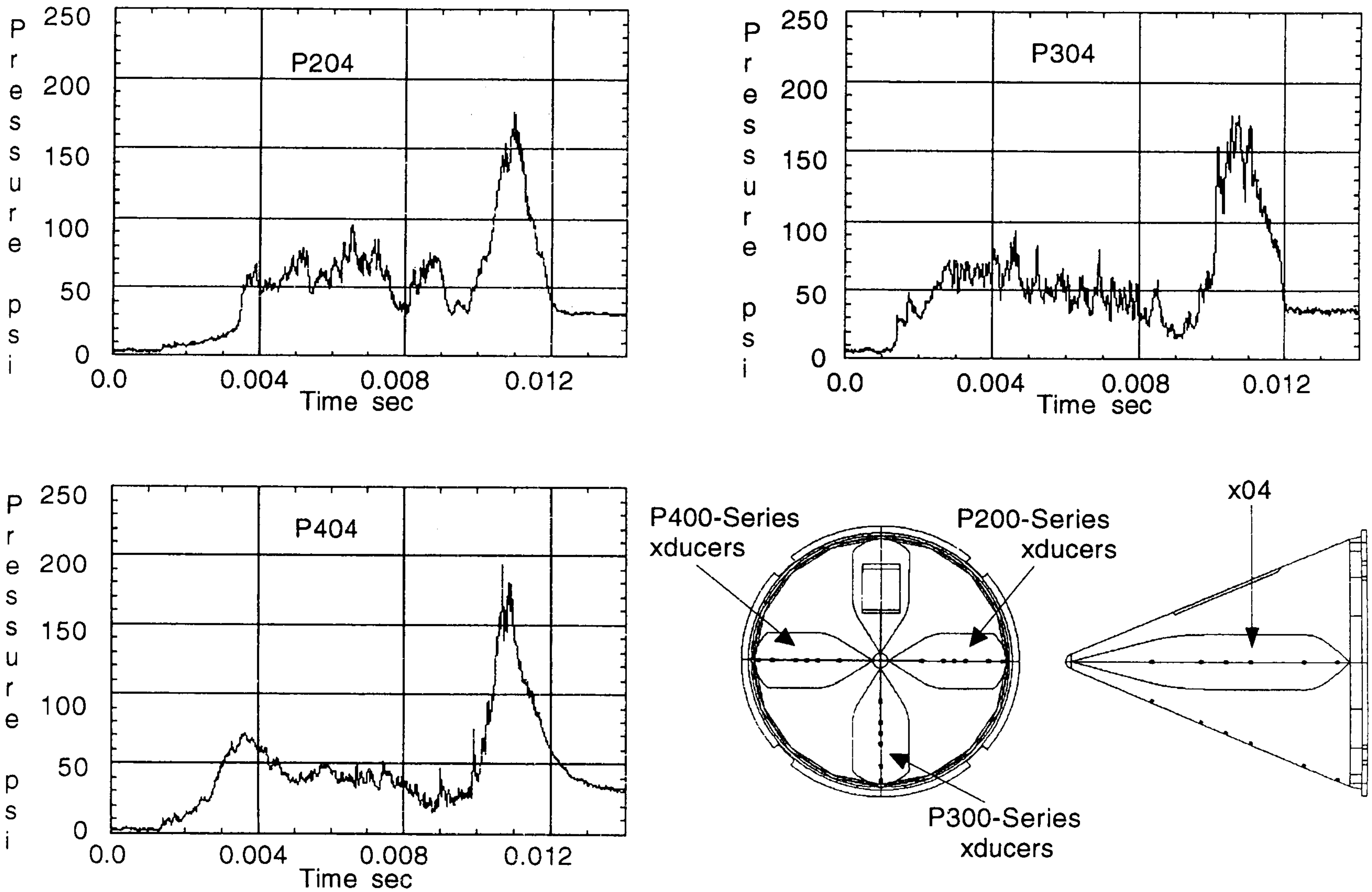


Figure 10. Continued

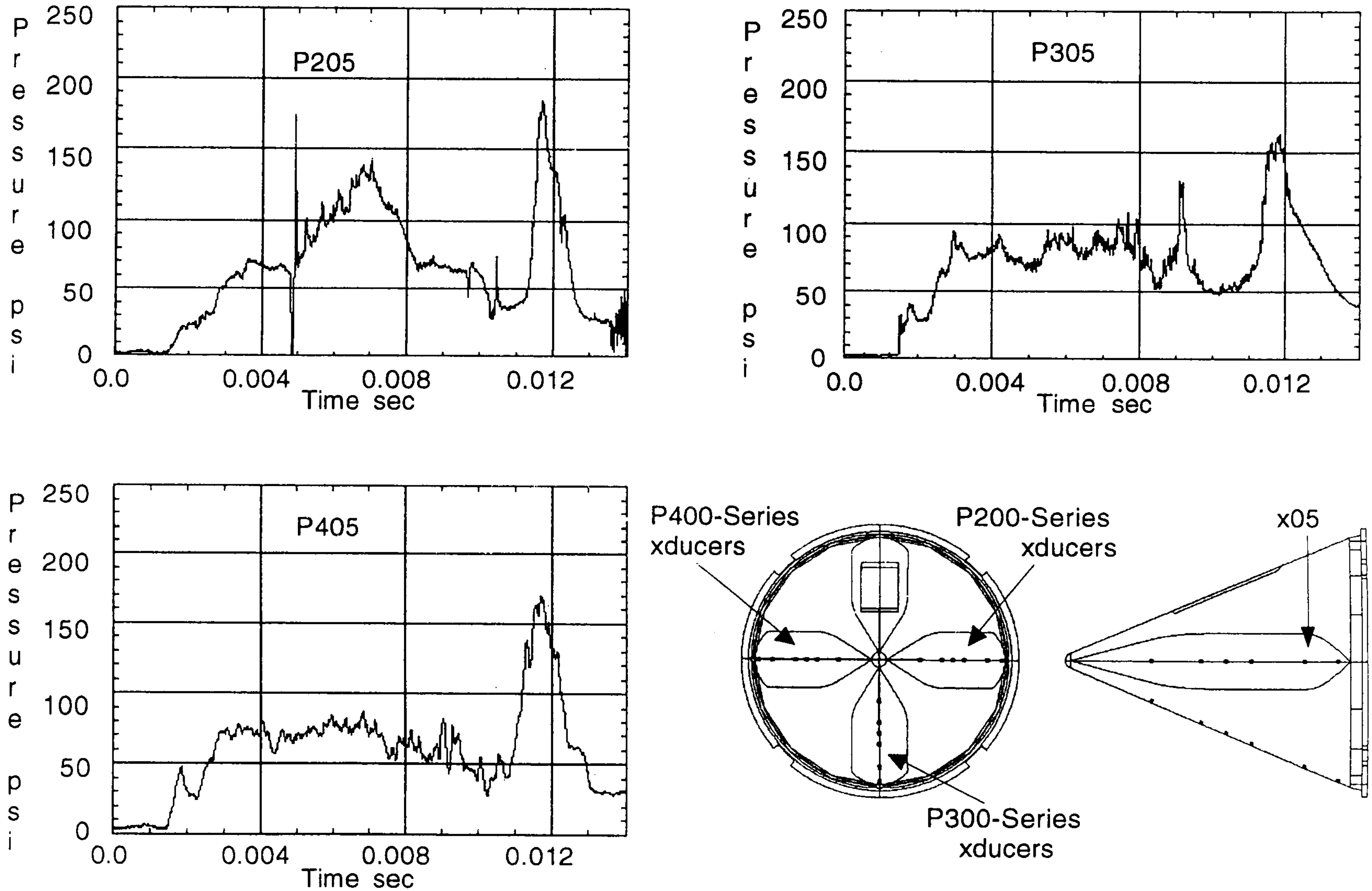


Figure 10. Continued

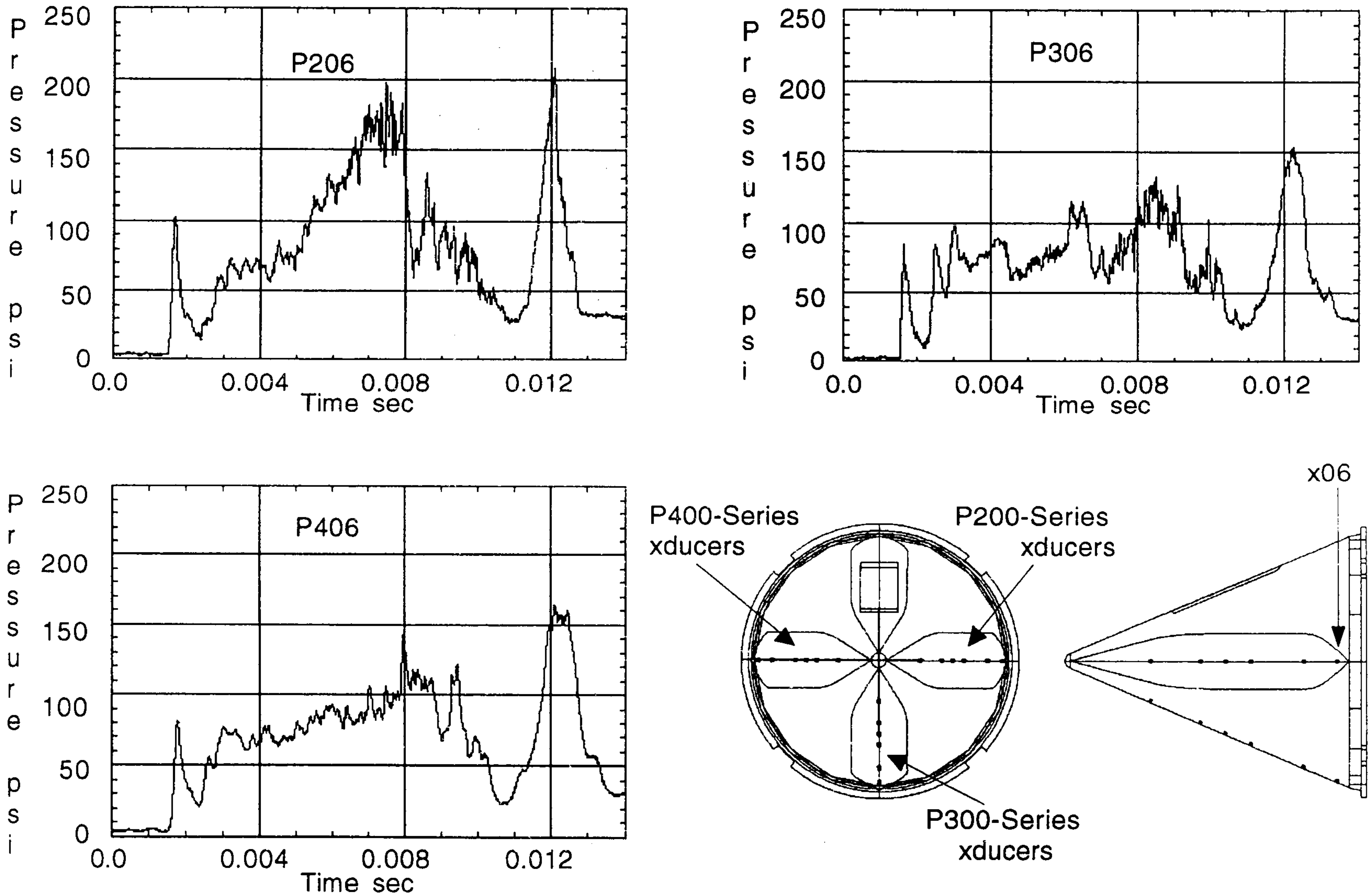


Figure 10. Concluded

first assumption made was that the bow shock remains upstream of the shroud. This is important for describing the properties of the flow filling the cavity, which were now assumed to be those of fluid downstream of a normal shock. Mass flow into the cavity is defined by the product of the density, velocity, and capture area at the mouth of the shroud (Figure 11). The simplification of the flow inside the shroud is now manifested by assuming the mass added to the internal volume of the cavity is uniformly distributed.

The instantaneous mass of the fluid within the cavity is simply calculated by multiplying the mass flow by the time elapsed since nosecap deployment. From this information, the instantaneous density is simply the instantaneous mass divided by the cavity volume. It then follows that the instantaneous pressure throughout the cavity is the product of the density, the fluid gas constant and the static temperature (Figure 11).

At the same time, external flow about the shroud causes static pressures on the petals which temporarily hold the shroud petals together while pressure is building inside. The static pressure on the petal external walls is calculated using a wedge oblique shock solution from the free stream conditions, according to petal angle. The wedge solution was assumed over the cone solution because at the initial angle of 13 degrees, the difference in solutions is relatively small, and after rotation begins, the cone effectively goes away, breaking up into four individual wedge-like petals.

The forces acting both internally and externally on the petals are calculated by multiplying the surface static pressures by the surface areas. The resultant forces are assumed to act at the centroid of the petal surface areas. A moment arm extending from the

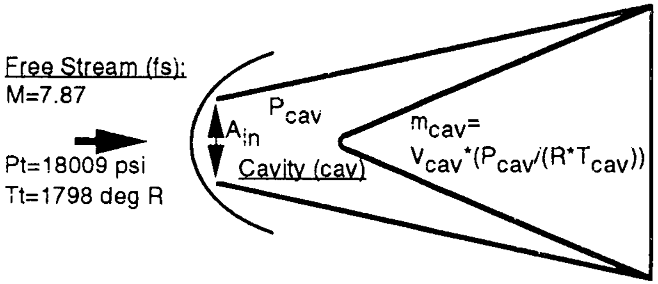


a. Initial Condition (t=0)

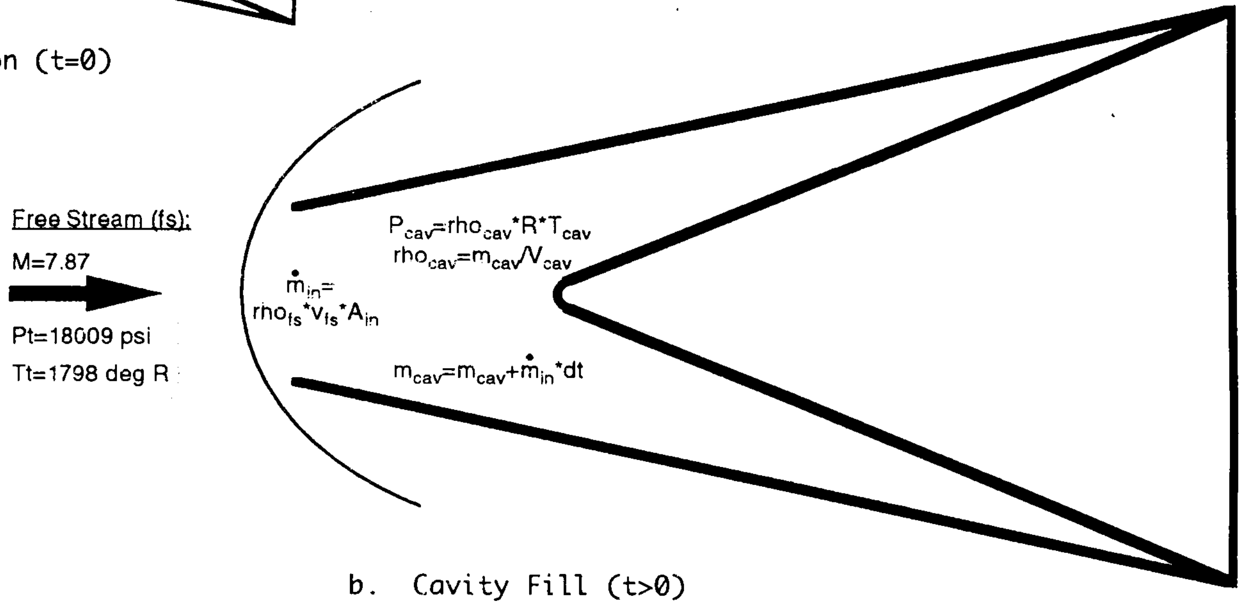


b. Cavity Fill (t>0)

Figure 11. Cavity Flow Properties Description

petal hinges to the petal centroids multiplied by the pressure forces reveals the opposing moments about the petal hinge. When the moment about the petal hinges caused by the pressure forces within the cavity becomes greater than the moment caused by the external pressure forces, the petals begin to rotate away from the forebody (Figure 12).

Petal angular acceleration is determined by dividing the sum of the moments about a petal's hinge by the petal moment of inertia about the hinge. Moments of inertia about the petals' hinges and about their centers of gravity (used to describe petal motion after unhinge) were provided by MDSSC.

As petal motion continues, gaps between the petals widen, allowing the mass trapped in the cavity to escape. Mass flow through the gaps is assumed to be choked in the plane of the gap defined by the shortest distance between any two petals (Figure 12). The bow shock is assumed to continue to stand upstream of the cavity opening until the mass flow into the cavity equals the mass flow escaping through the petal gaps. At the time the entering and exiting mass flows become equivalent, a moving normal shock is assumed to be positioned in the plane of the shroud petal tips (the most upstream shroud cavity opening - Figure 7).

## Vent and Travel

Two methods were investigated to attempt to describe the shock motion as it travelled downstream within the cavity. The first method ran under the assumption that the pressure of the fluid in the cavity between the plane of the shock front and the base of the

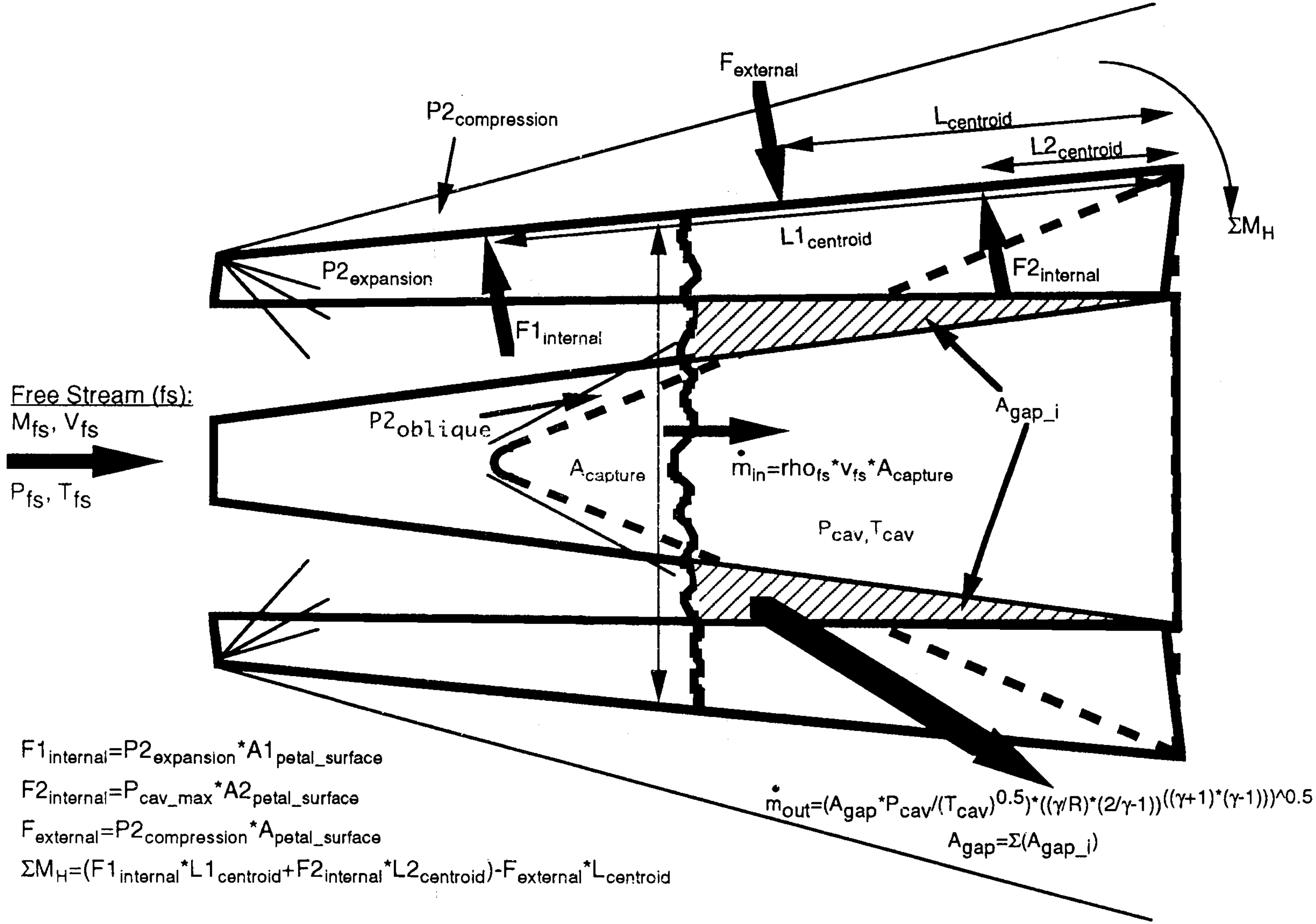


Figure 12. Petal Rotation Description

petals/tetracone remained constant as the shock moved. Shock motion was therefore determined by establishing where the shock front would have to be located for a given set of cavity conditions and petal angle in order to maintain the constant pressure.

The second method determined shock motion by establishing where the shock front would have to be to maintain an entering to exiting mass flow ratio of one. In both cases, the entering mass flow is determined from the fluid properties entering at the shock front plane, and the exiting flow is determined by the fluid properties venting through the petal gap areas downstream of the shock front plane.

Pressures on the forebody are assumed to be equal to the shroud cavity pressure while the shock is upstream of the forebody nose. As the shock front travels along the forebody, the pressures upstream of the front are assumed to be the static cone surface pressure for a 23 deg (half-angle) cone exposed to the free stream. Pressures downstream of the shock front are assumed to be the pressure of the fluid in flux between the shock front and the base of the petals/tetracone. Pressure on the forebody in the immediate vicinity of the shock front is assumed to be the total pressure downstream of a normal shock calculated from the free-stream conditions with an adjustment to Mach number to account for the shock's velocity (Figure 8).

During shock motion within the cavity, petal motion is now calculated with a consideration for the different pressure forces applied to the petal surface areas. First, for each incremental angle, the external pressure force is re-calculated (using a wedge solution as indicated earlier). Initially the flow is compressed over the petals' external surfaces, however after the petals pass through the horizontal plane, a Prandtl-Meyer expansion must be assumed and calculated as was shown in Figure 5.

The internal pressure on the petals downstream of the shock front are assumed to be the pressure of the fluid in flux between the shock front and the base of the petals/tetracone. The internal pressure on the petals upstream of the shock front is calculated as was the pressure on the petals' external surfaces, with expansion giving way to contraction as the petals rotate through the horizontal plane (Figure 5).

An instantaneous restraining moment about the petal hinges is calculated from the varying external pressure forces in the manner mentioned earlier. The liberating moment about the petal hinges is calculated from a sum of the moments generated by the internal pressure forces on either side of the shock front. Instantaneous centroids of the internal petal surface areas are calculated to determine the moment arms from the petal hinges to the assumed centers of pressure (Figure 12).

The petal hinges were designed to release at a specific petal rotation angle (Cayse [5]). Following petal release, the radial motion of the petals away from the forebody is calculated according to the differential pressure forces acting in the radial direction. As separation occurs, the additional gap area now developing between the base of the petals and the base of the tetracone is calculated as a growing annulus.

The event is concluded when the shock front plane crosses the base of the tetracone forebody (FS100).

# CHAPTER IV

# CODE DEVELOPMENT

To put in practice the concepts associated with what we will now call the moving shock theory, a FORTRAN computer code was written. Many challenges confronted the author in writing the code. The details of the methods used follow.

## Geometry

The most important foundation for the computational description of the shroud separation event was an accurate shroud/forebody geometry model. The ultimate goal was (is) to develop a code which can easily be adapted for various geometries. For the purposes of this experiment, however, it was important to use a specific benchmark to most accurately recreate the event in question. Therefore, the design details of the full scale HEDI wind tunnel model (used in the NSWC Tunnel 9 ground test (Cayse [5])) were used as the basis for the code to best produce data comparable to HEDI ground/flight tests.

To model the tetracone forebody, equations provided by N. Rajendraw of SAIC were used which described quarter sections of the tetracone as a function of axial location. A typical tetracone quarter profile (and its defining equation) is presented in Figure 13. To model the four identical shroud petals, details regarding

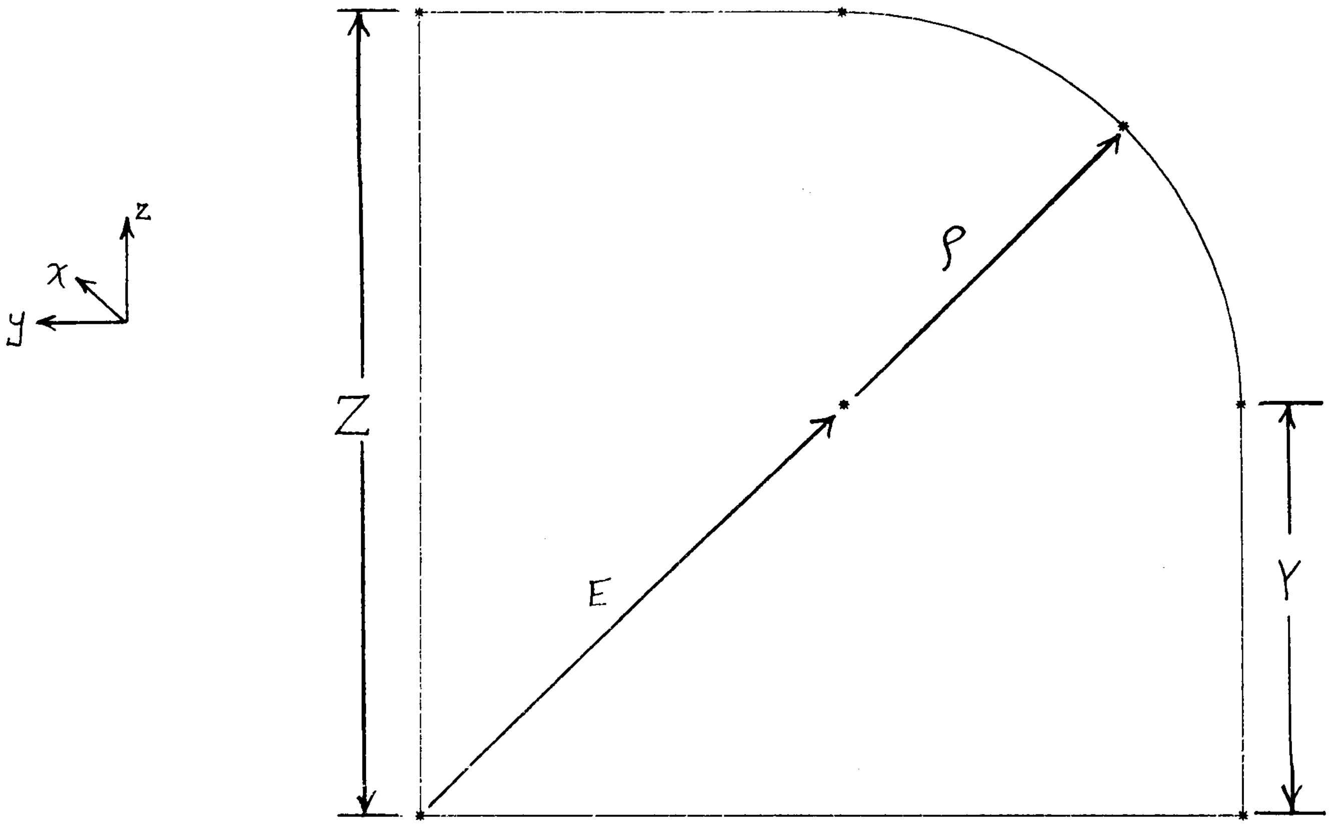


$Y = Const. * f(x)$ $Z = x * \tan(\mu)$

$\mu = 23°$ $\rho = Z - Y$ $E = Y * 2^{0.5}$

Figure 13. Typical Tetracone Quarter Section Profile at Station x.

specific petal profile dimensions were extracted from drawings provided by MDSSC. A typical petal profile is presented in Figure 14.

An attachment point representing the hinge axis between the base of the petals and the base of the tetracone forebody was defined as flight station (FS) 100. FS 100 is a basic point of reference used throughout the geometry development within the code.

With the basics of the hardware geometry defined, the specific flow areas and volumes could be calculated. To calculate a capture area, the instantaneous petal rotation angle was combined with the instantaneous shock position to arrive at a cross section of captured flow within the petals. By determining a radius from the axis of symmetry to a rotated petal's interior surface in the plane of the moving shock front, and by determining the gap distance between petals in the same plane, the captured flow cross section was calculated. If the tetracone was present in the plane of the shock, its cross sectional area at that position was calculated and subtracted out to obtain the total flow area (Figure 9).

The volume used for determining the properties of the fluid contained in the cavity downstream of the shock front was calculated by performing a numerical integration of flow cross sections from the shock location to the base of the model (FS 100). Integration proceeded by making incremental steps from the shock front plane back to FS 100, calculating the flow area cross sections at each step using the method described above. Each area was multiplied by the axial step distance to give an incremental volume, then all volume increments were added to reveal the total integrated volume downstream of the shock front plane.

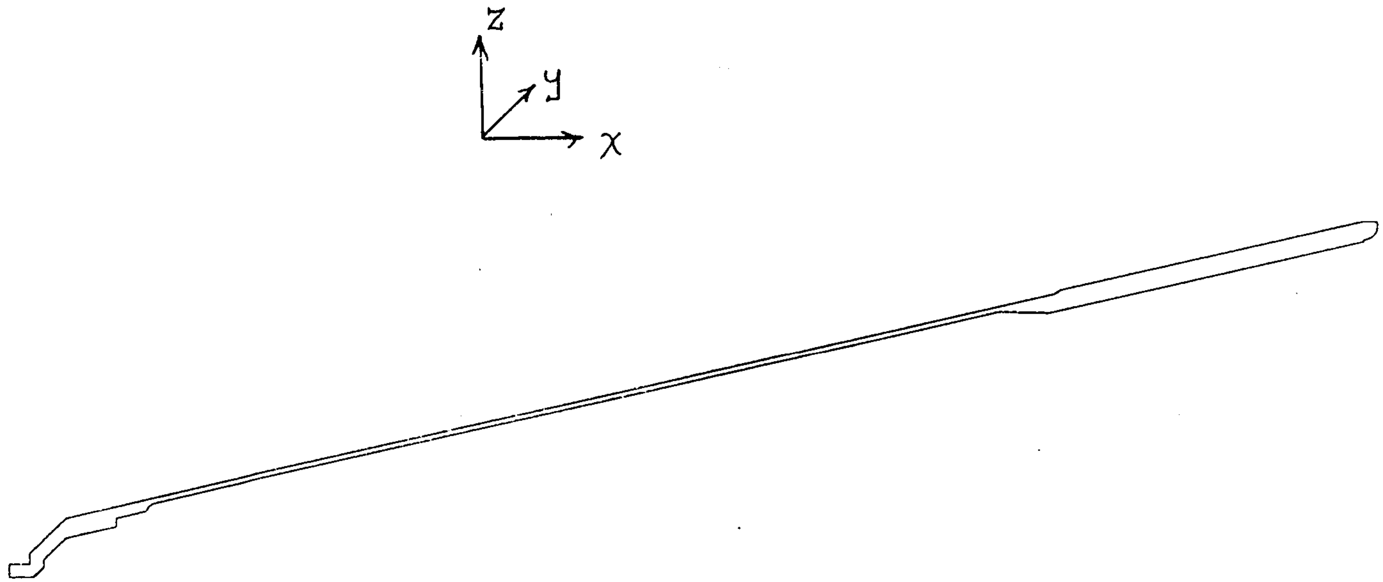


Figure 14. Typical Shroud Petal Profile

The results of flow area cross section calculations from petal tip to base for selected petal angles are presented in Figure 15. The area under each curve is of course the representative captured volume. Geometry development equations are presented in the Appendix.

## Description of Code

The code written is called "SHRDSEP". A flow diagram outlining its major functions, the subroutines called, and its method of progression is presented in Figure 16. Fluid equations are presented in the Appendix.

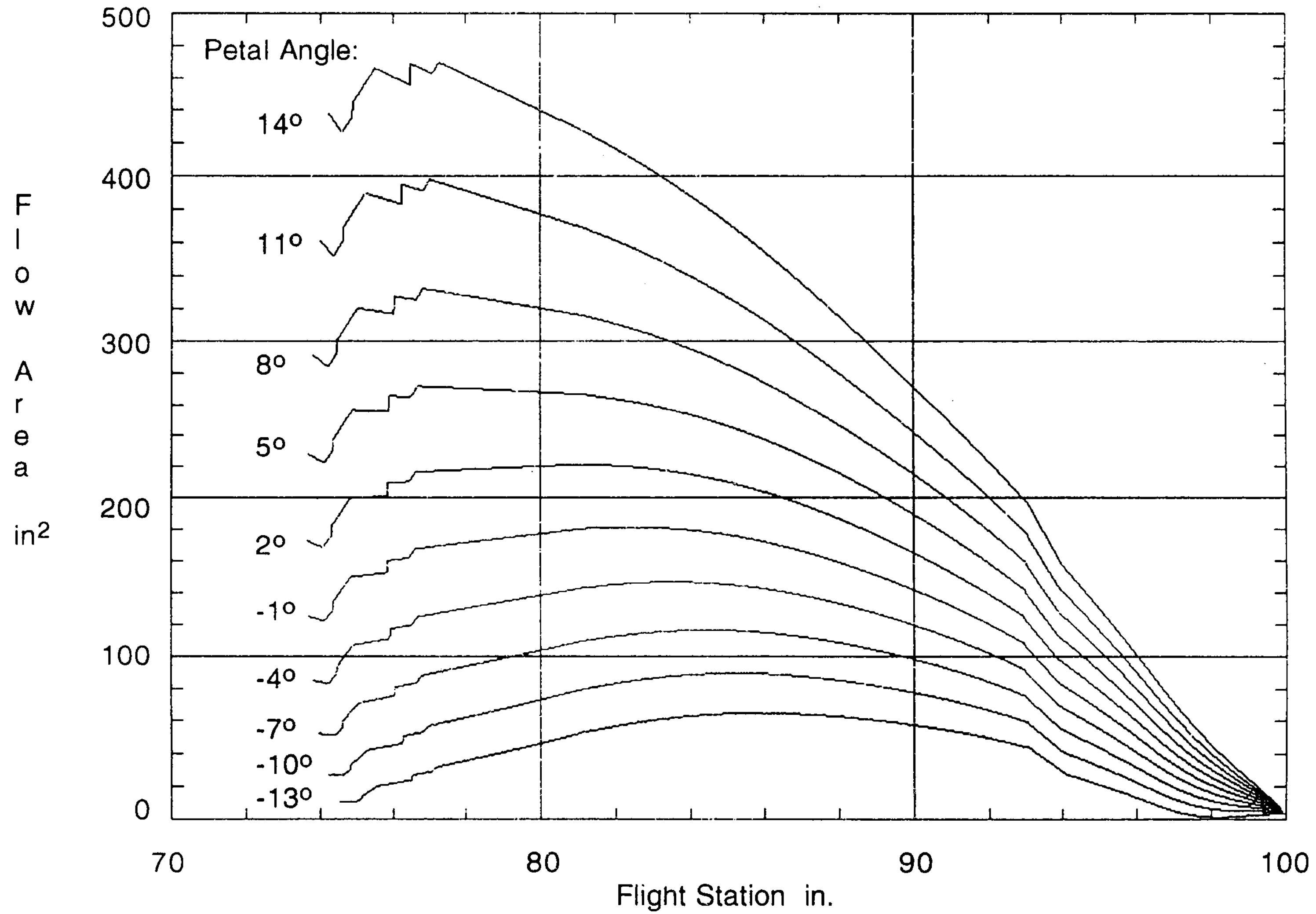


Figure 15. Axial Flow Cross Section Within Opening HEDI Shroud Petals

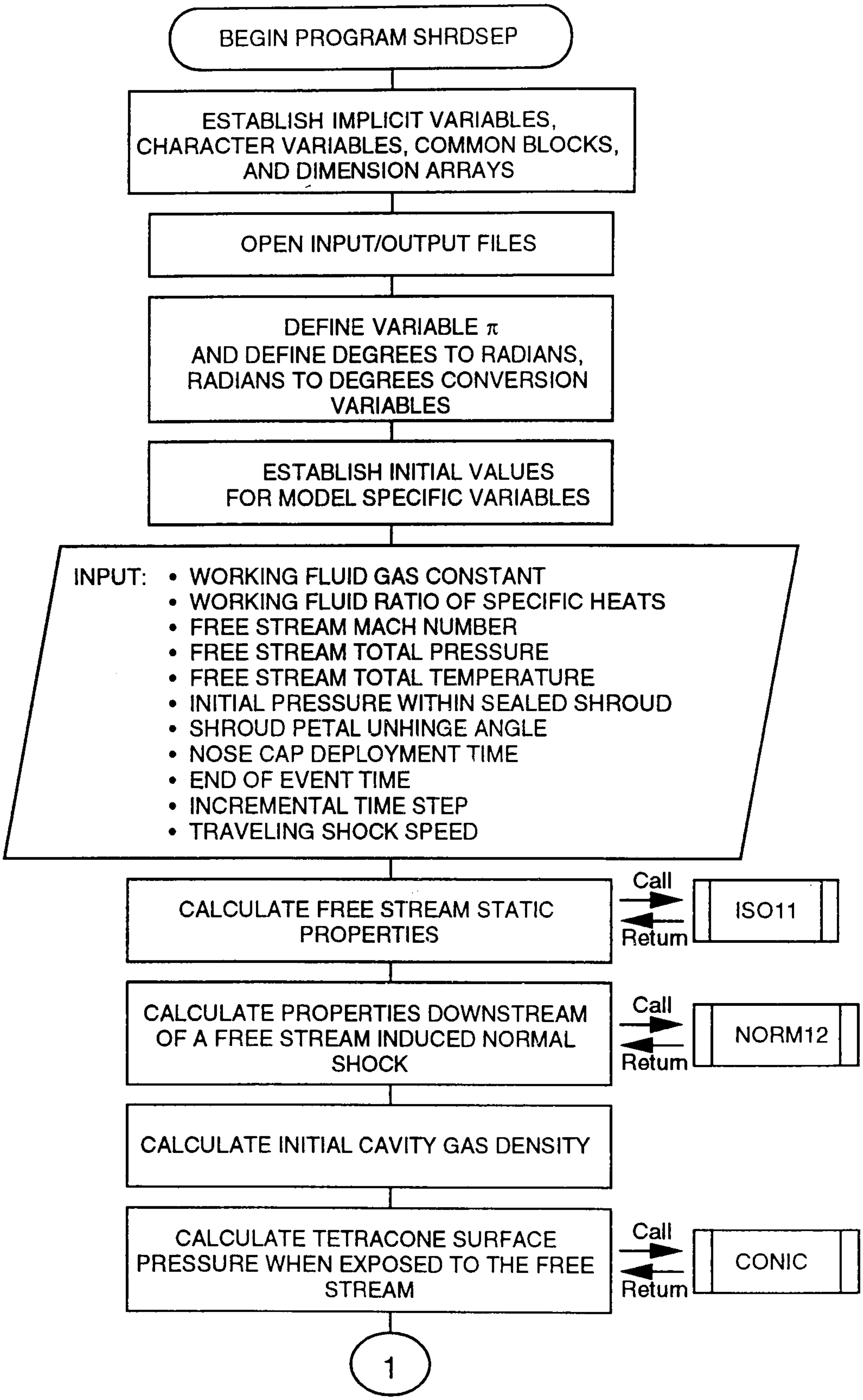


Figure 16. SHRDSEP Flow Diagram

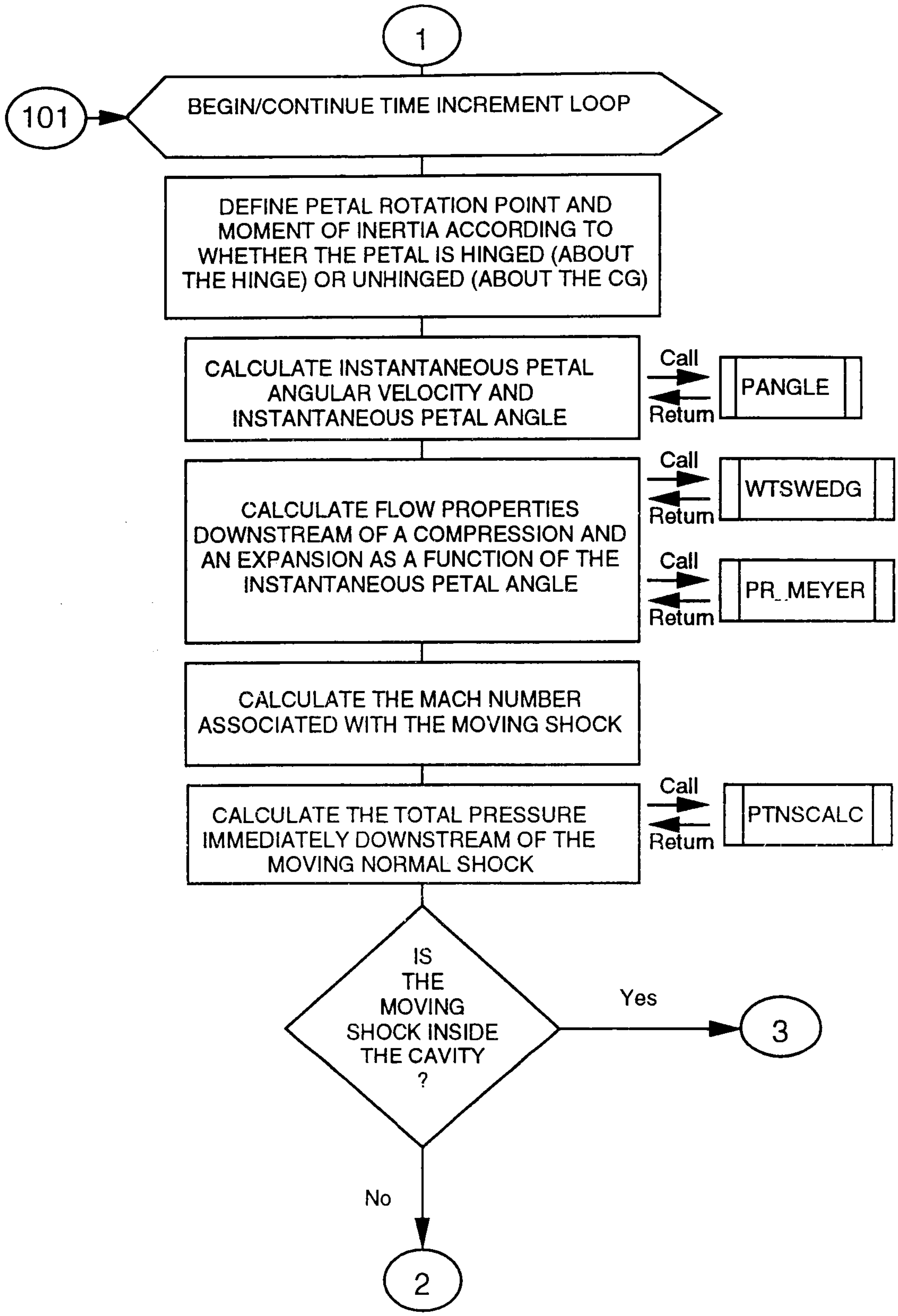


Figure 16. Continued

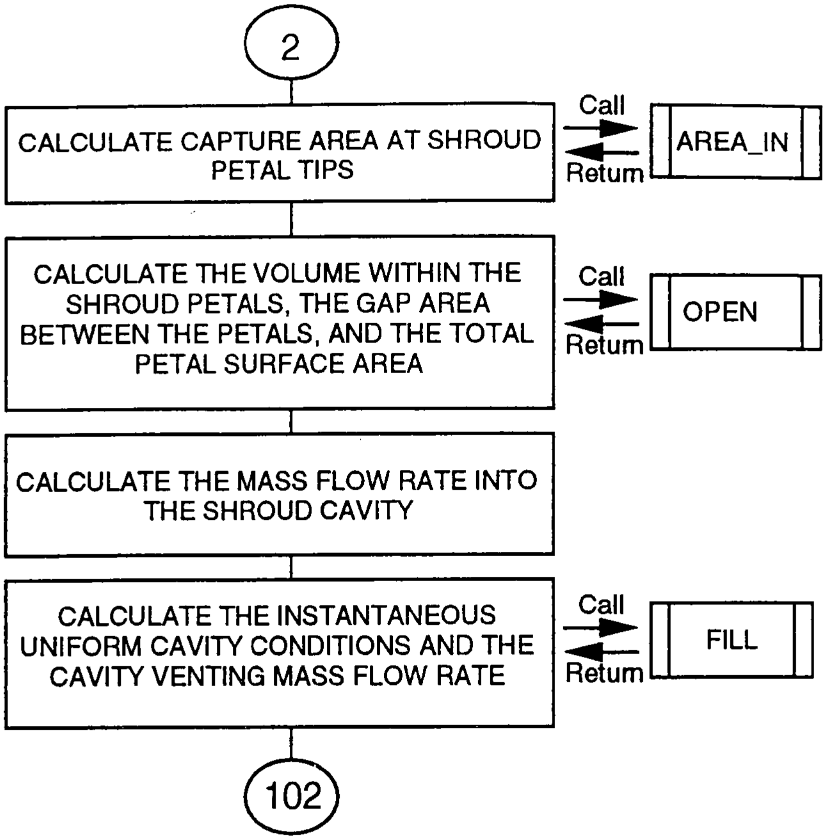


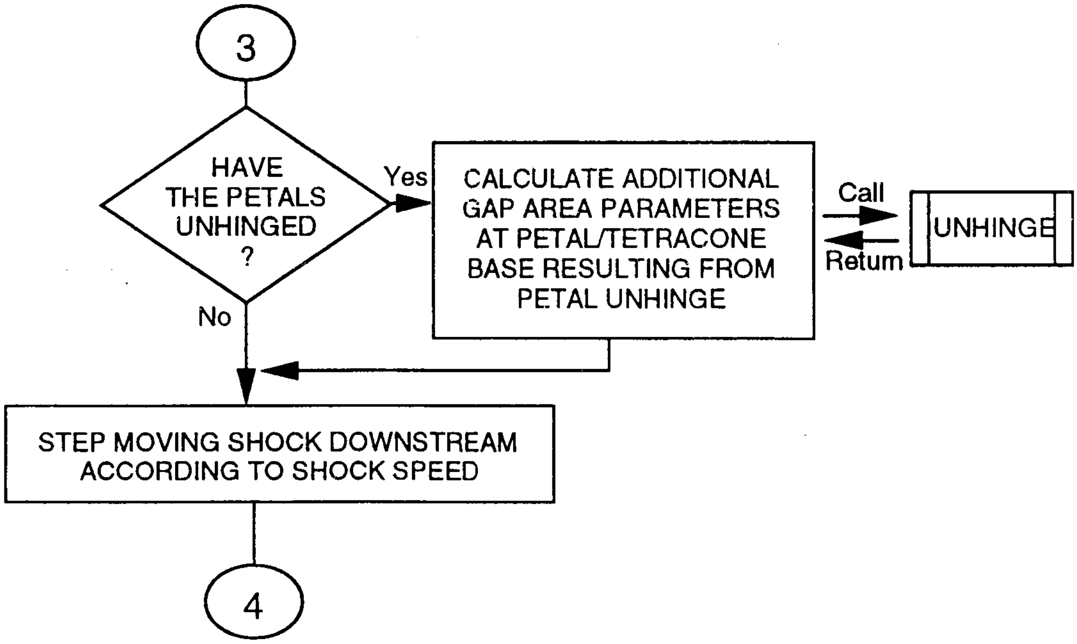


Figure 16. Continued

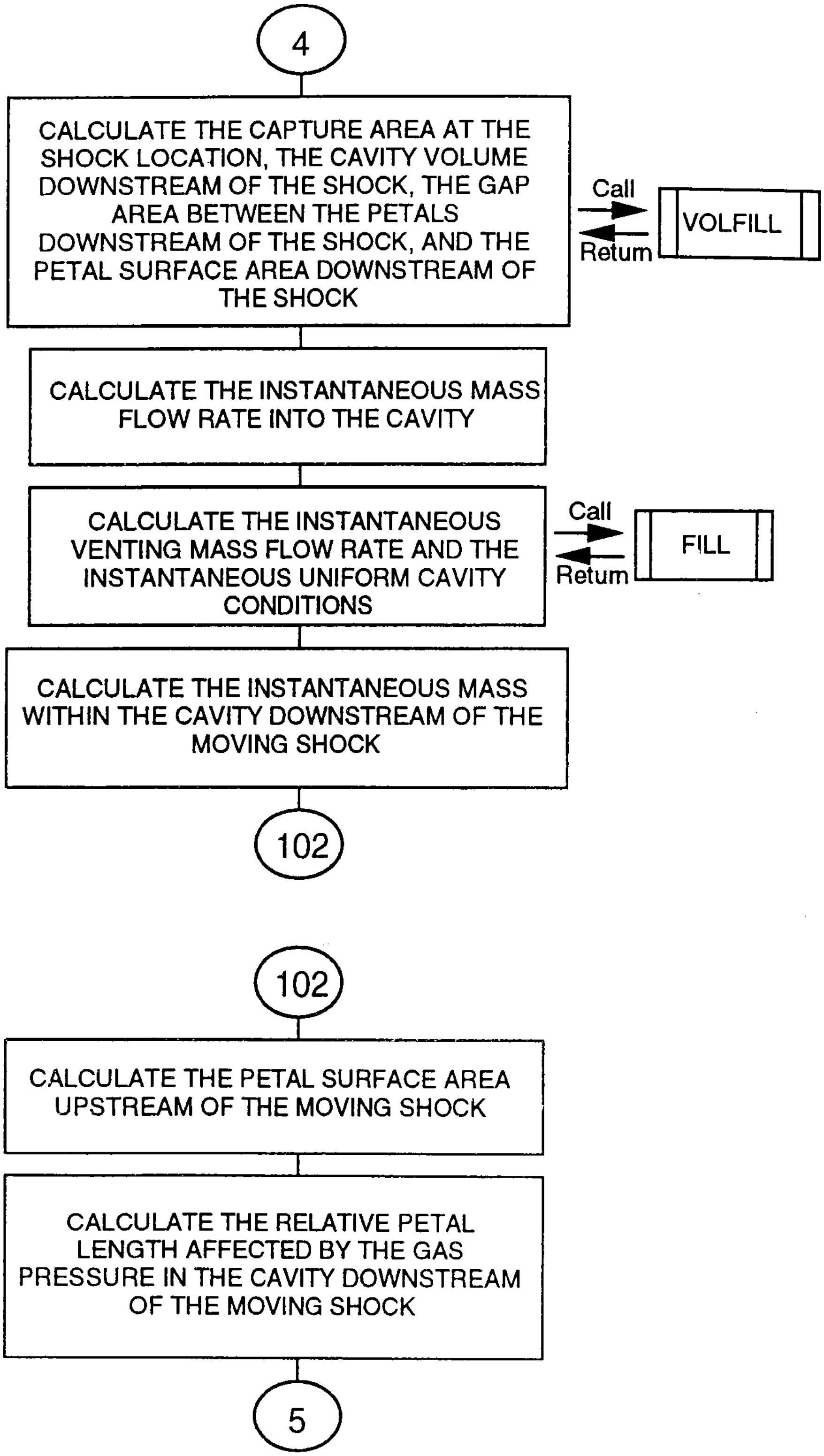


Figure 16. Continued

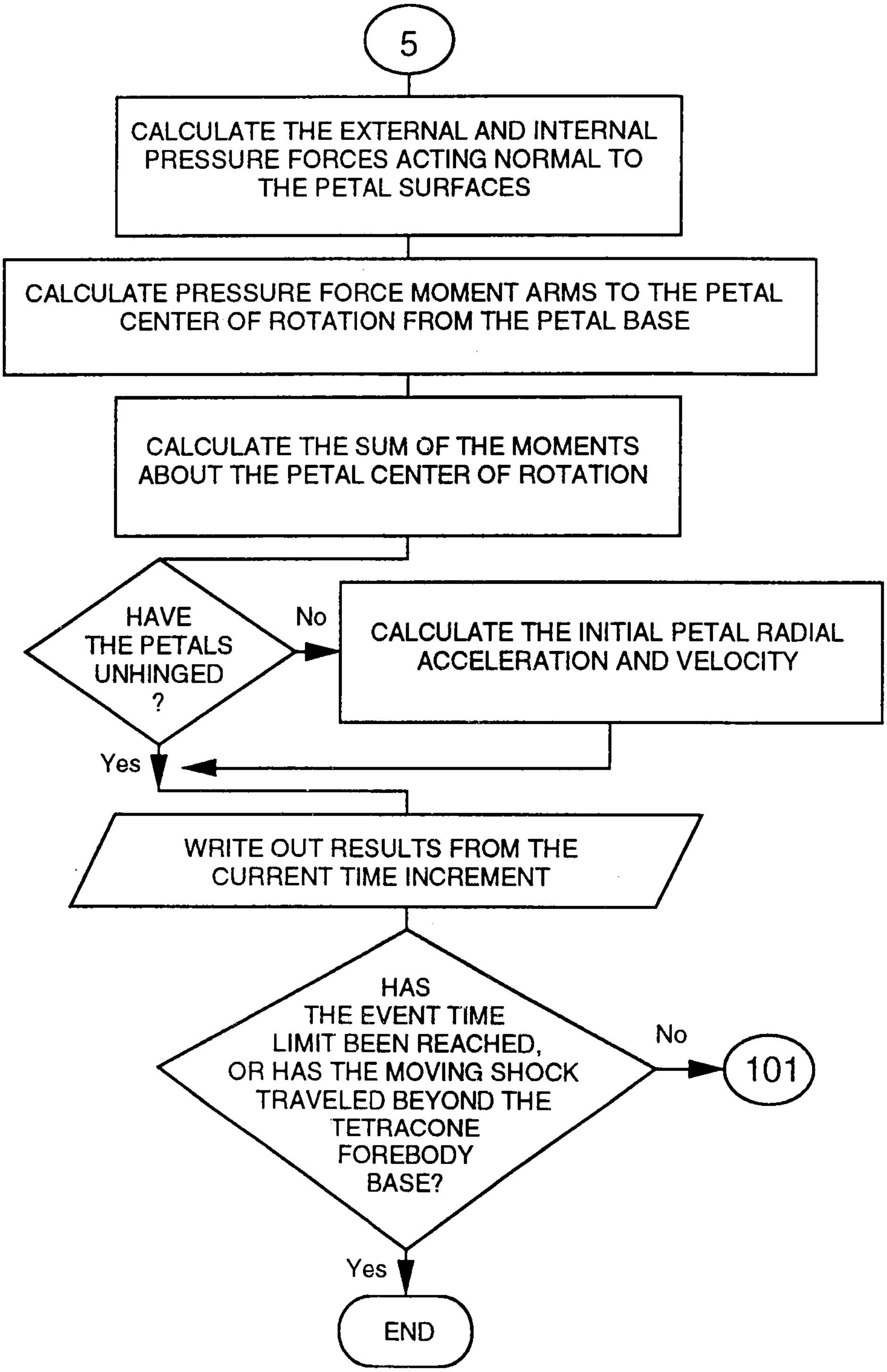


Figure 16. Continued

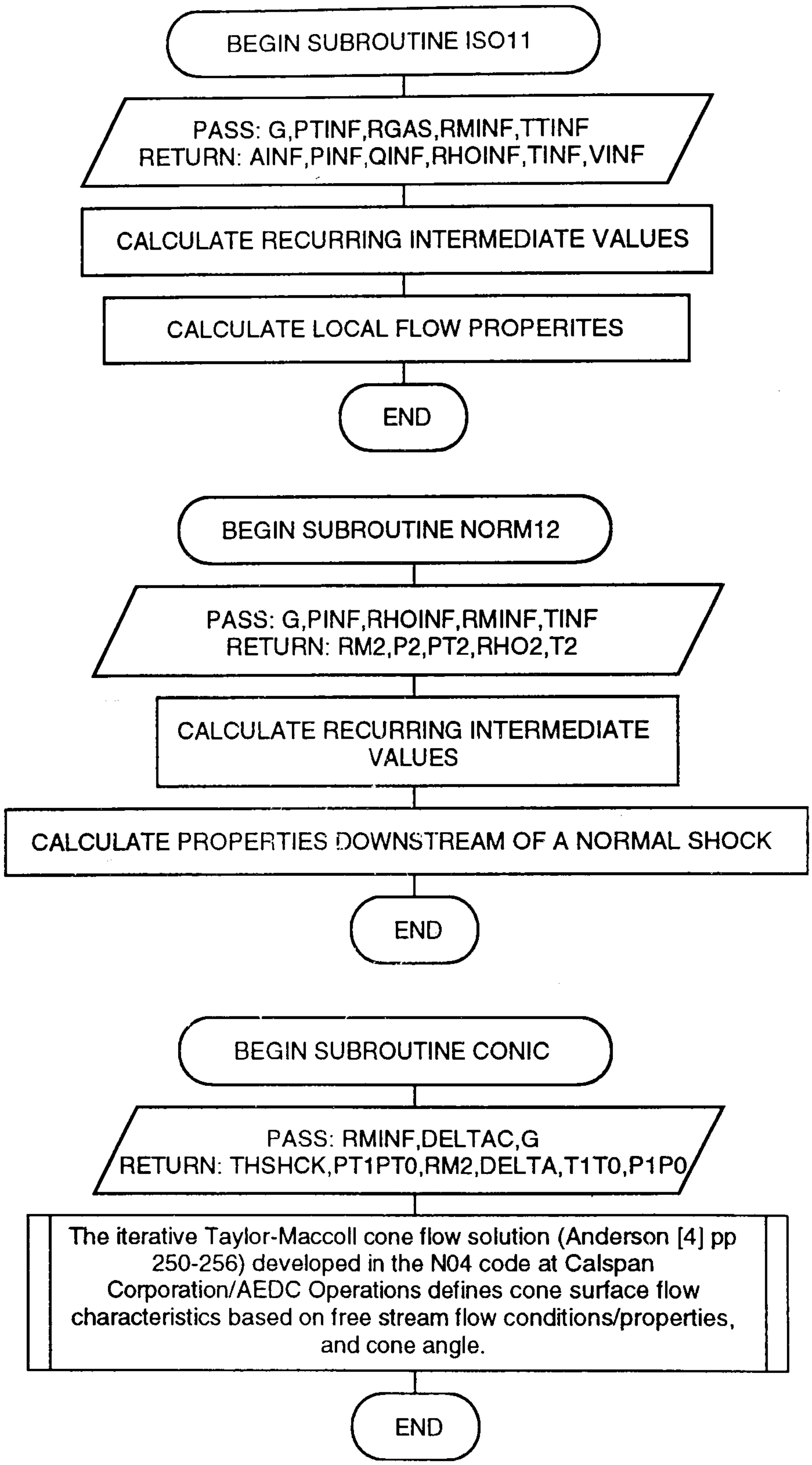


Figure 16. Continued

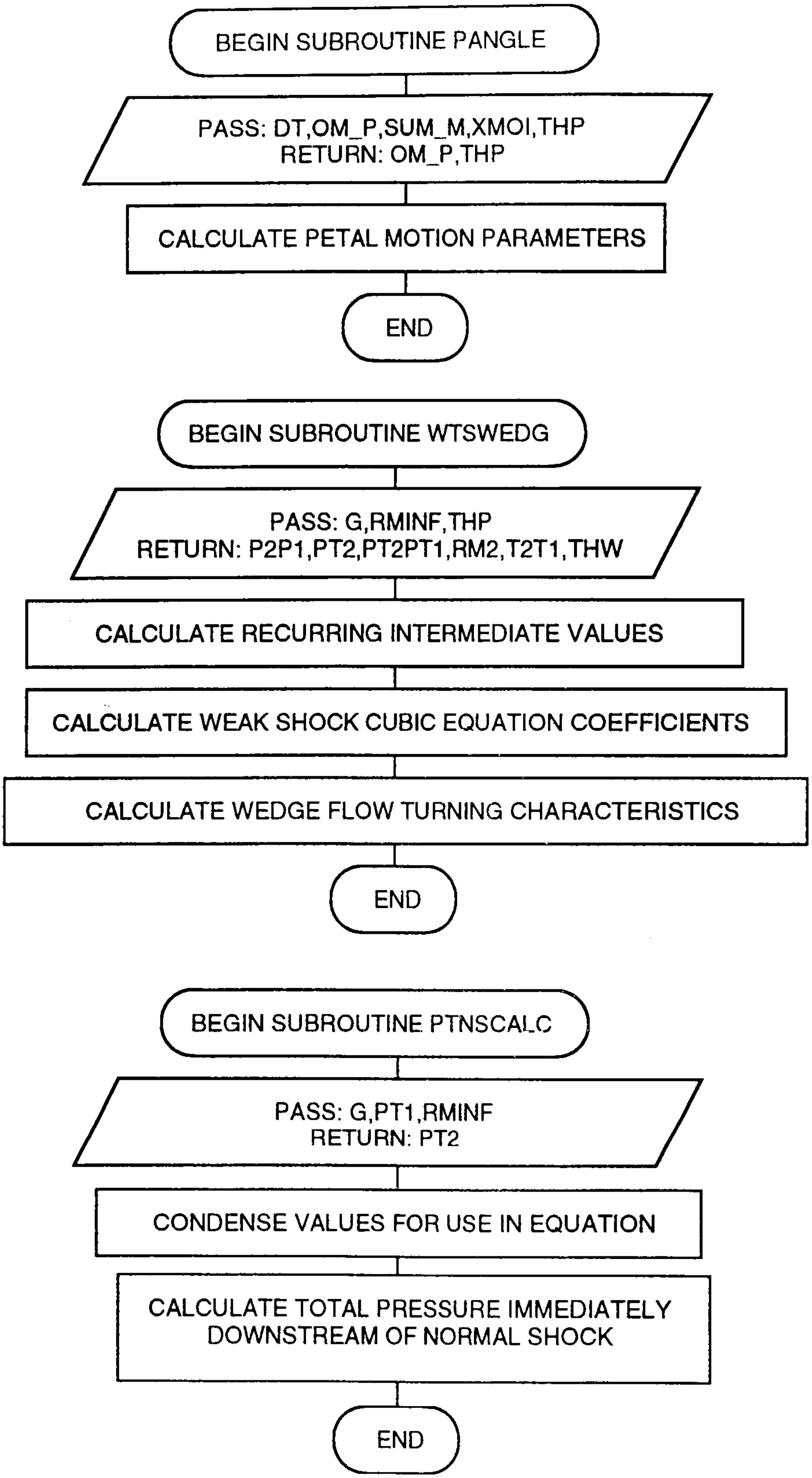


Figure 16. Continued

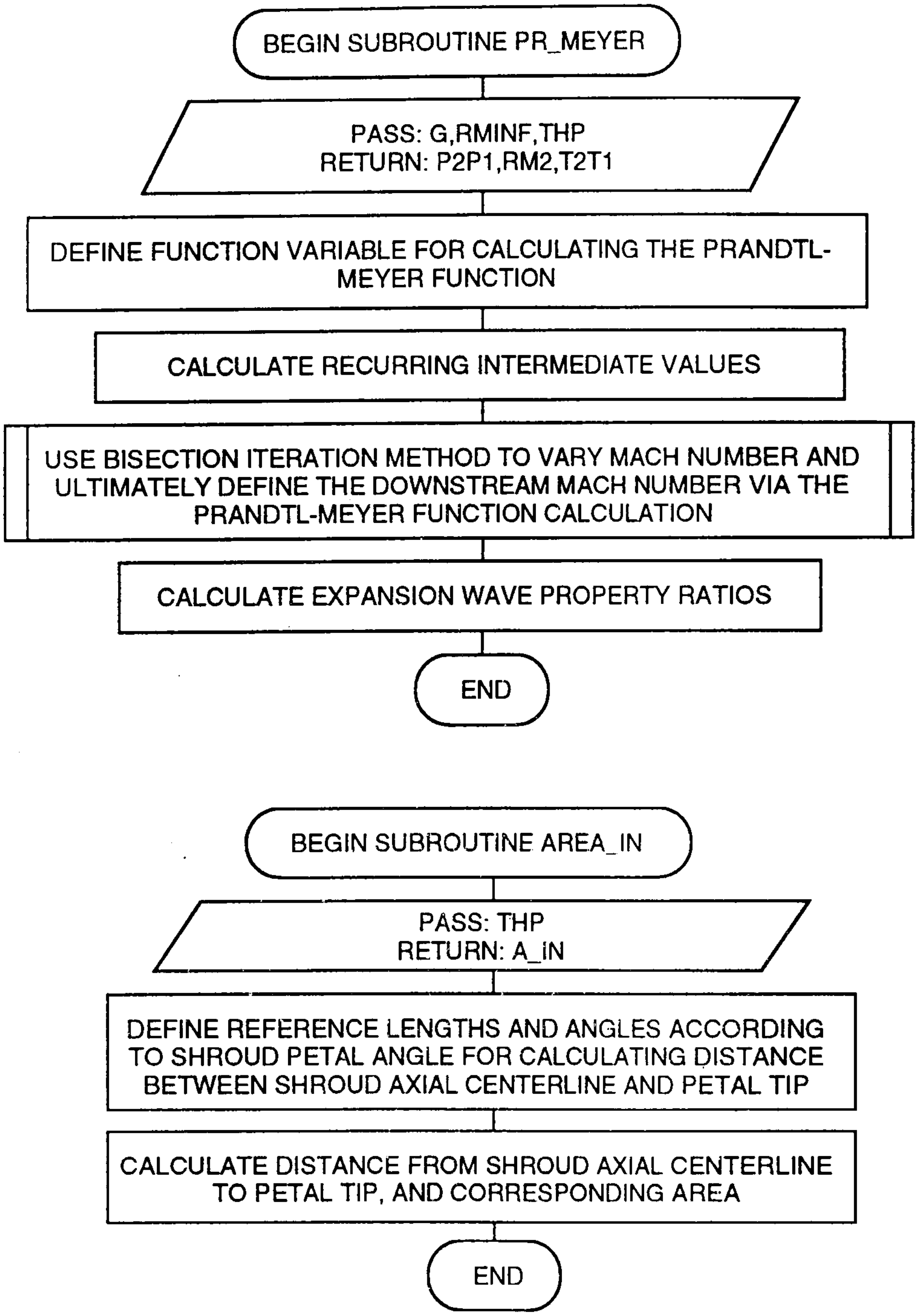


Figure 16. Continued

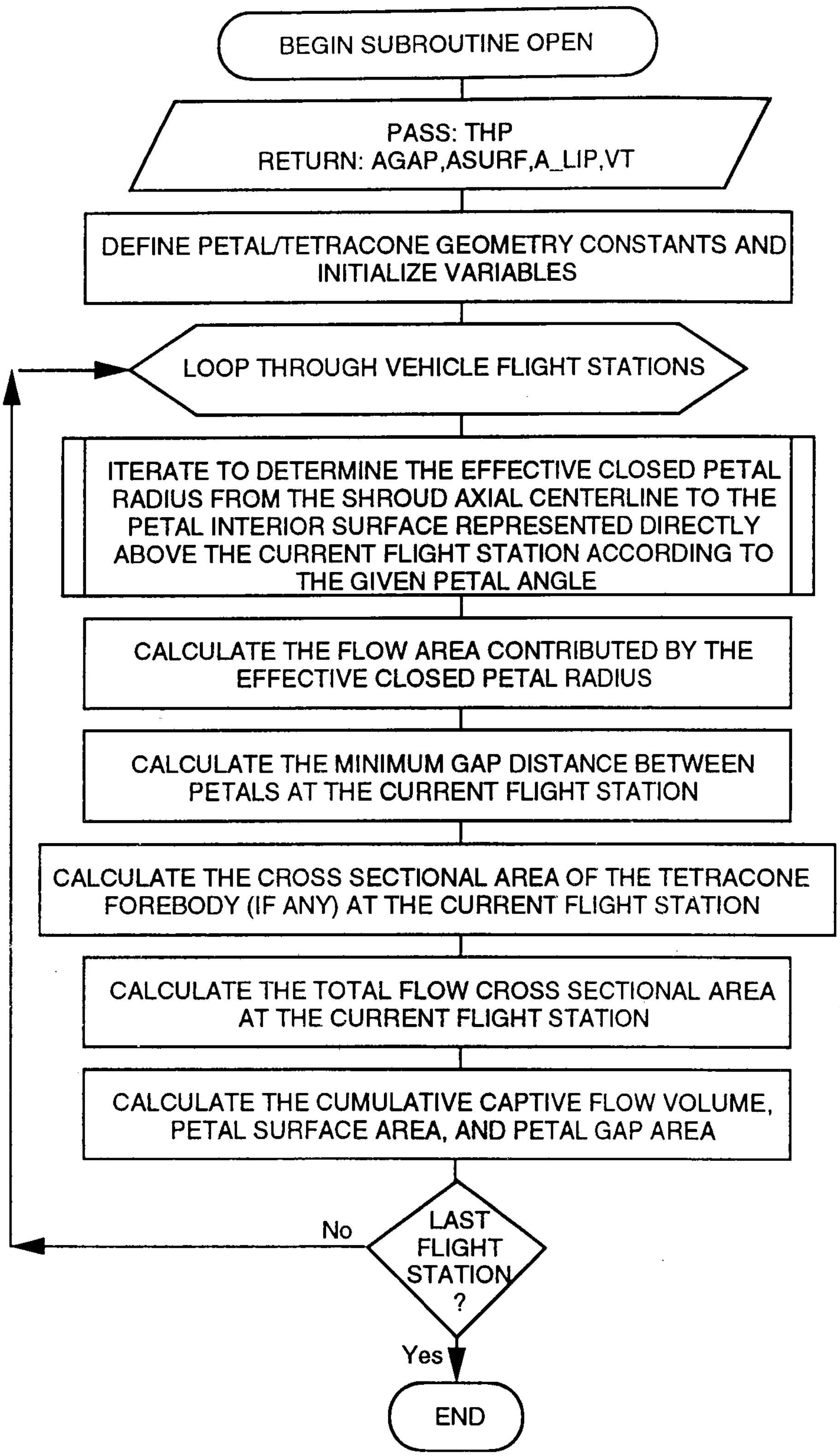


Figure 16. Continued

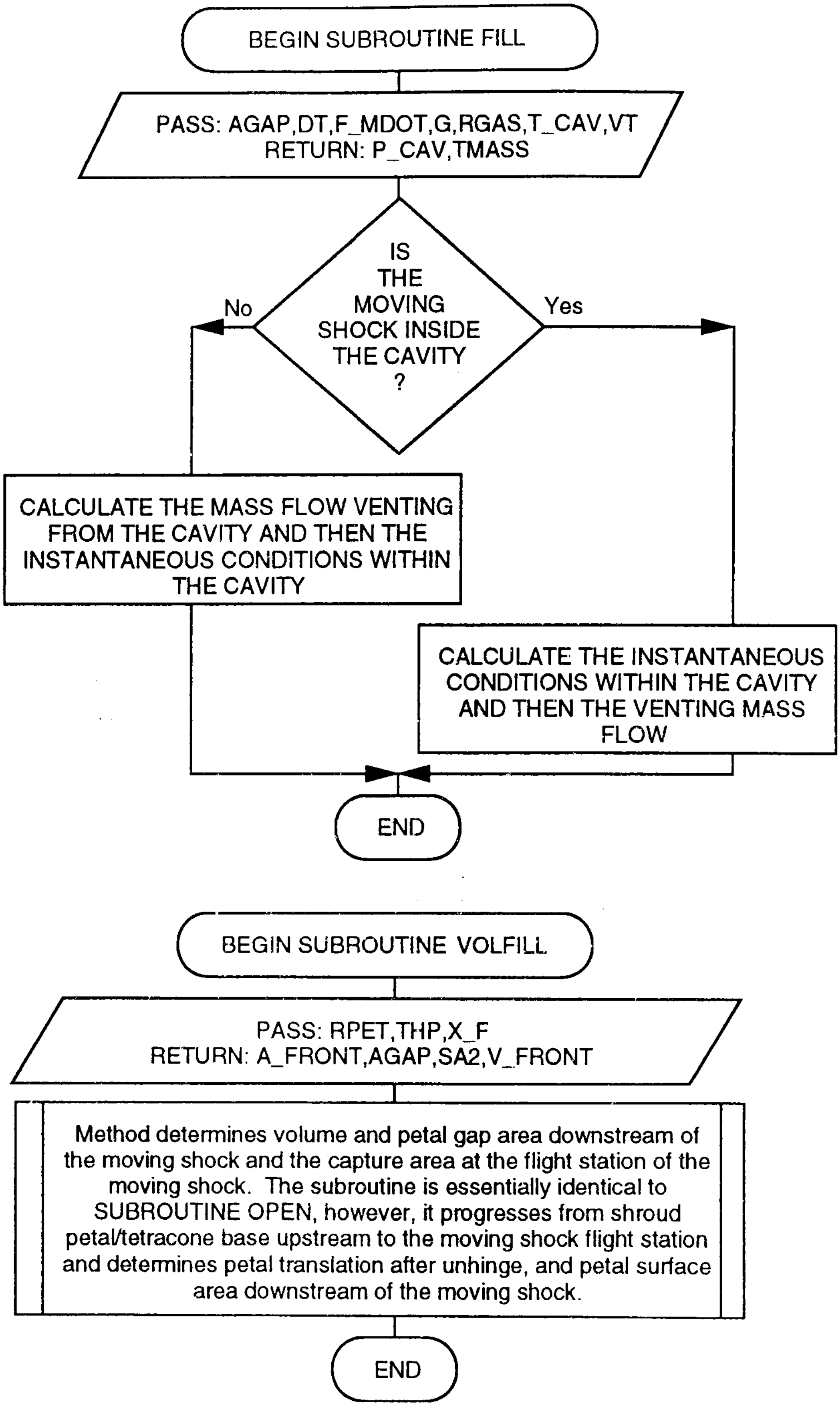


Figure 16. Continued

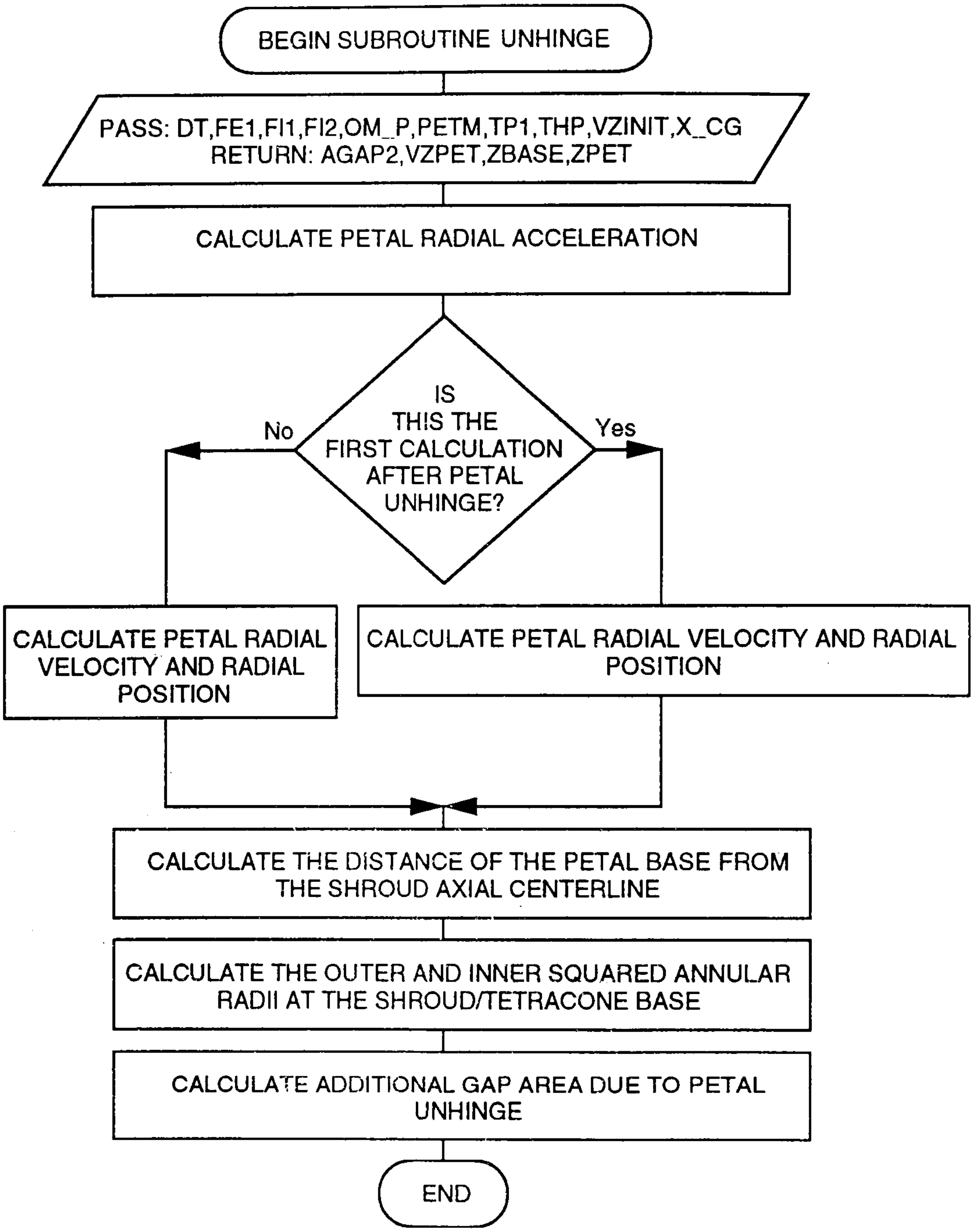


Figure 16. Continued

CHAPTER V

# DISCUSSION OF RESULTS

The original intent of the development of the program was to obtain a first order design tool for predicting the pressure histories and petal motions for shrouded seeker interceptor designs similar to the HEDI design. To truly accomplish this goal, it would be necessary for the program to independently determine the shock motion characteristics based on some controlling phenomenon. An exhaustive attempt was made to characterize just such a phenomenon within the scope of this investigation. A brief description of the methods attempted follows:

1. The pressure in the cavity is allowed to build and vent with the capture area remaining at the petal tips until the fill/vent mass flow ratio becomes less than 1. At this time the fill period cavity pressure has peaked.

   Shock motion through the cavity now begins at the petal tips. Traveling shock position is determined by assuming the pressure trapped downstream of the shock front remains constant at the fill period peak value. In order to meet this criteria, the shock must be moved downstream as the petals continue to open, thus defining the shock speed.

   The problem with this approach was that it created a ramp up to a constant pressure which remained until pulse passage at a specific axial location. Additionally, the speed of the shock was relatively slow and resulted in low peaks for the pressure pulses.

2. Cavity pressure is again allowed to build until the fill/vent mass flow ratio reaches 1. At this time, the shock front is positioned at the shroud petal tips and the mass flow ratio is held constant at 1. To meet this criteria, the shock front is advanced to account for the increasing petal gap area.

   Unfortunately, the pressure within the cavity begins to taper off causing the venting mass flow rate to taper off. Combine this with the ever growing capture area allowing increased mass flow in, and the program reaches a point where it marches the shock front back upstream to maintain the balanced mass flow ratio.

3. A hybrid program was investigated which took the approach of (2) above. However, shock motion downstream was continued only while the motion was in the downstream direction (for a finite interval of time - user specified), at which time a shock speed was calculated. The calculated shock speed was held constant from then on.

   Mixed results were obtained from this approach, none of them were ever very satisfactory. Additionally, the approach was simply experimental and had no real physical basis.

The program developed and described was pursued then to verify the theory that the tetracone forebody pressure histories and the shroud petal motions could be the result of a pseudo normal shock traveling through the cavity as described. To accomplish this, empirical data from the comparison data set would have to be used.

## Ground Test Comparison

The program was run using the flow conditions from the HEDI NSWC Tunnel 9 Mach number 8 test. Specifically, the following inputs were specified for the ground test comparison run of the program:

| | |
|---|---|
| Working Fluid (Nitrogen) Gas Constant: | 1762.29 ft^2/sec^2-R |
| Working Fluid Ratio of Specific Heats: | 1.4 |
| Free Stream Mach Number: | 7.87 |
| Free Stream Total Pressure: | 18009 psi |
| Free Stream Total Temperature: | 1798 R |
| Initial Internal Cavity Pressure: | 3.73 psi |
| Petal Unhinge Angle: | -4 deg |
| Estimated Traveling Shock Speed: | 266.67 ft/sec |

To attempt to match the flow dynamics of the program with the ground test case, two empirical values from the ground test were incorporated. Specifically, the petal unhinge angle was obtained by analyzing the wind tunnel petal motion data to determine at what angle the petal motion characteristics changed, in general, for each petal. The result of the analysis revealed a value of -4 degrees, which is considerably different than the design value of 2 degrees. The speed of the shock traveling within the cavity was determined as discussed earlier by dividing the distance between the most upstream and most downstream pressure transducer by the elapsed time between their respective peak pressure pulse occurrences.

The results of the ground test comparison run are presented in Figures 17 and 18. Figure 17 compares the pressure histories calculated by the program at each of the six axial pressure transducer locations to the three transducer measurements at each axial location. Figure 18 compares the petal motion history

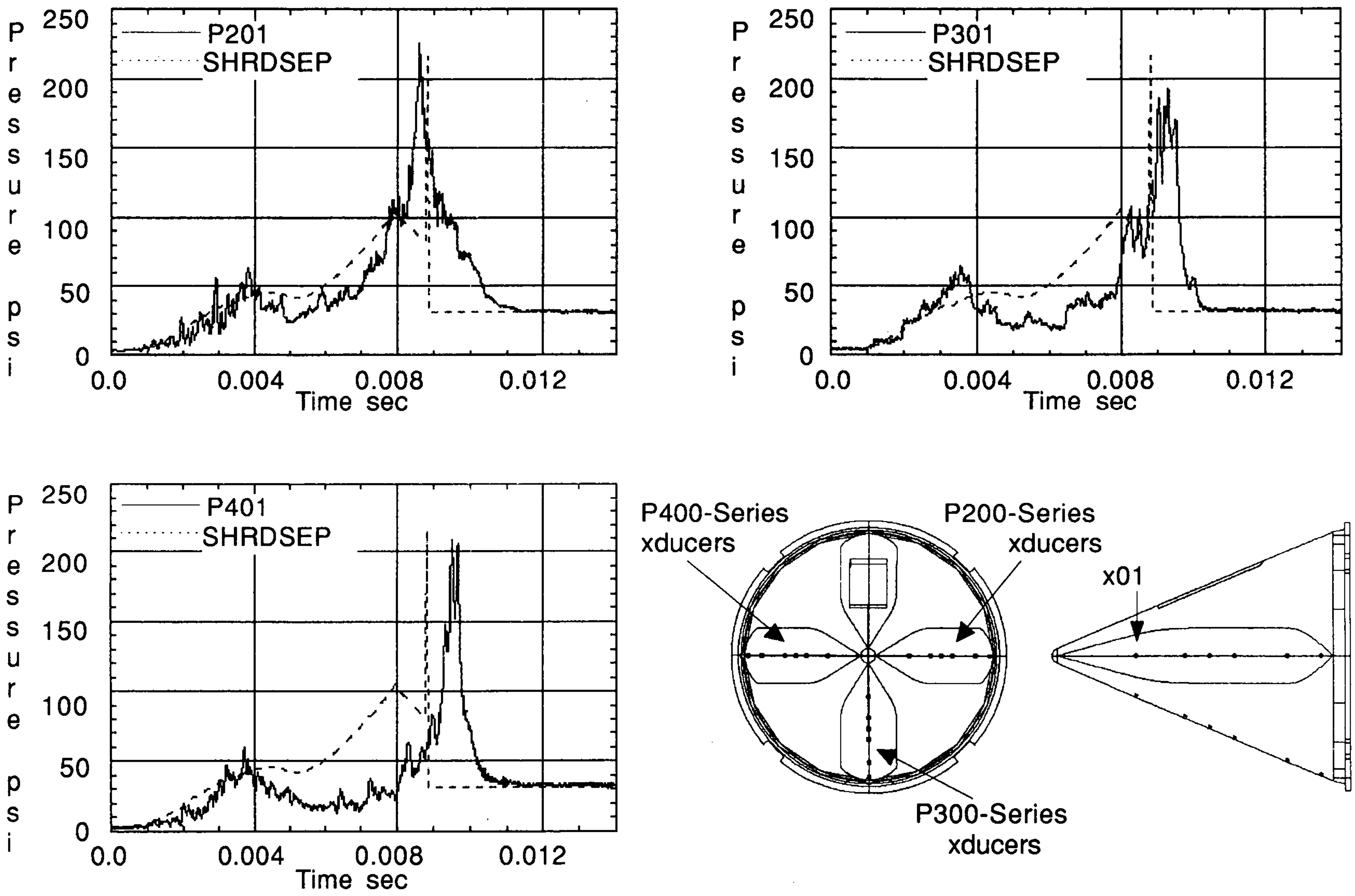


Figure 17. SHRDSEP vs HEDI NSWC Tunnel 9 Ground Test - Pressure Data

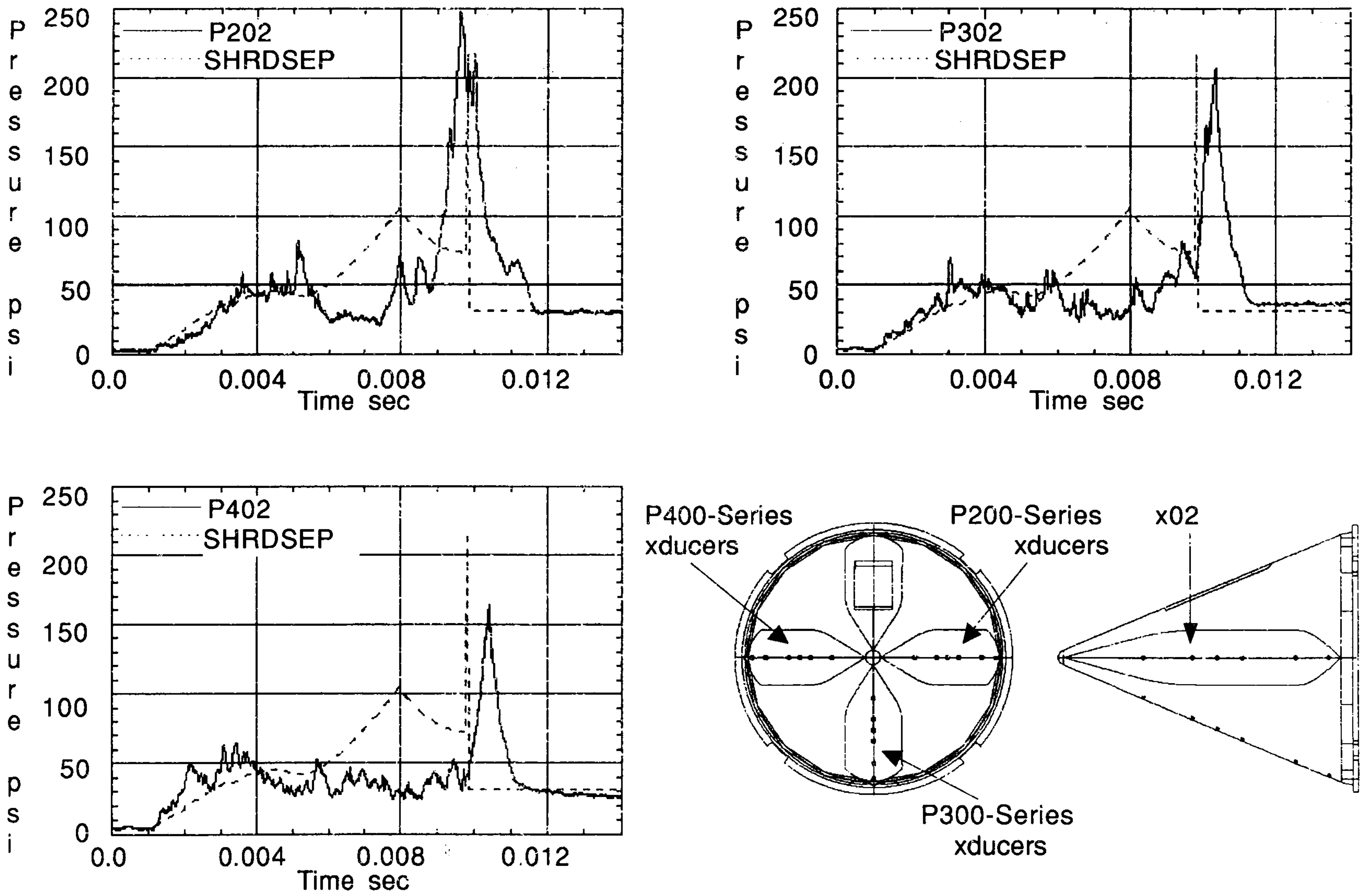


Figure 17. Continued

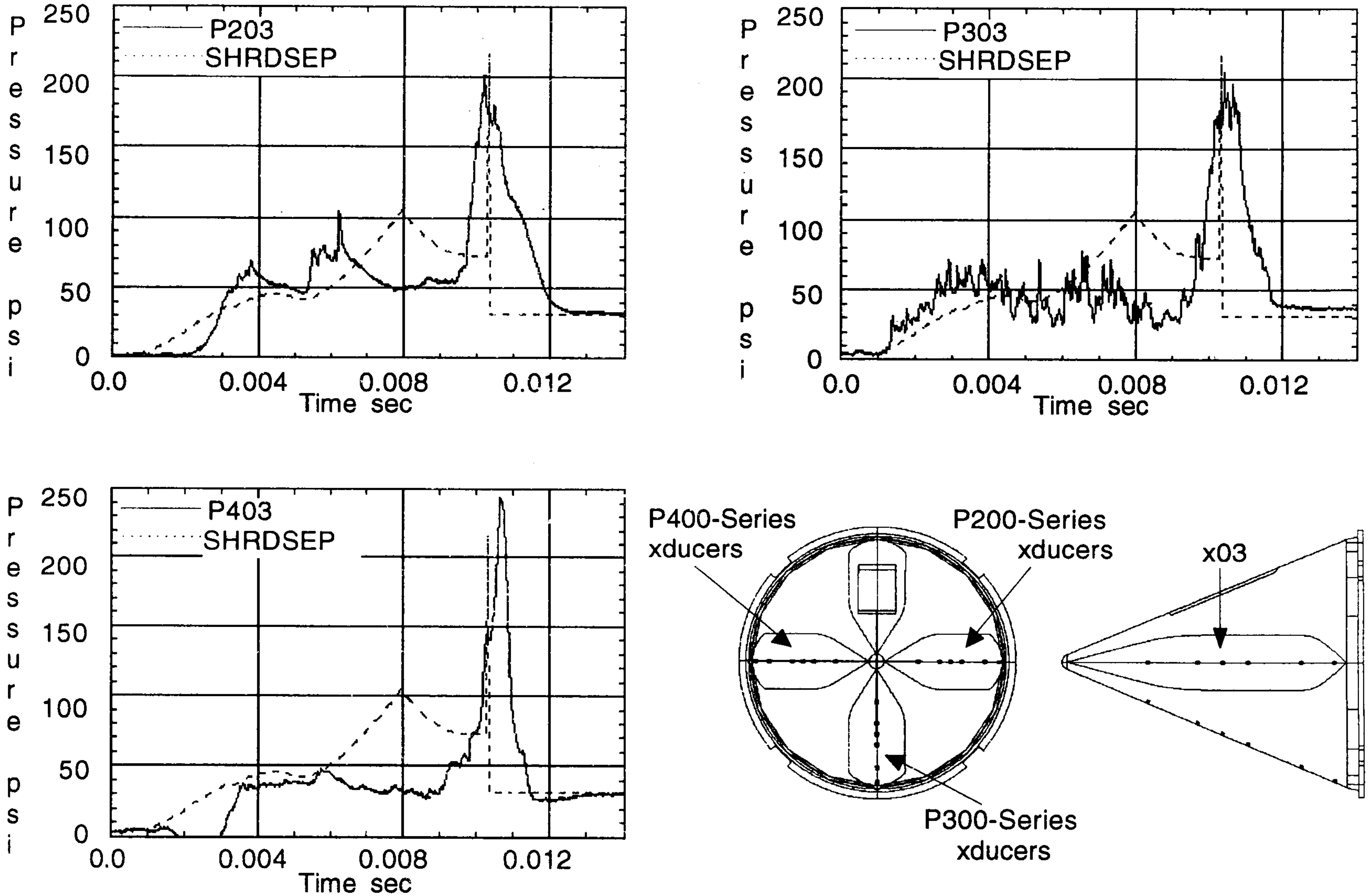


Figure 17. Continued

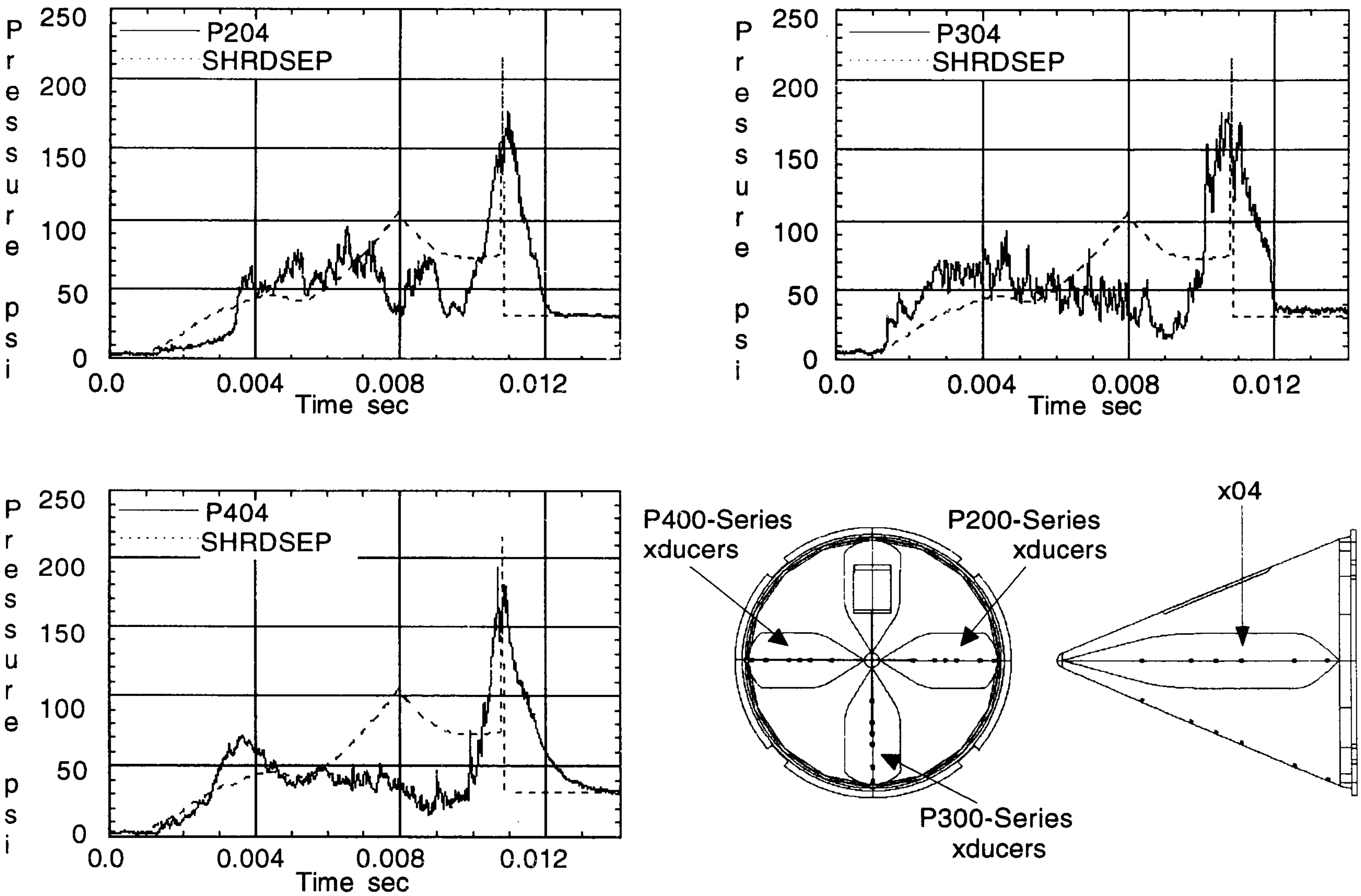


Figure 17. Continued

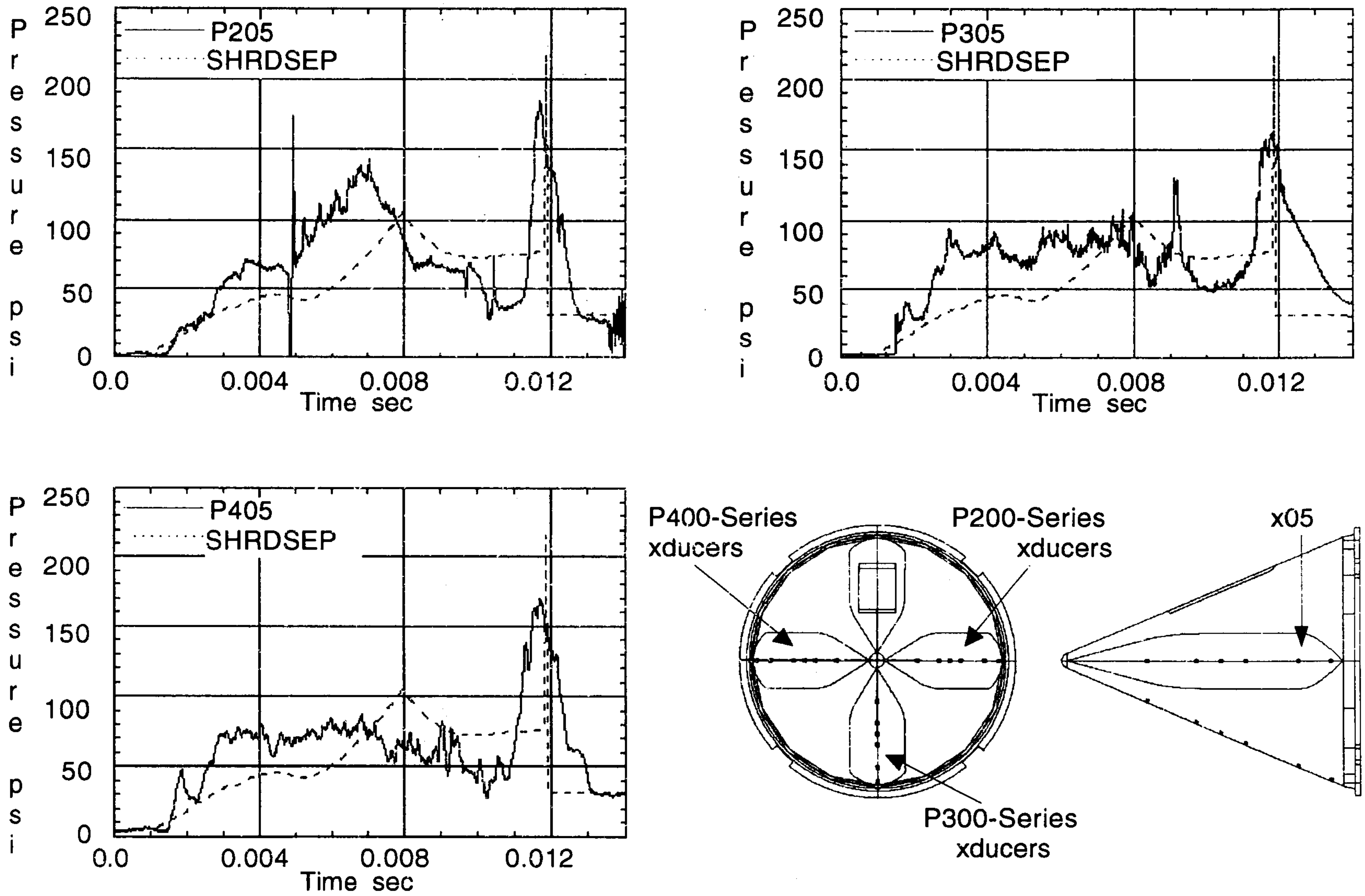


Figure 17. Continued

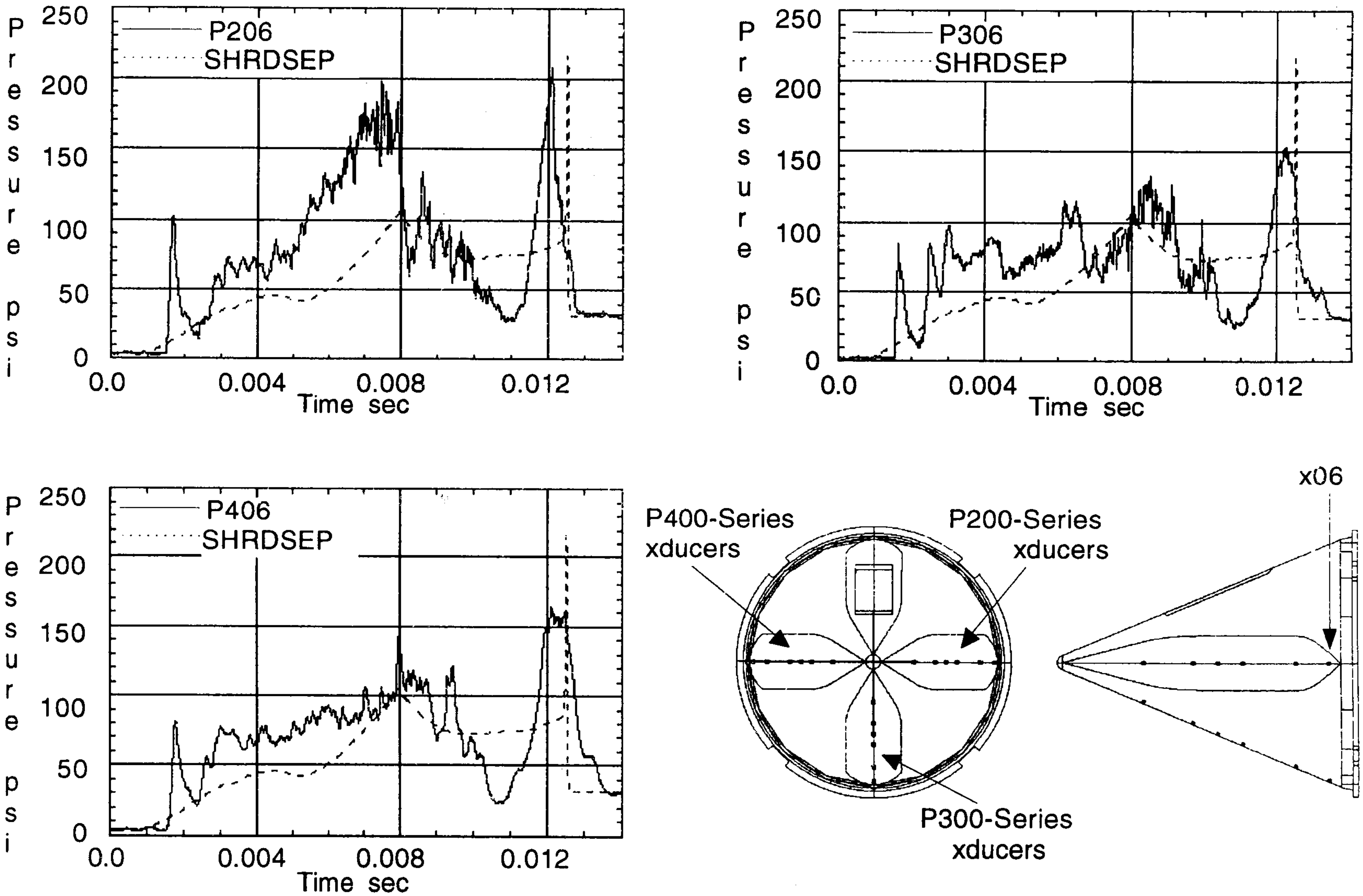


Figure 17. Concluded

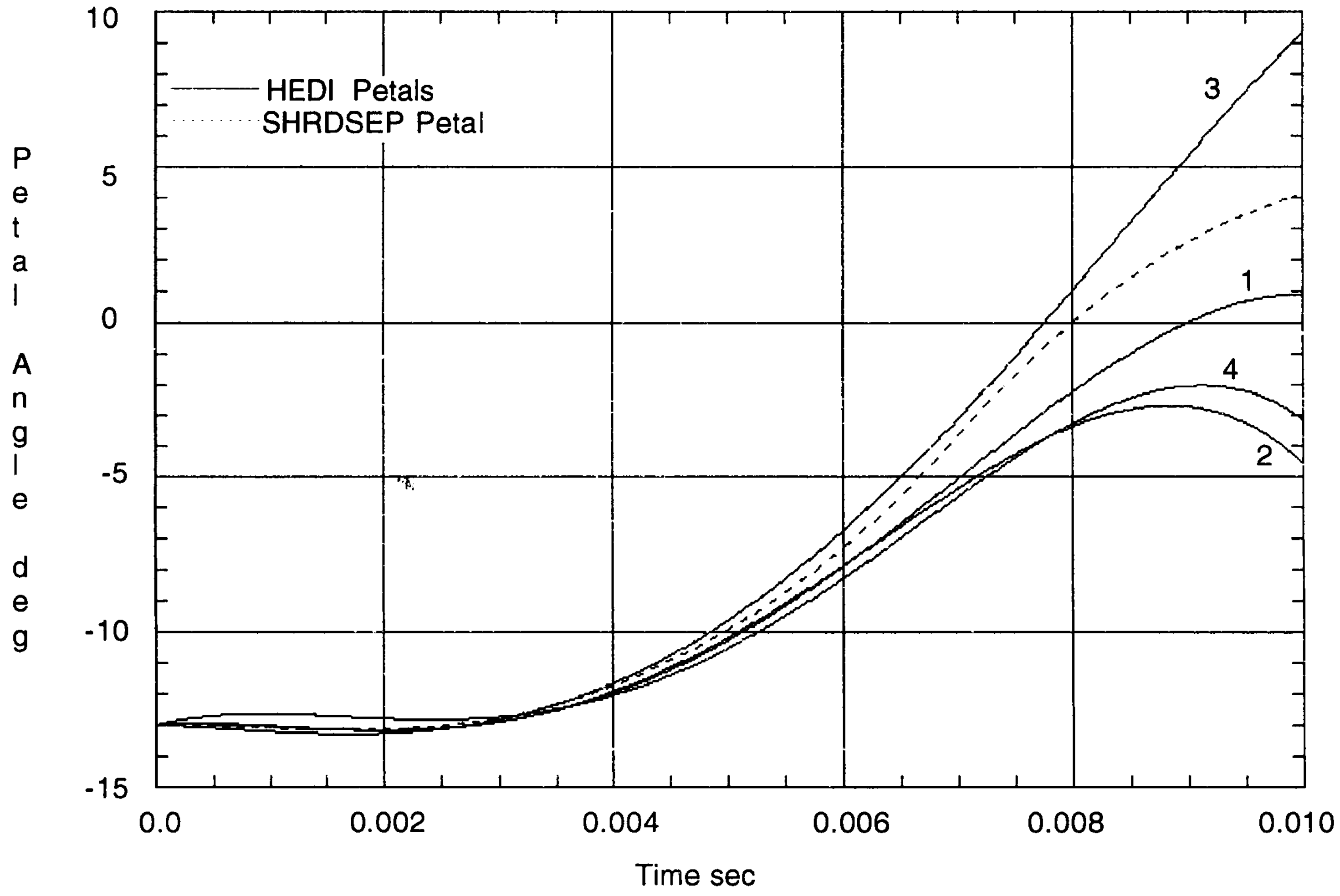


Figure 18. SHRDSEP vs HEDI NSWC Tunnel 9 Ground Test - Petal Motion Data

calculated by the program to the petal motion histories recorded during the ground test.

Analysis of the pressure data comparison plots gives solid credibility to the traveling pseudo normal shock theory pursued. It can be seen from Figure 17 that without exception, the cavity fill and early vent and travel period pressure profiles are closely matched. In addition, the peak values for the pressure pulses are nearly identically matched in time of occurrence and magnitude. The only trend not consistently modeled is the intermediate peak pressure generated by the program at approximately 8 milliseconds which corresponds to the time of petal unhinge.

Analysis of the petal motion data comparison plot also reveals promising results. The assumed axisymmetric motion of the four petals modeled by the program (represented by the generic petal in Figure 18) is not only bounded by the motions recorded by the four petals, it also reflects their characteristic trends.

Referring back to the one trend in the pressure profile comparisons (Figure 17) which is not as well matched by the program, it should be noted that the pressure histories for the most upstream transducers do match the program throughout the profile. Note the rapid divergence of petal 3 in the data presented in Figure 18. This non-symmetric petal deployment most likely caused a significant difference in the way the ground test model cavity vented. This fact provides at least one explanation as to why the intermediate pressure peak may not be witnessed later in the history when the more downstream transducers come into play.

## Flight Test Comparison

The program was run using the flow conditions from the last HEDI flight test at the time of shroud deployment. Specifically, the following inputs were specified for the flight test comparison run of the program:

| | |
|---|---|
| Working Fluid (Air) Gas Constant: | 1716.48 ft^2/sec^2-R |
| Working Fluid Ratio of Specific Heats: | 1.4 |
| Free Stream Mach Number: | 5.07 |
| Free Stream Total Pressure: | 2774 psi |
| Free Stream Total Temperature: | 2579 R |
| Initial Internal Cavity Pressure: | 9.3 psi |
| Petal Unhinge Angle: | -4 deg |
| Estimated Traveling Shock Speed: | 205 ft/sec |

The value used for the petal unhinge angle was -4 deg based on the ground test data. There was no data from the flight test to make any other determination. There were two pressure transducers on the forebody, both located on different faces of the tetracone, but at the same axial flight station (FS 92.2). Unfortunately this meant that there was no way of determining the speed of the shock empirically. Therefore, the shock speed value used was picked after a few trial and error iterations, the result of which placed the peak occurrence coincident with the measured peak occurrence. The intent here was to observe how the remainder of the pressure profile would compare.

Figure 19 presents the results of the program compared to the flight test data for the two transducers located at FS 92.2. Figure 19a does not compare very well. The profiles appear to be out of phase, and the peak pressure is off by a factor of 2. However, Figure 19b compares very well aside from the initial fill pressure

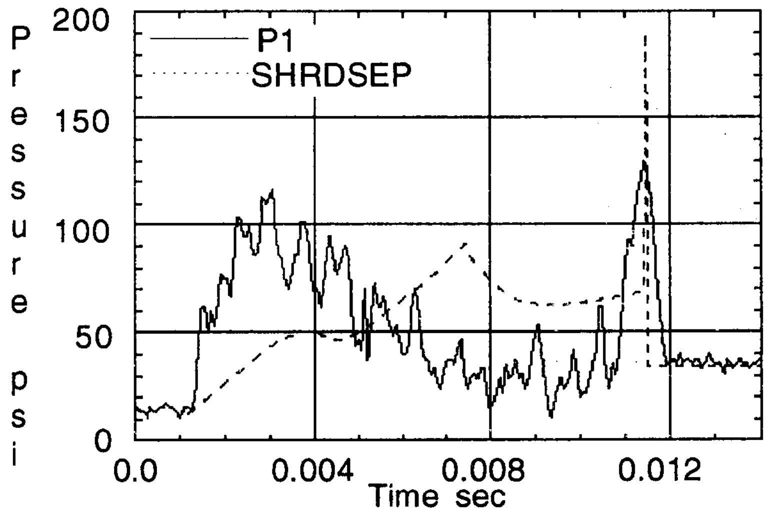


a. P1 (FS 92.2) vs SHRDSEP

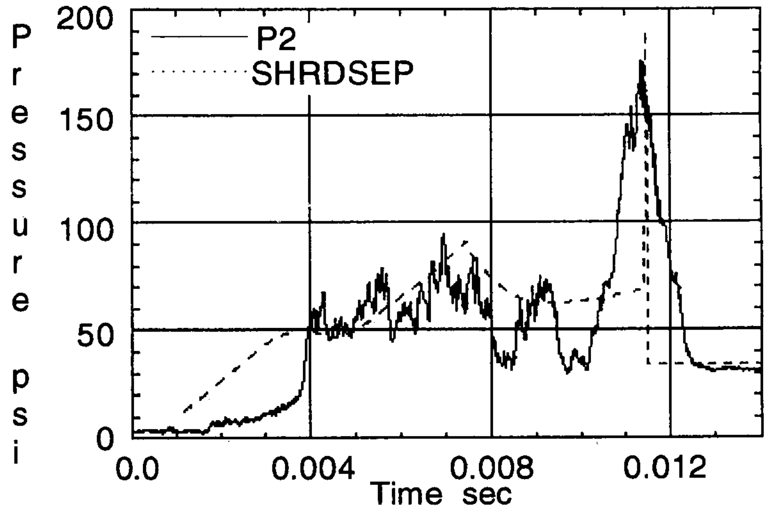


b. P2 (FS 92.2) vs SHRDSEP

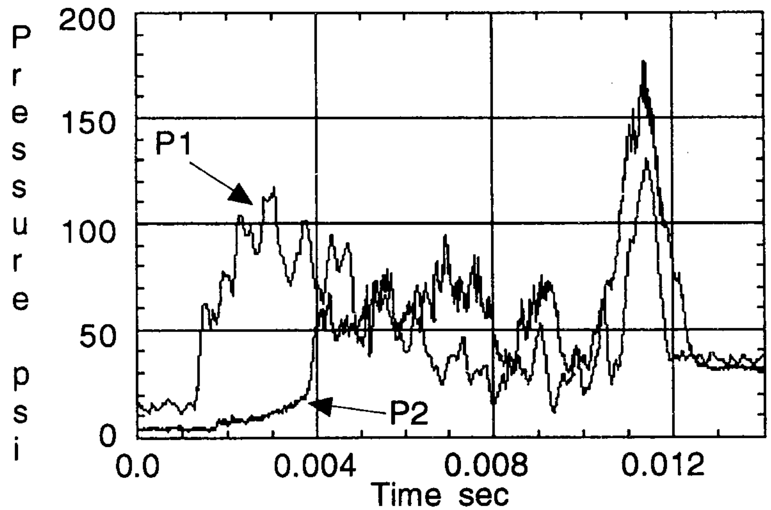


c. P1 vs P2

Figure 19. SHRDSEP vs HEDI Flight Test

variation. This comparison illustrates two points important to remember when using the program:

1. The program treats the captured flow as a bulk of mass with uniform properties throughout the cavity.

2. The program assumes uniform axisymmetric petal deployment.

The first point would explain why Figure 19b shows a difference in initial fill pressure. It is reasonable to believe that the actual cavity properties will have a density gradient resulting from various degrees of venting along the forebody axis of symmetry. Therefore, fluid properties downstream of the moving shock would be expected to become more uniform as the shock moves downstream and the density of the trapped mass increases significantly above initial levels.

The second point explains why such a radical difference can exist in the profiles of Figure 19a. Although the petal motion histories were not recorded during the flight test, it is reasonable to conclude that actual deployment of the petals was not symmetric, as was observed during the ground test. This means that there probably exist three-dimensional density gradients due to non-symmetric petal venting. Indeed, Figure 19c illustrates the difference between the two pressure transducers at the same axial location, but on different faces. Similar results can be observed in the ground test data.

Since there was no recorded petal motion data from the flight test, petal motion data could not be compared.

## CFD Comparison

The program was run using the flow conditions of the FEFLO CFD run (Chamberlin and Baltar [1]), which was run in support of the HEDI program. (It should be noted that hundreds of hours of Cray time were required to run the FEFLO solution.) Specifically, the following inputs were specified for the CFD comparison run of the program:

| | |
|---|---|
| Working Fluid (Nitrogen) Gas Constant: | 1740 ft^2/sec^2-R |
| Working Fluid Ratio of Specific Heats: | 1.4 |
| Free Stream Mach Number: | 8.86 |
| Free Stream Total Pressure: | 18009 psi |
| Free Stream Total Temperature: | 1769 R |
| Initial Internal Cavity Pressure: | 3.73 psi |
| Petal Unhinge Angle: | -3.4 deg |
| Estimated Traveling Shock Speed: | 300 ft/sec |

The only input not actually specified in the FEFLO run was of course the estimated traveling shock speed. This value was determined from study of the peak time histories resulting from the FEFLO run.

Figures 20 and 21 show the results of the comparison between the FEFLO output and the SHRDSEP output. Once again, the initial fill and vent/travel periods tend to agree fairly well for the first three axial transducer locations. The last two locations show encouraging trend profile comparisons. Unfortunately, all the comparisons show significant differences in magnitude and time of occurrence of the peak pressure pulse.

The FEFLO run was an attempt to model the ground test results. It was discovered late in the run that the free stream temperature (and therefore Mach number) were erroneously input. Despite this

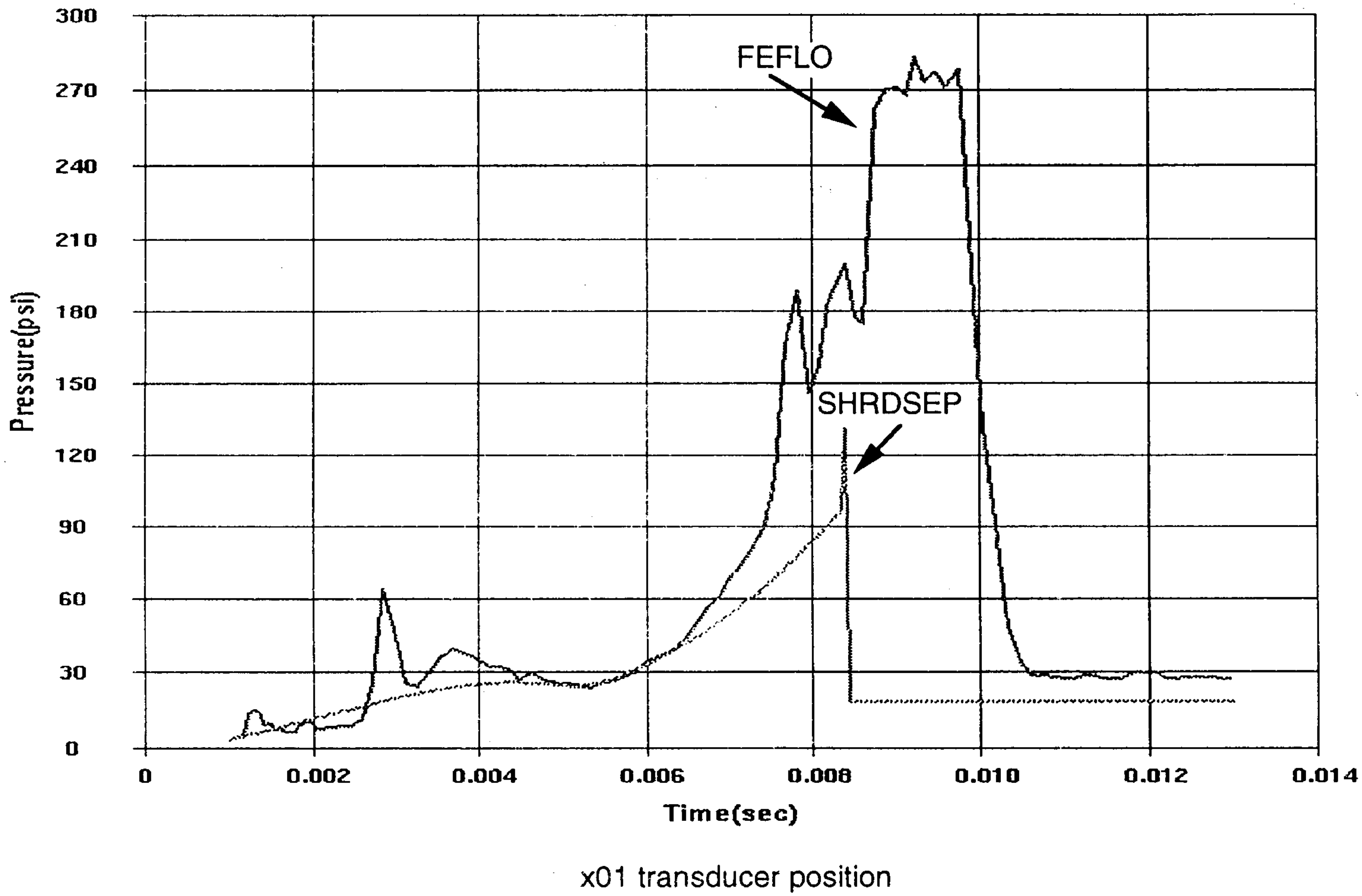


Figure 20. FEFLO vs. SHRDSEP Pressure Comparison

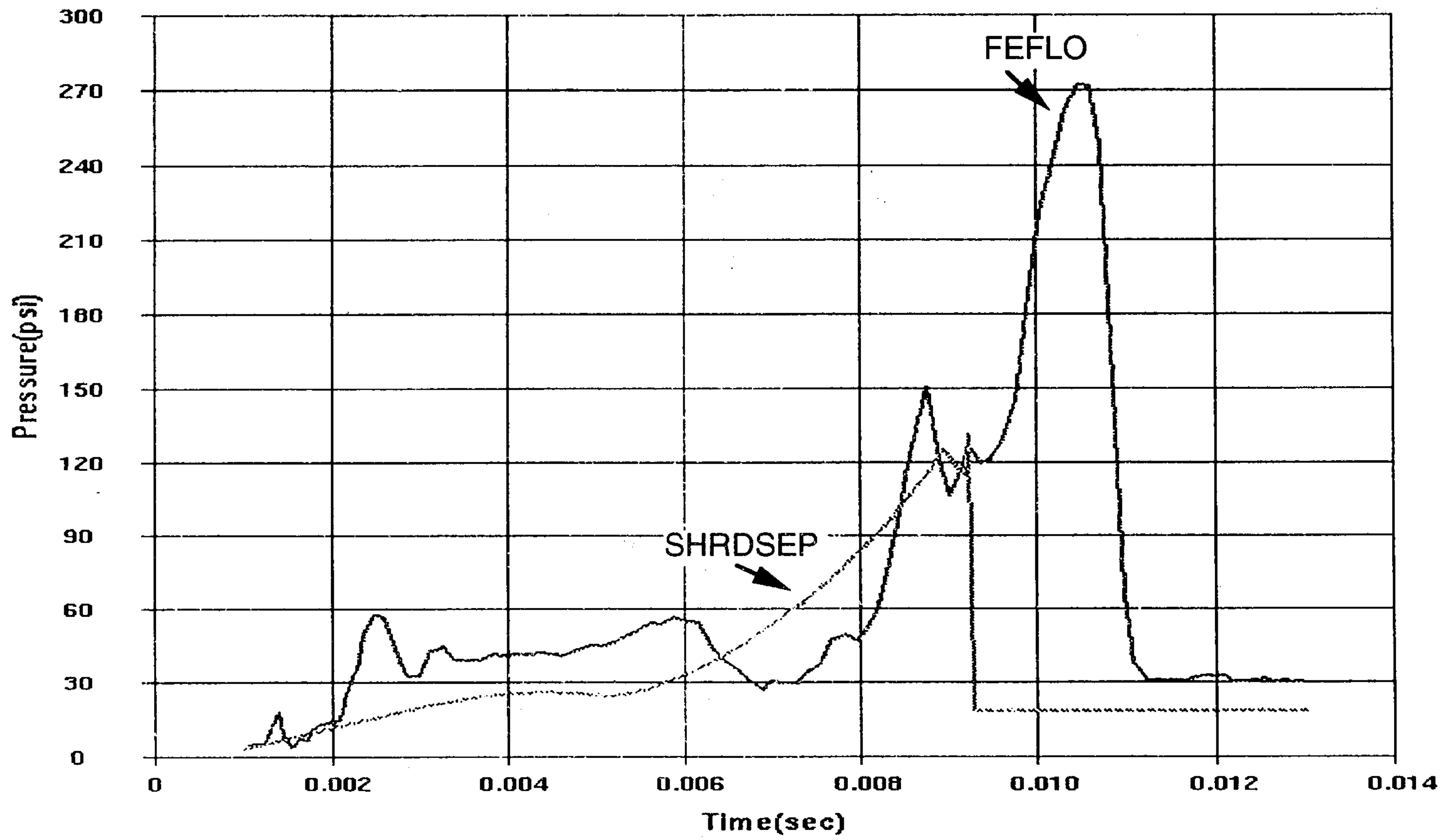


x02 transducer position

Figure 20. Continued

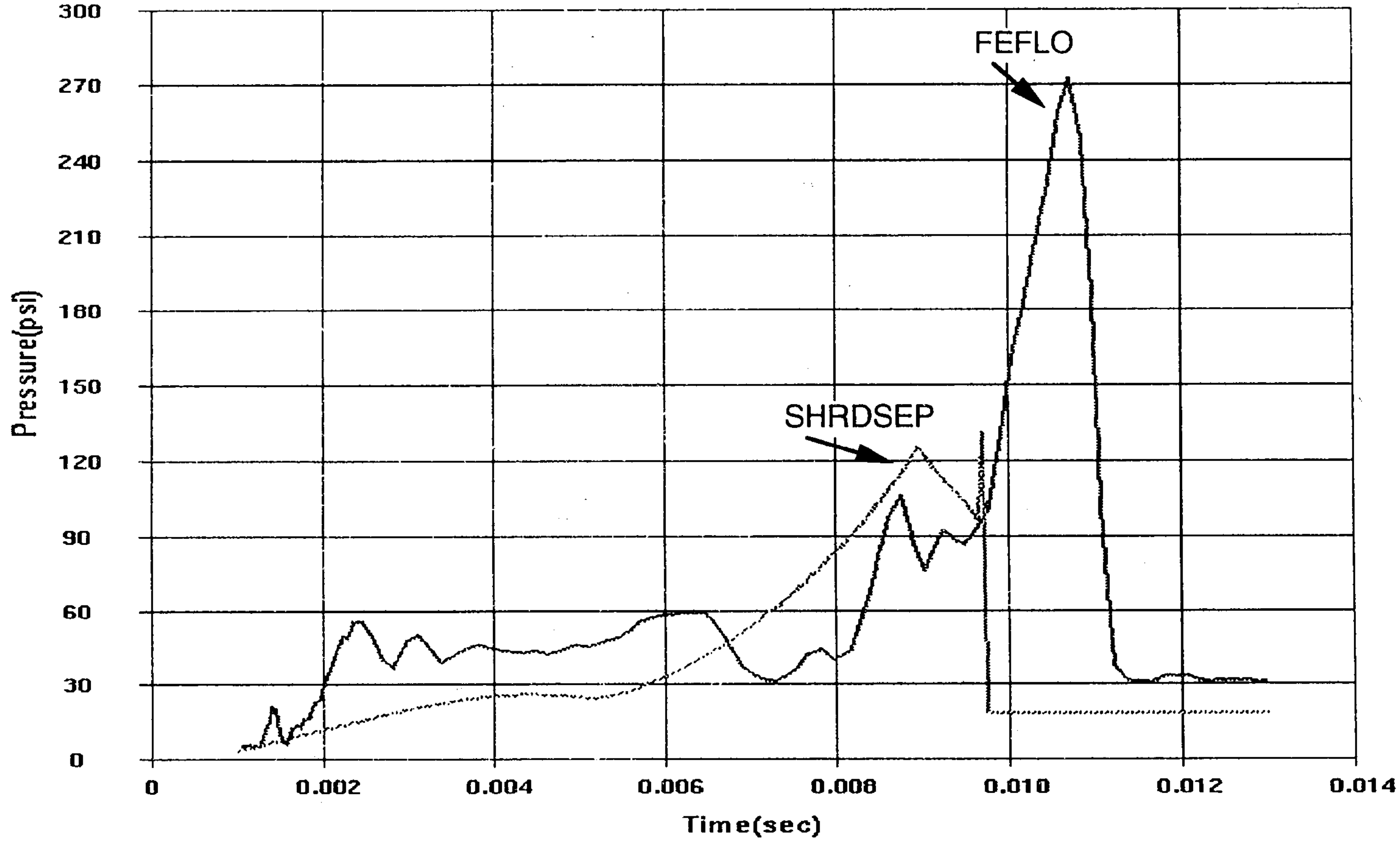


x03 transducer position

Figure 20. Continued

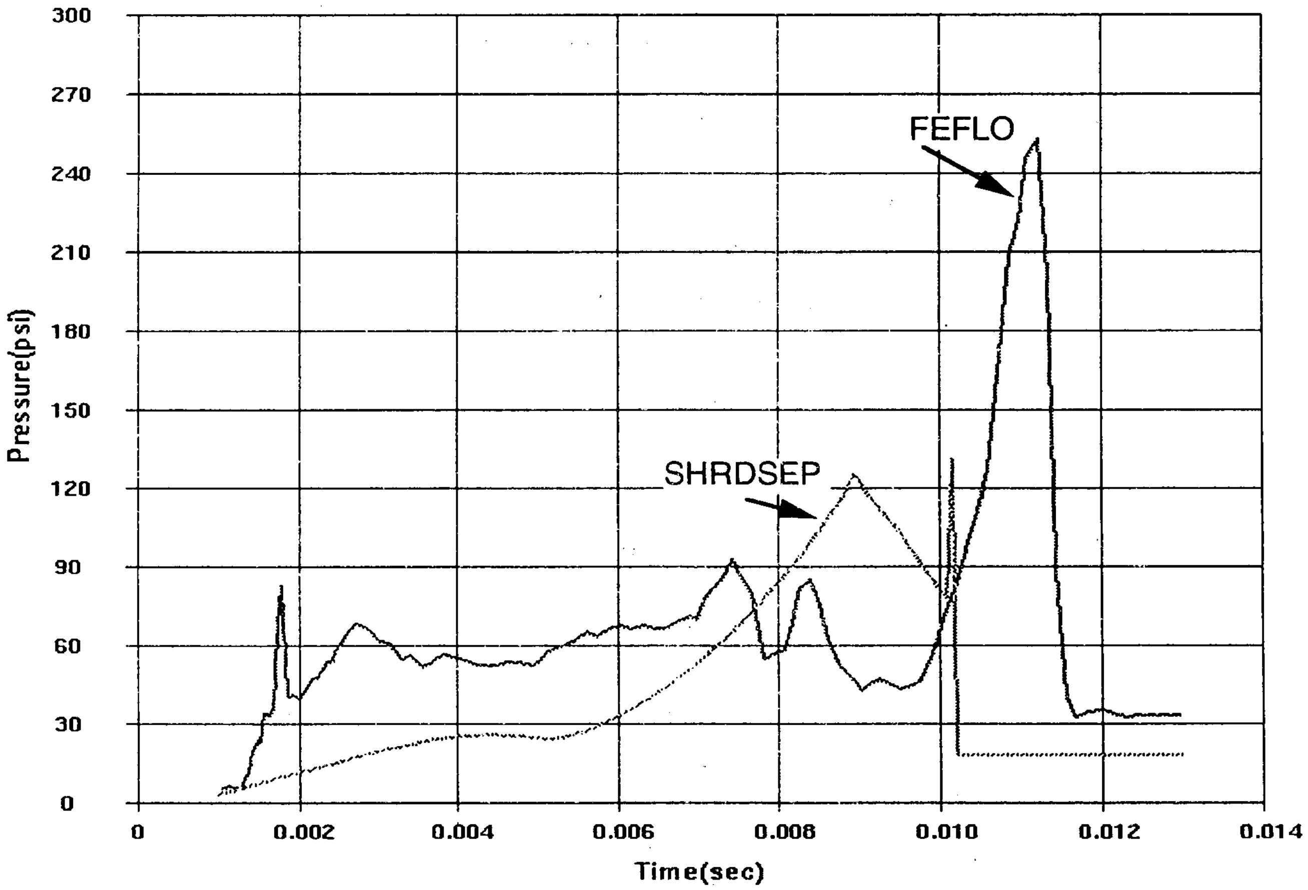


x04 transducer position

Figure 20. Continued

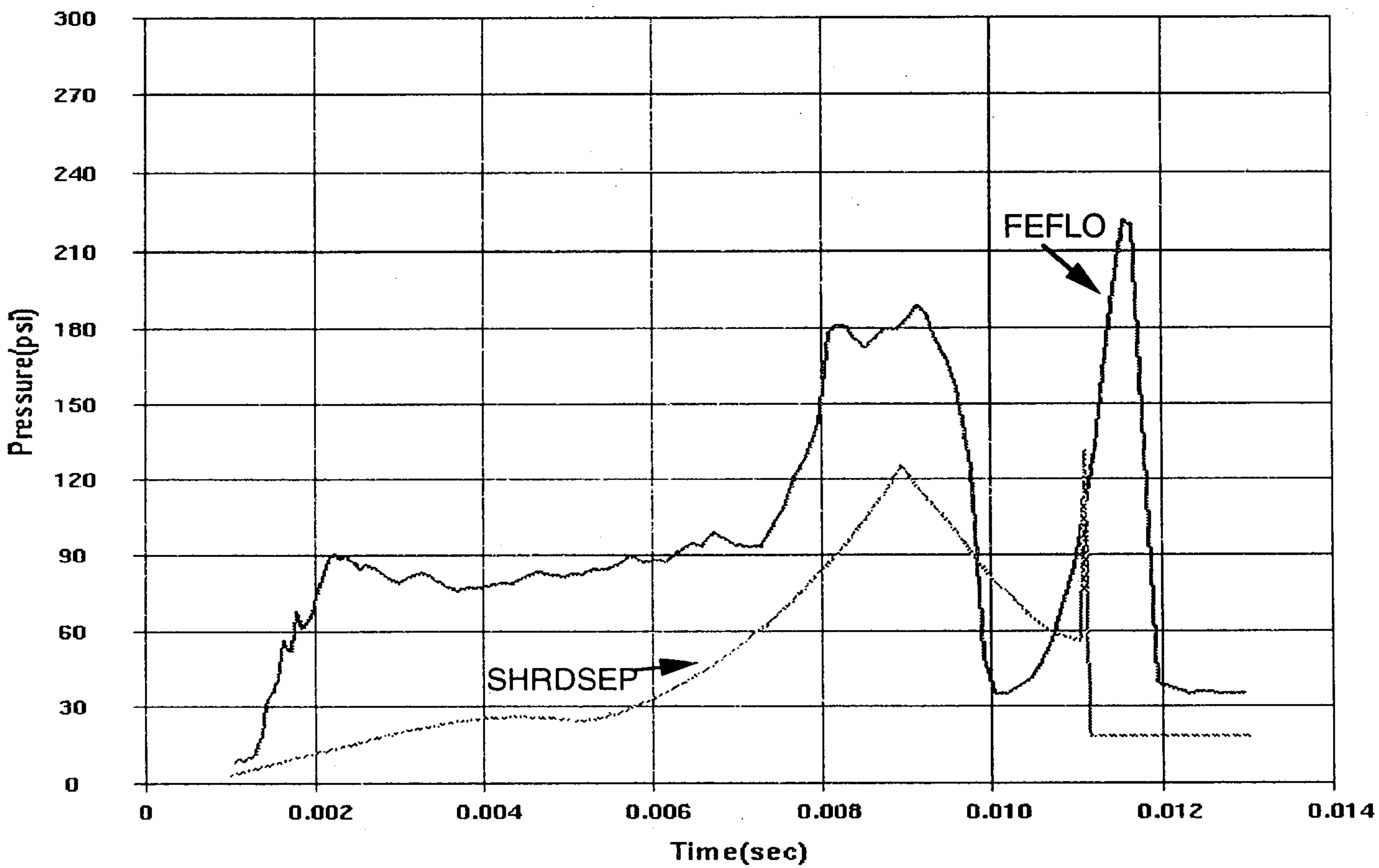


x05 transducer position

Figure 20. Continued

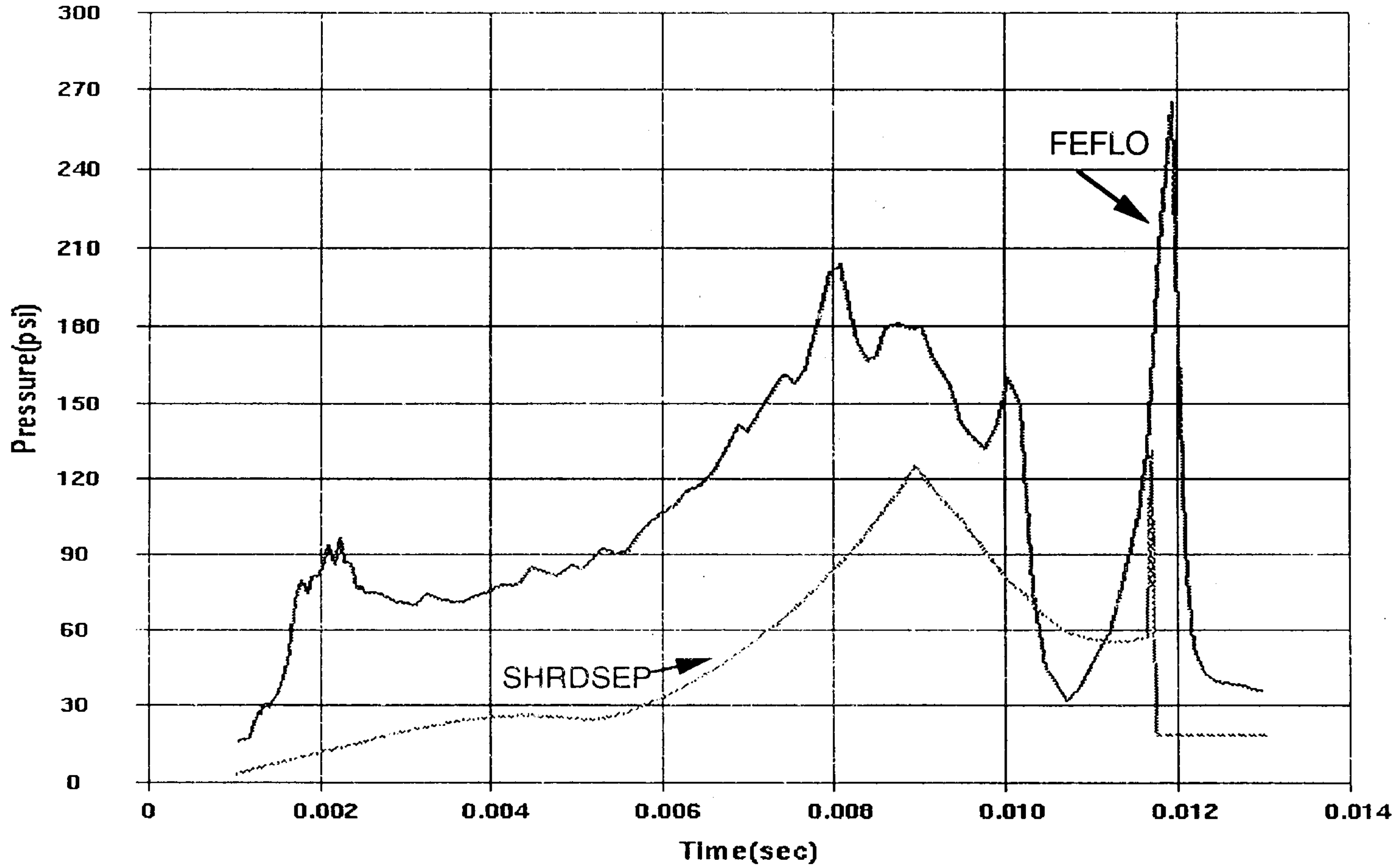


x06 transducer position

Figure 20. Concluded

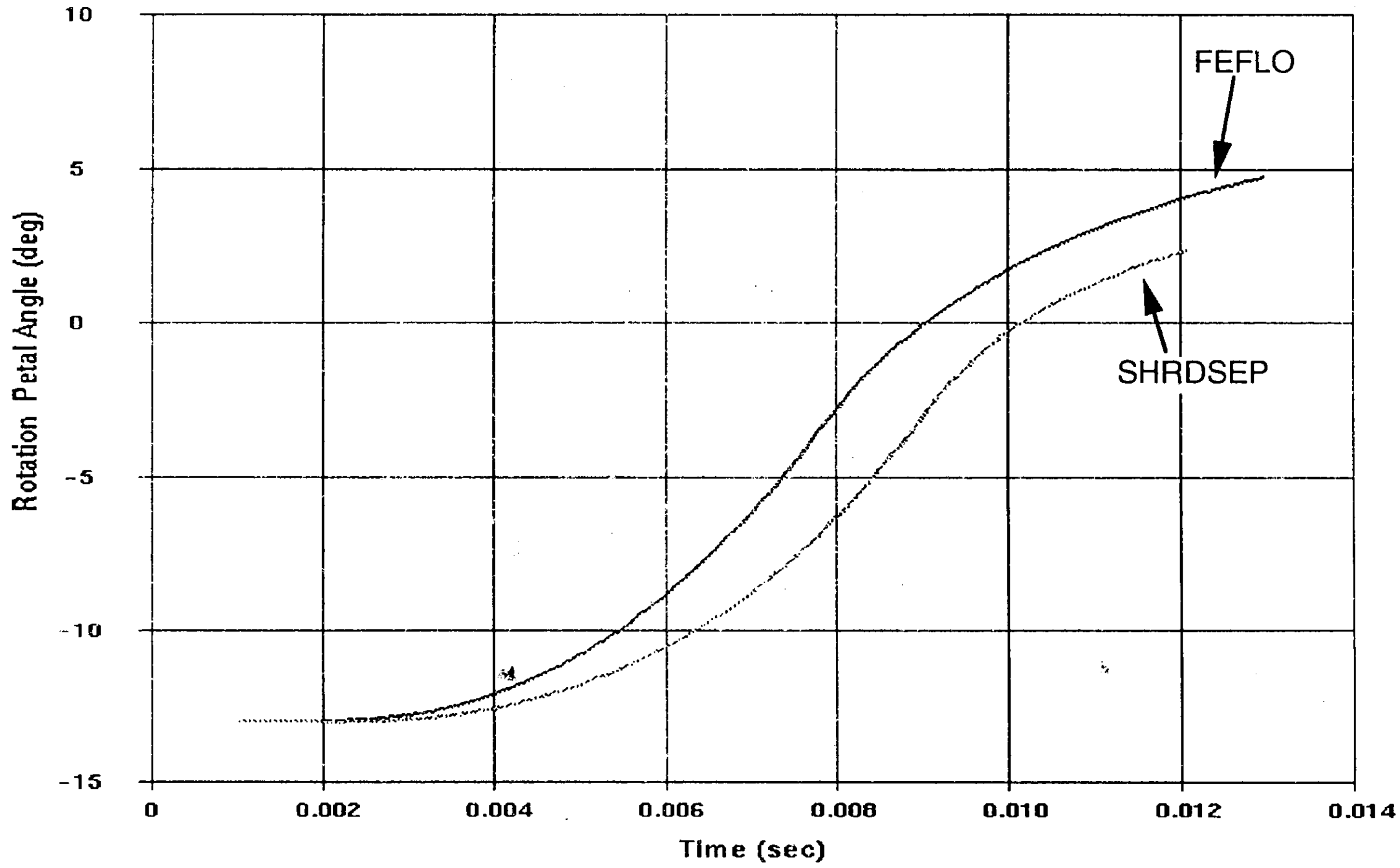


Figure 21. FEFLO vs. SHRDSEP Petal Motion Comparison

fact, the run was heralded a success because it still did an impressive job of matching the pressure and petal motion profiles. Concerning the difference in pressure magnitudes between the two profiles, it is interesting to note a passage from Chamberlin & Baltar [1]:

> "... It has been suggested (Cayse and Lumb [6]) that this spike is due to a normal shock which forms just prior to petal motion and which subsequently moves over the forebody as the petals rotate away. The present results demonstrate that a cavity shock, essentially normal to the local flow, interacts with the forebody bow shock and the petal lip shock to account for the high pressure pulse. Although the computation overpredicts the magnitude of the peak, its time history over the forebody is well characterized, with only a slight temporal delay due to the less rapid venting."

The generally higher pressures from the FEFLO results would lead one to believe that the resulting petal accelerations may be greater. Figure 21 shows that indeed, the FEFLO petal dsiplaces at a higher rate than the SHRDSEP petal, while the petals exhibit similar trends.

# CHAPTER VI

# CONCLUSIONS

The problem addressed in this effort was the characterization of the flow phenomenon which caused the large pressure transient measured on the HEDI forebody during the shroud separation event. The original intent of this effort was two fold. First, the investigation of the theory of a moving normal shock as the driver for the forebody pressure responses during shroud separation. Second, development of a first order independent design tool using the principles of the moving normal shock theory.

Approximations made include the assumption of uniform, one dimensional flow within the shroud during the separation event; choked flow exiting the shroud cavity through vent areas between shroud petals; specified constant speed normal shock movement downstream perpendicular to the axis of symmetry after the fill/vent mass flow ratio has reached 1; and capture area defined at the shock location with vent area defined downstream of the shock location after shock motion within the cavity has begun.

The results presented would indicate that as a whole, the moving normal shock theory developed by the methods of the investigation is reasonably good. The flow characteristics of this event are obviously much more complicated than what is assumed in the model presented. Nevertheless, significant accomplishments were made in matching pressure trend profiles (for all cases), matching pulse peak magnitudes (for the ground and flight test cases), and matching petal motion data (for the cases with available data).

The primary drawback in the conduct of this effort was the inability to define a reliable independent shock motion model within the context of this simplified model.

The model is recommended for use as a first order design tool assuming the following considerations are made:

- The geometry must be modified for the specific case being investigated.
- The petal release angle plays a strong roll in the outcome of the case run. The actual release angle may differ significantly from the design release angle. Until empirical data can be obtained, the design release angle should be used.
- Estimate of the shock speed must be based on the design deployment conditions and the geometry/mass properties of the shroud petals. This information will allow an engineering estimate of the event duration. With this known (or specified as a requirement) the engineer can subtract the time required for the fill/vent mass flow ratio to equal 1 (calculated by the SHRDSEP code) to find the duration of the shock motion. The shock speed estimate can then be calculated by dividing the cavity length by the shock motion duration.

# LIST OF REFERENCES

## LIST OF REFERENCES


[1] Chamberlin, Rex R. and Baltar, James Y., "Time-Accurate Calculation of Hypersonic Shroud Separation", AIAA Paper 93-0317, 1993.

[2] Tincher, D. J., "HEDI Shroud Screening Test (NASA LaRC)", MDC-H3219, McDonnell Douglas Space Systems Corporation, Huntington Beach, California, 1986.

[3] Edney, B., "Anomalous Heat Transfer and Pressure Distributions on Blunt Bodies at Hypersonic Speeds in the Presence of an Impinging Shock", The Aeronautical Research Institute of Sweden, Report 115, 1968.

[4] Anderson, John D., Modern Compressible Flow, McGraw-Hill Book Company, New York, 1982.

[5] Cayse, Robert W., "Analysis of HEDI Shroud Deployment Window Loads Test Data", SYT91-TP-003, SY Technology, Incorporated, Huntsville, Alabama, 1991.

[6] Lumb, Stewart B. and Cayse, Robert W., "Transient Aerodynamics of a High Dynamic Pressure Shroud Separation for a Ground Based Interceptor Missile", AIAA Paper 92-2820, 1992.

APPENDIX

## Geometry Equations

Cross sectional areas within the closed petals were calculated according to the radius of the petal cross section at a given flight station (FS). The radii used were developed from the petal drawings and calculated as follows:

| | | |
|---|---|---|
| Section 1: | Reff=1.802 | x1<X<x2 |
| Section 2: | Reff=(X-Xoff2)*TAN(45) | x2<X<x3 |
| Section 3: | Reff=(X-Xoff3)*TAN(45) | x3<X<x4 |
| Section 4: | Reff=(X-Xoff4)*TAN(13) | x4<X<x5 |
| Section 5: | Reff=(X-Xoff5)*TAN(13) | x5<X<x6 |
| Section 6: | Reff=1.05*X-11.858 | x6<X<x7 |
| Section 7: | Reff=(X-Xoff7)*TAN(13) | x7<X<x8 |
| Section 8: | Reff=6.886 | x8<X<x9 |
| Section 9: | Reff=(X-Xoff9)*TAN(13) | x9<X<x10 |

Where the Xoff"i" locations are the points on the X-axis (axis of symmetry) at which the extension of a line defining an angle on the petal profile intercepts the X-axis. All X distances are measured from the virtual orign of the 13 deg cone that defines the shroud. The cross sectional area is:

AP=PI*Reff**2

Cross sectional areas of the tetracone forebody were calculated according to the tetracone geometry equations provided by MDSSC. The areas were calculated as follows (AT-tetracone cross sectional area):

Section 1: THS=ASIN(1-((X-18.329)/RS)) x1<X<x2

AT=PI*(RS*COS(THS))**2

```
Section 2: Y=C1*(X-18.633)                  x2<X<x3
AT=4*Z**2-(Z-Y)**2*FMP                      C1=0.2658,
                                            Z=XT*TAN(23),
                                            XT=X-17.549,
                                            FMP=4.0-PI
Section 3: Y=a0+a1*XT+a2*XT**2+a3*XT**3     x3<X<x4
AT=4*Z**2-(Z-Y)**2*FMP                      a0=-2.937,a1=1.245
                                            a2=-0.108,a3=0.003
Section 4: Y=1.75                           x4<X<x5
AT=4*Z**2-(Z-Y)**2*FMP
Section 5: J=b0+b1*XT+b2*XT**2+b3*XT**3     x5<X<x6
Y=(J-Z)/(1.4142-1.0)                        b0=-131.162,
AT=4*Z**2-(Z-Y)**2*FMP                      b1=22.392,b2=-1.203
                                            b3=0.022
Section 6: RTCR=(X-XTCOFF)*TAN(13)          x6<X<x7
AT=PI*RTCR**2                               XTCOFF=1.744
```

Gap distances between the petals as they separate are calculated as a function of radial translation of the petal from centerline at a given flight station:

```
AMP=AAV-THP
THPT=ATAN((Rb-Reff)/(X20-X1P))
THDIFF=THPT-AMP
RTHP=Rb-(X20-X)*TAN(THDIFF)
DReff=RTHP-Reff
DGAP=2.0*DReff*SIN(45)
```

Area elements sum to a total captured cross sectional area defined by:

```
Atotal=AP+4*DGAP*Reff+DGAP**2
```

The total flow cross section is described by:

```
Aflow=Atotal-AT
```

## Fluid/Aeromechanical Equations

The instantaneous mass flow rate into the cavity:

```
F_MDOT=RHOINF*VINF*A_FRONT
```

The instantaneous mass flow rate out of the cavity:

```
V1=AGAP*P_CAV/(T_CAV**0.5)
V_MDOT=V1*((G/RGAS)*(2.0/(G+1.0))**((G+1.0)/(G-1.0)))**0.5
```

The instantaneous mass within the cavity:

```
TMASS=TMASS+V_MDOT*(CHKRAT-1.0)*DT
```

The instantaneous cavity density:

```
RHO_IN=TMASS/VT
```

The instantaneous cavity pressure:

```
P_CAV=RHO_IN*RGAS*T_CAV
```

External and internal pressure forces acting on the petal surfaces:

```
FE1=PPETEXT*(SAT/4.0)
FI1=PPETINT*(SA1/4.0)
FI2=PI2*(SA2/4.0)
```

Pressure force moment arms to the petal center of rotation from the petal base:

```
XPET1=((PETL-PETL2)-(2/3)*(PETL-PETL2)*XCONST)+PETL2-XUN
XPET2=(PETL2-(2/3)*PETL2*XCONST)-XUN
XPET3=(PETL-(2/3)*PETL*XCONST)-XUN
```

The sum of the moments about the petal center of rotation:

```
SUM_M=(FI1*XPET1+FI2*XPET2-FE1*XPET3)
```

Initial petal radial acceleration and velocity at time of petal unhinge:

```
AXINIT=(SUM_M/(X_CG*PETM))*COS(THP)
VZINIT=VZINIT+AZINIT*DT
```

Local Isentropic flow properties:

```
GOGM1=G/(G-1.0)
XMISO=1+((G-1.0)/2.0)*RMINF**2
PINF=PTINF/(XMISO**GOGM1)
TINF=TTINF*(XMISO**-1.0)
RHOINF=PINF/(RGAS*TINF)
VINF=((G*RGAS*TINF)**0.5)*RMINF
```

Properties downstream of a normal shock:

```
XM2=RMINF**2
GM1=G-1.0
GP1=G+1.0
GOGM1=G/GM1
CME=2*G*XM2-GM1
PT2=PINF*((GP1*XM2/2.0)**GOGM1)*(GP1/CME)**(1.0/GM1)
RM2=((GM1*XM2+2)/CME)**0.5
P2=PT2*(1+RM2**2*GM1/2.0)**-GOGM1
T2=T1*CME*(GM1*XM2+2)/(XM2*GP1**2)
RHO2=RHO1*(GP1*XM2)/(GM1*XM2+2)
```

Petal angular motion parameters:

```
AL_P=SUM_M/XMOI
OM_P=OM_P+AL_P*DT
THP=THP+OM_P*DT
```

Wedge compression parameters:

```
T2D=(TAN(THP))**2
XM2=RMINF**2
A=((G+1.0)*XM2+2.0)/2.0
B=T2D+1
C1=(-2.0*(A*T2D+1.0)-XM2)/B
C2=(A**2*T2D+2.0*XM2+1.0)/B
C3=-XM2/B
X=(3*C2-C1**2)/3.0
Y=(2.0*C1**3-9.0*C1*C2+27.0*C3)/27.0
PHI=ACOS(-Y*((-6.75/X**3)**0.5))
RM1ST2=2*((-X/3.0)**0.5)*COS((PHI/3.0)+240.0)-C1/3.0
THW=ASIN((RM1ST2/XM2)**0.5)
RM1N=(RMINF*SIN(THW))**2
P2P1=((2.0*G*RM1N-(G-1.0))/(G+1.0)
T2T1=(2.0*G*RM1N-(G-1.0))*((G-1.0*RM1N+2.0)/((G+1.0)**2*RM1N)
PT2PT1=(((G+1.0)*RM1N)/((G-1.0)*RM1N+2.0))**(G/G-1.0))*
((G+1.0)/(2.0*G*RM1N-(G-1.0)))**(1.0/G-1.0))
RM2=(((G+1.0)**2*RM1N*RMINF**2-4.0*(RM1N-1.0)*(G*RM1N+1.0))/
((2.0*G*RM1N-(G-1.0))*((G-1.0)*RM1N+2.0)))**0.5
```

Wedge compression parameters:

```
GRAT=(G+1.0)/(G-1.0)
GRATI=1.0/GRAT
XNUM(RM)=(GRAT**0.5)*ATAN((GRATI*(RM**2-1.0))**0.5)-
ATAN((RM**2-1.0)**0.5)
TTOP=1.0+((G-1.0)/2.0)*RM2**2
TBOT=1.0+((G-1.0)/2.0)*RMINF**2
P2P1=T2T1**(G/(G-1.0))
```

# VITA

Peter Evan Fryberger was born in Summit, New Jersey on 20 August 1963. He attended elementary schools in the Warren Township, New Jersey School District and graduated from Watchung Hills Regional High School in Warren, New Jersey in June, 1981. That same June he entered Florida Institute of Technology, then transferred to The University of Texas at Austin in September, 1983 where in December, 1986 he received the degree of Bachelor of Science in Aerospace Engineering. In March, 1987 he entered The University of Tennessee Space Institute of Tullahoma, Tennessee and in May, 1993 received a Master of Science degree in Mechanical Engineering.

He is presently employed as a Member of the Technical Staff at SY Technology, Incorporated in Huntsville, Alabama.